Bragg Grating Based Sensors in Microstructured Polymer optical Fibres: Accelerometers and Microphones

Alessio Stefani

Ph.D. Thesis

December 2011

DTU Fotonik
Department of Photonics Engineering

Bragg Grating Based Sensors in Microstructured Polymer Optical Fibers: Accelerometers and Microphones

Alessio Stefani

Ph.D. Thesis

December 23rd 2011

DTU Fotonik
Department of Photonics Engineering
Technical University of Denmark
Ørsteds Plads 345V
DK-2800 Kgs. Lyngby
Denmark

Preface

The work presented in this thesis has been carried out as part of my Ph.D. project in the period January 1st 2009-December 23rd 2011.

The work took mainly place at DTU Fotonik (Department of Photonics Engineering), Technical University of Denmark. A three months research stay was spent at the Department of Electronic Engineering, Macquarie University, NSW, Australia and a one month research stay was spent at the Instituto de Engenharia de Sistemas e Computadores (INESC) do Porto, Portugal.

The project was financed by the Danish National Advanced Technology Foundation and supervised by

- Ole Bang, Professor, DTU Fotonik, Technical University of Denmark, Kgs. Lyngby, Denmark
- Wu Yuan, Ph.D., Singapore Institute of Manufacturing Technology, Singapore

The results of the thesis were presented for public examination and debate on February 27th 2012 at the Technical University of Denmark. The evaluation committee consisted of Doctor Kay Schuster (Institute of Photonics Technology Jena, Germany), Professor Søren R. Keiding (University of Aarhus, Denmark) and Professor Karsten Rottwitt (Technical University of Denmark).

Alessio Stefani, March 13th 2012

Acknowledgments

First I would like to sincerely thank my supervisor Ole Bang for giving me the possibility to work on this project and for his trust, support, motivation and guidance, which made the work interesting, constructive and challenging, but also pleasant.

A big thank you to Scott for the discussions, for having shared work, failures and successes. Thanks to all the project partners, in particular Søren from Brüel & Kjær; Bjarke, Nicolai and Ole from Ibsen; and Ole from DPA Microphones; for the pressure, enthusiasm, support and for the great job done during the project. Without them I wouldn't have been able to achieved what I did. Thanks to Graham for hosting me at Maquarie and for making the time Down Under a great experience and to Matthias for all the collaborations and projects together. Thanks to John Canning and Kevin Cook for their time and the possibility to work with them at Sidney University, even if for just a short time. Thanks also to José Manuel and Orlando for hosting me at INESC and for always being enthusiastic and motivated. Thanks also to the COST actions 299 and 1001 for financial support, but mostly for making possible many collaborations and creating great possibilities for networking. Thanks also to David Webb, Kyriakos Kalli and all the guys at Aston University for very fruitful collaborations. Thanks to all the people who showed interest in this work and wanted to collaborate, it was a big push every time in keep doing it and doing it better. Many thanks to Frank, Martin and Jan from the workshop, for the priceless amazing work. They are behind many results even if it's rarely mentioned. Thanks to all my colleagues for help, discussions, fun, coffee breaks and

cakes.

Thanks to Michael and Kristian for making working big fun without reducing the scientific level and value of it. It's been a pleasure to work we you guys! And thanks also for being great friends! Thank you Michael! also for the useful and ironic comments on the thesis manuscript. Thanks to all my friends for making life so good and taking away the pressure when necessary. In particular thanks to: Chiara, Vale, Carolina, Lina, Francesca and Birgit; for making the last three years so much better.

Finally a huge thank you goes to my family that supported me and believed in me all the time without doubts even if they were far and it was hard to accept.

Abstract

With the growing interest towards fiber Bragg grating sensors and the growing ability in manufacturing polymer optical fibers, the development of polymer fiber Bragg sensors has catched the attention of industries with the goal of developing high performance sensors.

This thesis presents the development of fiber sensors based on polymer optical fiber Bragg gratings. The whole process from the preform to the device is discussed and reported. A presentation on the fiber drawing technique used is given. Issues encountered when working with polymer fibers and solutions concerning fiber cleaving and gluing of polymer to silica fibers are discussed. The realization of gratings in polymer fibers is shown with two different techniques: the UV phase mask technique and the direct writing technique reported here for the first time for polymer fibers. Realization of gratings in PMMA step index fibers and in microstructured fibers made of PMMA and TOPAS is reported. The gratings have been written at both 1550 nm, to take advantage of components made for telecommunications, and 850 nm, to exploit the lower loss of polymers and the fast acquisition electronics at this wavelength. A technique for writing multiplexed gratings is shown and temperature compensation of strain sensors, by using two adjacent gratings, is demonstrated. Humidity insensitivity in a strain sensor based on a TOPAS fiber is also shown.

In order to investigate the possibility of using viscoelastic materials, such as polymers, in dynamic sensors, dynamic mechanical characterization of polymer fibers was made and it is presented.

The investigated and produced fiber Bragg gratings in microstruc-

tured polymer optical fibers were used to produce optical accelerometers. The accelerometers and their characterization are reported. Finally the realization of an optical microphone based on polymer fiber Bragg gratings is reported.

Resumé (Danish abstract)

Med den voksende interesse for fiber Bragg-gitter sensorer og forbedringen i fremstilling af polymer optiske fibre, har udviklingen af polymer fiber Bragg sensorer fanget opmærksomheden af industrier som ønsker at udvikle højtydende sensorer.

Denne afhandling præsenterer udviklingen af fibersensorer baseret på polymer optisk fiber Bragg sensorer. Hele processen fra præform til sensor diskuteres og redegøres. En præsentation gives af den anvendte fibertrækningsteknik. Udfordringer i arbejdet med polymerfibre og løsninger vedrørende fiberkløvning og limning mellem polymer og silikatglas fibre diskuteres. Realiseringen af gitre i polymerfibre demonstreres med to forskellige teknikker: UV-fasemaske teknikken og direkteskrivning teknikken. Fremstilling af gitre i PMMA trinindeksfibre og i mikrostrukturerede fibre lavet af PMMA og TOPAS præsenteres. Gitre er fremstillet til både 1550 nm, for at drage fordel af komponenter lavet til telekommunikation, og til 850 nm, for at udnytte polymerers lavere tab og den hurtigere detektionselektronik ved denne bølgelængde. En teknik til at skrive multipleksede gitre vises og temperaturkompensering af tøjningssensorer ved brug af to tilstødende gitre demonstreres. Ufølsomhed overfor fugtighed i en tøjningssensor baseret på en TOPAS fiber vises også. For at undersøge muligheden for at bruge et viskoelastisk materiale såsom polymer i dynamiske sensorer, er der udført og præsenteret en dynamisk-mekanisk karakterisering af polymerfibre.

De undersøgte og fremstillede Bragg gitre i mikrostrukturerede polymer optiske fibre er blevet brugt til at producere optiske accelerometre. Accelerometrene og deres karakterisering rapporteres. Til sidst

beskrives realiseringen af en optisk mikrofon baseret på polymer fiber Bragg gitre.

Summary of Original Work

This thesis is based on the following journal publications:

Paper 1 A. Stefani, K. Nielsen, H.K. Rasmussen and O. Bang, "Cleaving of TOPAS and PMMA microstructured polymer optical fibers: Core-shift and statistical quality optimization", Optics Communications, vol. 285, pp. 1825-1833 (2012).

Paper 2 W. Yuan, A. Stefani, M. Bache, T. Jacobsen, B. Rose, N. Herholdt-Rasmussen, F.K. Nielsen, S. Andresen, O. Brøsted Sørensen, K. Styhr Hansen and O. Bang, "Improved thermal and strain performance of annealed polymer optical fiber Bragg gratings", Optics Communications, vol. 284(1), pp. 176-182 (2011).

Paper 3 A. Stefani, W. Yuan, C. Markos and O. Bang, "Narrow Bandwidth 850 nm Fiber Bragg Gratings in Few-Mode Polymer Optical Fibers", IEEE Photonics Technology Letters, vol. 23(10), pp. 660-662 (2011).

Paper 4 I.P. Johnson, W.Yuan , A Stefani, K Nielsen, H.K. Rasmussen, L. Khan, D.J. Webb, K. Kalli and O. Bang, "Optical fibre Bragg grating recorded in TOPAS cyclic olefin copolymer", Electronics Letters, vol. 47(4), pp. 271-272 (2011).

Paper 5 W. Yuan, A. Stefani, and O. Bang, "Tunable Polymer Fiber Bragg Grating (FBG) Inscription: Fabrication of Dual-FBG Temperature Compensated Polymer Optical Fiber Strain Sensors", IEEE Photonics Technology Letters, vol. 24(5), pp. 401-403 (2012).

Paper 6 A. Stefani, M. Stecher, G.E. Town and O. Bang, "Direct Writing of Fiber Bragg Grating in Microstructured Polymer Optical Fiber", IEEE Photonics Technology Letters doi: 10.1109/LPT.2012.2197194.

Paper 7 A. Stefani, S. Andresen, W. Yuan and O. Bang, "Dynamic characterization of polymer optical fibres", submitted to IEEE Sensors Journal.

Paper 8 W. Yuan, L. Khan, D.J. Webb, K. Kalli, H.K. Rasmussen, A. Stefani and O. Bang, "Humidity insensitive TOPAS polymer fiber Bragg grating sensor", Optics Express, vol. 19(20), pp. 19731-19739 (2011).

Paper 9 A. Stefani, S. Andresen, W. Yuan, N. Herholdt-Rasmussen, and O. Bang, "High Sensitivity Polymer Optical Fiber Bragg Grating Based Accelerometer", IEEE Photonics Technology Letters, vol. 24(9), pp. 763-765 (2012).

Other scientific reports associated with the project:

1. W. Yuan, A. Stefani, O. Bang, T. Jacobsen, B. Rose, N. Herholdt-Rasmussen, F.K. Nielsen, S. Andresen, O. Brøsted Sørensen and K. Styhr Hansen, "Fiber-optical microphones and accelerometers based on polymer optical fiber Bragg gratings", invited talk, paper 7726-1, SPIE Photonics Europe 2010, April 12th, 2010.

2. W. Yuan, A. Stefani, O. Bang, S. Andresen, F.K. Nielsen, T. Jacobsen, B. Rose and N. Herholdt-Rasmussen, "Fiber-optical Accelerometers Based On Polymer Optical Fiber Bragg Gratings", oral presentation 561, Advanced photonics and renewable energy 2010 optics & photonics congress, June 23th, 2010.

3. G.E. Town, W. Yuan, A. Stefani and O. Bang, "Grating Writing and Growth at 325nm in Non-Hydrogenated Silica Fiber", poster 710, Advanced photonics and renewable energy 2010 optics & photonics congress, June 24th, 2010.

4. W. Yuan, A. Stefani, S. Andresen and O. Bang, "Tensile Strain and Temperature Characterization of FBGs in Preannealed Polymer Optical Fibers", oral presentation 106, OECC conference, July 9th, 2010.

5. A. Stefani, W. Yuan, S. Andresen and O. Bang, "Polymer optical fiber Bragg grating sensors: measuring acceleration", oral presentation 596, 19th Australian Conference on Optical Fibre Technology, December 7th, 2010.

6. I.P. Johnson, D.J. Webb, K. Kalli, W. Yuan, A. Stefani, K. Nielsen, H.K. Rasmussen and O. Bang, "Polymer PCF grating sensor based on poly(methyl methacrylate) and TOPAS cyclic olefin copolymer", SPIE Optics + optoelectronics, April 19th, 2011.

7. W. Yuan, A. Stefani, K. Nielsen, H.K. Rasmussen, D.J. Webb, K. Kalli and O. Bang, "870nm Bragg grating in single mode TOPAS microstructured polymer optical fibre", poster 7753-166, 21st international conference on optical fiber sensors, Ottawa, May 18th, 2011.

8. A. Stefani, W. Yuan, S. Andresen and O. Bang, "Viscoelastic limit of polymer optical fibers: characterization of the dynamic response", oral presentation 81, The 20th international conference on Plastic Optical Fibers, September 14th, 2011.

9. L. Khan, I.P. Johnson, W. Yuan, A. Stefani, K. Nielsen, H.K. Rasmussen, D.J. Webb, K. Kalli and O. Bang, "Humidity sensitivity of TOPAS optical fibre Bragg grating", The 20th international conference on Plastic Optical Fibers, September 15th, 2011.

10. A. Stefani, M. Stecher, G.E. Town and O. Bang, "Fiber design and realization of point-by-point written fiber Bragg gratings in polymer optical fibers", oral presentation, paper 842617-7, SPIE Photonics Europe 2012, April 12th, 2012.

11. "A reason to Bragg", Electronics Letters, vol. 47(4), p. 228, 2011.

Other scientific reports published during the project:

1. M.H. Frosz, K. Nielsen, P. Hlubina, A. Stefani and O. Bang, "Dispersion-engineered and highly-nonlinear microstructured polymer optical fibres", oral presentation 7357-4, SPIE Europe Optics + Optoelectronics 2009, April 22nd, 2009.

2. M.H. Frosz, A. Stefani and O. Bang, "Highly sensitive and simple method for refractive index sensing of liquids in microstructured optical fibers using four-wave mixing", Optics Express, vol. 19, pp. 10471-10484 (2011).

3. M. Stecher, S. Duerrschmidt, K. Nielsen, A. Stefani, H.K. Rasmussen, P.U. Jepsen, G.E. Town, O. Bang and M. Koch, "Mode profiling of THz fibers with dynamic aperture near-field imaging", 36th International Conference on Infrared, Millimeter, and Terahertz Waves, October 4th, 2011.

4. M. Stecher, C. Jansen, M. Ahmadi-Boroujeni, R. Lwin, A. Stefani, M. Koch, and G.E. Town, "Polymeric THz 2D Photonic Crystal Filters Fabricated by Fiber Drawing", submitted to Transactions on Terahertz Science and Technology.

5. M. Stecher, C. Jansen, M. Ahmadi-Boroujeni, R. Lwin, A. Stefani, O. Bang, M. Koch, and G.E. Town, "Fiber Drawn 2D Polymeric Photonic Crystal THz Filters", CLEO 2012.

Contents

Chapter 1

Introduction to the thesis

The recent developments of microstructured polymer optical fibers (mPOFs), after their first fabrication in 2001 [1], and the subsequent success in writing fiber Bragg gratings (FBGs) in this type of fibers [2] have opened new possibilities towards sensor development. Taking advantages of material properties of polymers providing high sensitivity to both strain and temperature, exploiting different behaviours of different polymers in terms of water and biomolecule affinity, together with the advantages of microstructured fibers in terms of dispersion optimization, accessibility to the propagating field and endlessly single mode guidance, microstructured fibers appear to be optimal candidates for Bragg grating sensors. Nevertheless the high material loss of the most commonly used polymers, together with a technology that just started to develop, poses severe problems and limitations to it.

1.1 Main contribution and thesis organization

This work presents the development, realization and characterization of sensors based on microstructured polymer optical fiber Bragg gratings. During the project the design and fabrication of mPOFs in various materials was carried out. Solution to practical issues in handling polymer fibers, such as cleaving and gluing, were also considered. FBG writing

and process optimization in various polymer fibers and with different techniques has been done. Finally the mPOF FBGs have been used as the active sensor device. Basic strain and temperature sensors have been characterized. Moreover the mPOF FBGs have been employed as sensing element in more complex sensor designs for accelerometers and microphones.

The thesis is organized as follows: first, a background introduction on state of the art and basic concepts in polymer fibers, Bragg gratings and fiber sensors is given. The background introduction is followed by a presentation of the work done during the project. The work is presented through the description of the relevant publications produced during the project with the explanation of the connection between them and by additional sections for the description of the unpublished work. Finally conclusions and outlooks are given.

Chapter 2

Background introduction

2.1 Polymer optical fibers

In the history of the development of optical fibers, polymer optical fibers (POF) find their first appearance at the very beginning. In fact already some of the earliest fibers in the '50s were made out of polymers [3]. The need and goal to achieve lower transmission loss pushed silica fibers forward compared to polymer fibers, which have an intrinsically higher loss. In fact for silica fibers the limiting factors are Rayleigh scattering at short wavelengths (UV and visible), impurities and absorption due to water vibrational levels at long wavelengths (visible and near infrared). The loss mechanisms in optical fibers are listed in Table 2.1. For polymer fibers the absorption bands given by the C-H vibrational levels limit transmission in the long-wavelength ($> 800\ nm$) region. Towards shorter wavelengths the C-H absorption diminishes, but the Rayleigh scattering increases (proportional to λ^{-4}) creating a region of minimum loss around 550 nm. Since carbon-hydrogen bonds are basic constituents of polymers, overcoming the limit of the absorption given by their presence in the material seems to be impossible. A way to solve the problem is by substituting the hydrogen atoms with heavier elements. A heavier constituent will shift the excitation of vibrations towards higher wavelengths, reducing the loss and increasing the usable range of wavelengths. Both deuterium [4] and fluorine [5] have been

Type of mechanism	Mechanism	Origin
Intrinsic	Absorption	Vibration modes Electronic transitions
	Rayleigh scattering	Density fluctuations Orientation fluctuations Composition fluctuations
Extrinsic	Absorption	Organic pollutants Dust
	Scattering	Micro-fractures Bubbles
	Out-coupling loss	Micro and macro bends

Table 2.1: Loss mechanisms in optical fibers as outlined in Ref. [7].

used for substitution of hydrogen. However the production of such materials is not trivial, it's expensive and, in the case of fluorine, creates hydrofluoric acid as a by-product, which complicates the safety of the manufacturing process. For these reasons, and for the difficulties in purchasing them, these materials are not the most used for fabrication of polymer optical fibers. In fact, fibers made of poly(methyl methacrylate) (PMMA) are more widely used [3]. In Fig. 2.1 a comparison of loss of silica fibers, PMMA fibers and fibers made with a fluorinated polymer (CYTOP) is shown. The lowest loss measured in a polymer fiber is about 10 dB/km around 1100 nm in a graded index fiber made with CYTOP [5]. The theoretically predicted minimum loss is 0.3 dB/km at 1300 nm [6] and is almost two orders of magnitude lower than what has been experimentally achieved. This value is close to the loss of silica fibers and would change completely the perspectives on polymer fibers if achieved.

Two processes can be used for fabrication of polymer optical fibers: drawing from a solid preform or directly from liquid (which could be unpolymerized material or the polymer in a melt state). The first is also the one more commonly used for silica fibers and the fiber guiding properties are determined when producing the preform. The desired

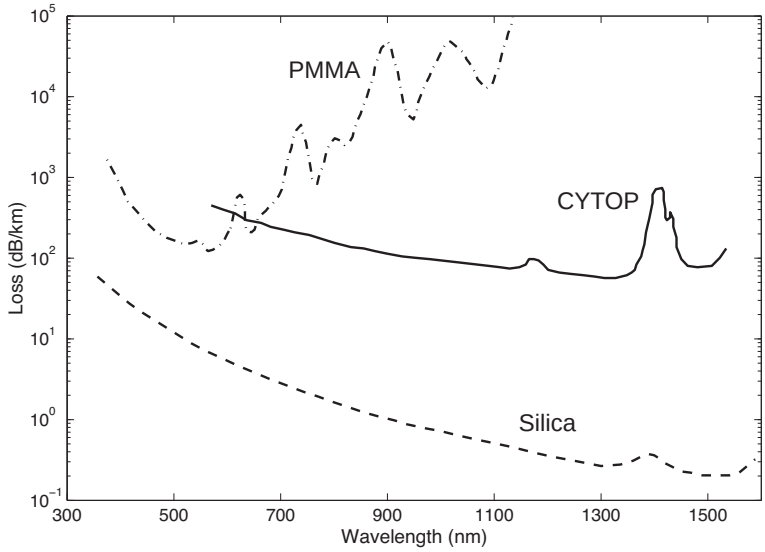

Figure 2.1: Transmission loss of fibers made of silica, PMMA and CYTOP fluorinated polymer, as in Murofushi *et al.* [8].

refractive index profile in a preform for all-solid POF has been realized by centrifuging during polymerization, by interfacial gel polymerization, by using dopants (usually dyes) or by using different polymers with similar mechanical properties [3]. The latter is the easiest and more used technique. It produces step-index fibers with a high refractive index difference. This factor strongly influence the acceptance and confinement properties of the fiber. For a step index fiber the numerical aperture (NA) is determined by the difference between the refractive index of the core (n_{core}) and that of the cladding ($n_{cladding}$):

$$NA = \sqrt{n_{core}^2 - n_{cladding}^2}. \tag{2.1}$$

The numerical aperture together with the dimension of the core determines the guiding properties of the fibers. Directly related to the NA is the V parameter (normalized frequency), which is strictly connected

to the number of modes propagating in the fiber, and it's given by:

$$V = \frac{2\pi a}{\lambda} NA, \tag{2.2}$$

where a is the fiber core radius and λ is the free space wavelength. Both high NA (high refractive index difference) and a large core would be preferred in the manufacturing process. The first because it's more controllable, the second because it reduces the loss due to scattering at the interfaces. The drawback is that both factors contribute to make the fiber multi mode (the single mode behaviour is achieved for $V < 2.405$). Working against the single mode operation is also the wavelength. Due to the lower loss region, it would be better to work at lower wavelengths, which again increases the normalized frequency and poses even more strict geometrical and manufactural limits when single mode behaviour is required.

Single mode behaviour is anyway not always required. In fact, there is a big interest towards low loss highly multimode polymer fibers for short range communications, where the need for lower costs compensates for the lower data transmission capability. These fibers are generally thick (from 0.5 to 1 mm) and have a graded index core profile. However, communications is not the only field of interest for polymer optical fibers.

There have been several reasons for keeping the interest in polymer optical fibers even after silica fibers have improved and the difference in loss between the two reached a practically unbridgeable difference. The two most important reasons are the lower cost of production and the higher flexibility of the material itself compared to silica. Other material properties that make polymer appealing are: the lower density that makes it lighter than glass; the higher elasticity, quantified in a lower Young's modulus (3 GPa compared to 72 GPa of silica); the higher elastic limit (maximum 10% strain compared to 1% in silica); and the higher thermal expansion and thermo-optic coefficients [3].

With these characteristics polymer fibers find applications as the basis for sensors, where the material advantages can be exploited even when the fiber has high loss. Moreover, sensor performance can be

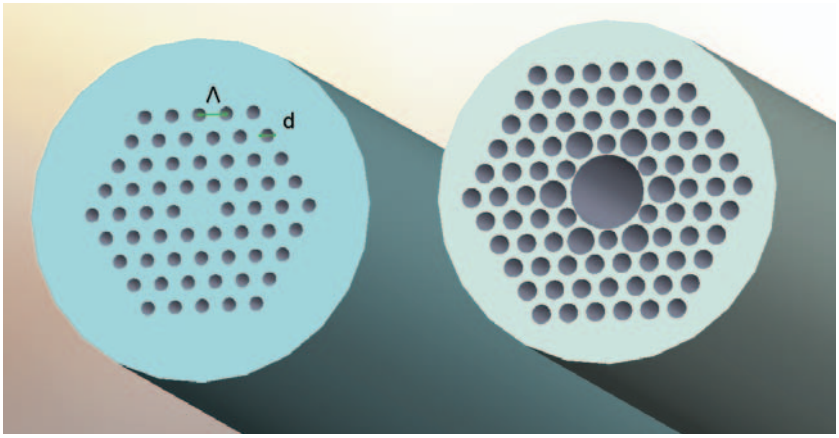

Figure 2.2: Schematic representation of a solid core photonic crystal fiber (left) and of a hollow core bandgap fiber (right). In the figure, d is the hole diameter and Λ is the hole to hole distance (pitch).

improved by modifying the fiber through functionalizing the cladding, by increasing the evanescent field with a tapered section, by inscribing long period gratings (LPGs) and FBGs. Further improvement could be achieved by single mode behaviour and by introducing a microstructure in the fiber [3, 9].

2.1.1 Microstructured polymer optical fibers

Microstructured optical fibers (also called photonic crystal fibers, PCFs) have been first demonstrated in silica in 1996 by Knight *et al.* [10]. They can be roughly divided in two classes based on the guiding principle: those that guide using total internal reflection and those where confinement is due to the absence of a solution to Maxwell's equations for the electromagnetic field in the cladding (a so called photonic bandgap). An example of each type of fiber is shown in Fig. 2.2. Major advantages given by the photonic crystal structure are the possibility to control/tailor the dispersion, and the exceptional endlessly single mode guiding principle [11]. This not only means that the same fiber can be

used for single-mode guidance over a broad range of wavelengths, but also that the dimensional restrictions required for single mode guiding at low wavelengths are relaxed.

In this dissertation only microstructured fibers guiding by total internal reflection are considered. In these fibers the microstructure acts as a mechanical "doping" of the cladding, which effectively reduces the cladding refractive index. In a microstructure with holes organized in a hexagonal lattice the endlessly single mode guiding is obtained with the ratio between the hole diameter, d, and the pitch (hole to hole distance), Λ, being: $d/\Lambda < 0.42$ independently from the fiber material [11]. Fig. 2.3 shows the guiding regime depending on the hole to pitch ratio and the wavelength to pitch ratio [12].

Microstructured fibers have not only been made with silica, but also in other materials, like soft glasses [13] and polymers. In 2001 van Eijkelenborg *et al.* [1] reported the first fabrication of a microstructured polymer optical fiber. The preform for an mPOF can both be a stack of tubes (as in the case of silica PCFs) or it can be a bulk cylinder of plastic in which the hole-pattern is extruded, casted or drilled [3]. This particular feature gives the possibility of obtaining any kind of hole-pattern, enabling the development of specific fibers for each application. Many different microstructure designs have been developed and used up to now. The most used is a uniform hexagonal structure with equally spaced holes, all with the same dimension (as in Fig. 2.2). A different number of rings has been used depending on the final application. More rings decrease the confinement loss, but reduce for example the accessibility to the core from the side. Some other mPOF structures fabricated until now are: graded index mPOF (GImPOF) [14, 15], hollow core mPOF (HCmPOF) [15, 16], high birefringence fibers [15, 17], rectangular core [15], twin cores [15], multi core [18], suspended core [19,20] and randomly microstructured [21]. The use of dopants as dyes has also been shown [18,22]. As for POFs different materials have been used for mPOFs: polycarbonate (PC) [23], TOPAS [19, 20], biodegradable materials [24] and the most commonly used PMMA [3].

Microstructured polymer fibers have not only been used for optical wavelengths but also as waveguides for THz radiation [25, 26].

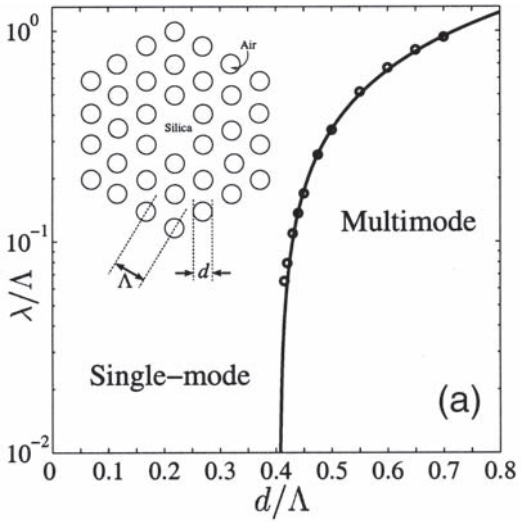

Figure 2.3: Single-mode–multimode phase diagram, as in Mortensen *et al.* [12].

Aside from the loss, the practical use of polymer optical fibers, and particularly of thin microstructured fibers, is reduced by the difficulties in handling these fibers. For example cleaving is a quite relevant issue. The hot blade technique has been found to have the best results [27], but, even if the knowledge is there, many current and potential users find themselves fighting to have good cleaving results. Another issue is connectorization and bonding with standard components made of silica.

2.2 Fiber Bragg gratings

Fiber Bragg gratings consist of a modulation of the refractive index of the fiber along the propagation axis. Each refractive index variation produces a reflection of the propagating radiation. If the modulation and the wavelength are so that all the reflected components interfere

constructively a mirror for specific wavelengths is created (Fig. 2.4). The constituent relation for a homogeneous grating (with a constant periodical index modulation) is:

$$\lambda_B = 2n_{eff}\Lambda \tag{2.3}$$

where λ_B is the reflected Bragg wavelength, n_{eff} is the effective refractive index and Λ is the period of the refractive index modulation.

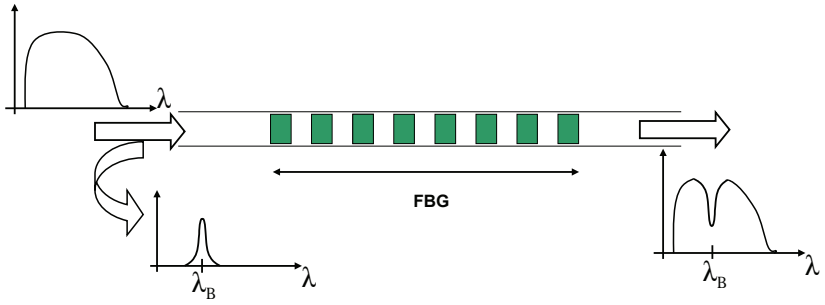

Figure 2.4: Fiber Brag grating working principle.

What mainly influenced the interest and ability of writing gratings into fibers is the photosensitivity of the material to UV light. This was discovered in 1978 by Hill *et al.* [28], but even though the impact of the discovery was immediately understood, it took about a decade before it was put into practical use [29]. The photosensitivity of the fibers can be enhanced with various techniques, but the standard procedures are the increase of the amount of Germanium (and other dopants) content in the core and hydrogen loading of the fibers before exposure [29]. The technique that is commonly used for grating inscription is the phase mask technique, which uses UV light radiation for exposure. Interferometric techniques are also often used in order to have more flexibility on the resulting grating wavelength [30]. A third technique, that as well allows flexibility in the determination of the profile of the refractive index change and does not require photosensitivity since it is based on a two photon absorption process, is the point by point writing technique [31].

Various types of gratings [30] and many refractive index modulation profiles can be obtained and are used nowadays [29, 32].

Fiber Bragg gratings have been written also in microstructured fibers [33]. The grating is written by illuminating the fiber with light coming from the side, but the light is diffracted due to the microstructure, which complicates the writing process [34]. Nevertheless the photosensitivity of silica fibers and the use of techniques, as hydrogen loading and doping of the core, to enhance the photosensitivity are sufficient to compensate for it.

Fiber Bragg gratings find applications as filters, mode converters, laser mirrors, chromatic dispersion compensators and sensors [29, 32].

2.2.1 Fiber Bragg gratings in polymer optical fibers

Photosensitivity of polymers was first reported by Tomlinson *et al.* in 1970 [35]. The refractive index change was induced by irradiation with 325 nm UV light produced with a HeCd laser. Despite this early discovery, the first report of Bragg gratings in polymer optical fibers dates to 1999 [36]. The physical mechanism behind polymer photosensitivity has been the cause of discussions and speculations. In fact, starting from the work of Tomlinson *et al.* it was supposed that the increase in refractive index could have been caused by extra cross-linking and polymerization due to the UV light exposure. A detailed study on UV light effect on PMMA has been done and it well explains the processes involved in refractive index modification [37]. However, this study explains the consequences of material-light interaction limited to short irradiation wavelengths (193 nm and 248 nm). It also reports about the use of 308 nm as exposure wavelength, but with this wavelength no refractive index change was documented. Most of the reported FBGs in polymer fibers were written with exposure at 325 nm. It should be considered that the material preparation and composition and the fiber fabrication process might change the fiber properties, leading to uncertainties in the interpretations of the results. It is indeed widely accepted that the refractive index change is given by the polymerization of the unreacted monomers, see, e.g., Ref. [38] and references therein.

As with silica fibers, Bragg gratings have been demonstrated in polymer fibers of both the solid type and microstructured type [2]. In the latter, the fiber is made of only one material, so some of the factors that can change from experiment to experiment are eliminated. The reported gratings have been inscribed using HeCd continuous wave (CW) UV radiation at 325 nm wavelength with 30 mW power. The inscription times for mPOFs are on the order of several tens of minutes to hours [7]. In order to reduce the writing times or increase the grating strength the use of dopants or co-polymers in the core was successfully reported [39–41].

Typical applications of Bragg gratings in polymer optical fibers are: tunable filters [38], laser mirrors [42] and sensors. Various Bragg wavelengths have been written up to now in polymer fibers, going from the wavelength where there are commercially available cheap components: 1550 nm [2]; to lower wavelengths where the losses of polymer fibers are lower: 927 nm [43], 827 nm [44].

2.3 Optical fiber sensors

The development of fiber optics has been mostly driven by the telecommunication sector. At the same time, optoelectronics has quickly improved both related to optic communications and as a self sustained sector (e.g. with the development of displays, disc players, etc.). The fiber sensor industry has taken advantage of these two factors. Because of the high costs of the components, fiber optic sensors have tried at first to fill the gaps left open by other types of sensors, more than competing with them. As the costs reduce over time, the advantages of optical fibers sensors over conventional ones make them suitable also to cover other market areas and consequently the research driving them forward is intensified. The main advantages of fiber optic sensors are their light weight, high sensitivity, high bandwidth and environmental ruggedness. The big interest in the field is also given by the ability of fiber sensors to cover a wide range of applications. In fact they can be used to sense rotation, acceleration, electric and magnetic field, temperature, pressure, sound, vibrations, position, strain, humidity, viscosity,

chemical and biological agents, and many other sensor applications [45].

Fiber sensors use many different configurations, working principles and materials. They can be all-fiber or integrated with components of different nature, detect based on amplitude variations, polarization or spectral detection, be configured as interferometers, be multiplexed, localized or distributed, embedded, and they can be made with fibers of different materials (e.g. silica or polymer) [45].

2.3.1 Polymer optical fiber sensors

More than any other field, the field of optical fiber sensors exploits the material properties of polymers, rather than just their reduced cost compared to other materials. The automotive sector is probably the major user of polymer fiber based sensors, but it is not the only one. POF sensors have been demonstrated and used for numerous applications. As already mentioned the thick multimode polymer fibers are the most used, for their easy handling properties. They find many applications also in the sensors field ranging from stress, temperature, humidity, chemical sensors to wind speed sensors and so on [9, 46, 47]. Works on single mode POF have also been reported for strain sensing [48, 49], temperature sensing [50] and for ultrasound sensors [51, 52]. All are reported in an interferometric configuration. Also Bragg grating POF sensor have been developed and will be discussed later on, in section 2.3.3.

Microstructured polymer optical fiber sensors

Two main advantages lead the development of mPOF sensors: the possibility of having a single mode fiber and the accessibility to the evanescent field in the microstructure. The first is mainly used for fiber Bragg grating based sensors. Sensors not based on Bragg gratings usually do not need the fiber to be single mode. MPOFs sensors for: gas detection [53, 54], aqueous solutions analysis [55, 56], pH determination [57], Raman spectroscopy [58], biosensing [19, 20, 59], hydrostatic pressure and temperature measurements [17, 60]; were reported. Some of the

working principles are evanescent field [61], plasmonic resonances [62], fluorescence [19, 20, 59], and change in birefringence [17, 60].

Taking advantage of the possibility of having single mode fibers, grating based sensors find numerous applications when based on microstructured polymer optical fibers. A first category is long period grating sensors. This type of sensors benefit of the possibility of tailoring the dispersion of microstructured fibers, to which the sensitivity is related [63]. Moreover the possibility of infiltrating the holes with liquids and gases influences the mode propagation both in the core and in the cladding, giving several parameters that can be optimized for specific applications. Long period grating sensors in mPOFs were demonstrated for strain sensing [64, 65], to be sensitive to water content and surrounding medium refractive index [66, 67], to humidity and temperature [68].

2.3.2 Fiber Bragg grating sensors

One class of fiber sensor which is widely used and which allows detection of a large number of parameters is fiber Bragg grating sensors. Bragg grating sensors provide localized sensing, but through the possibility of being multiplexed, which is one of their strongest advantages, they can also provide quasi-distributed measurements. The sensing principle consists in the detection of a shift of the Bragg wavelength. The shift imposed could be due to a modification of the grating physical properties (such as length) or of the effective refractive index experienced by the radiation. Given these considerations, the use of Bragg gratings finds applications for mechanical and environmental parameter measurement. What is considered the most important use of FBGs sensors is the creation of so called “smart structures”. Embedded in various materials, multiplexed and able to detect various parameters, they produce a network of sensors which gives full information of structures such as buildings, roads, bridges and dams. Such a network would give more information on the history and status of the structure under examination, making possible immediate repairs, but also reducing costs and improving safety preventing structural damages and collapses [45]. The

same principle of smart structures can also be applied in sectors different from structural engineering, e.g. healthcare monitoring [69]. FBG based sensors have been demonstrated for strain, temperature, pressure, acceleration, vibrations, electric and magnetic field and chemicals detection [32, 45, 70, 71].

When compared to other kinds of sensors FBG based sensors have the advantages of multiplexing possibilities, of being small and compact, inexpensive, insensitive to optical power fluctuations and with direct relation between what is measured and what one wants to quantify.

Although the fibre gratings are themselves inexpensive and easy to produce, the systems for monitoring the grating are often expensive and complicated. Different ways to monitor FBGs have been proposed, but in general a broadband light source and a wavelength detection system is used. A second disadvantage of FBG sensors is the simultaneous dependence of the grating on more than one parameter at the same time. Typically the influence of temperature needs to be removed for detection of other parameters which have the same time scale of temperature variation (e.g. quasi-static strain). Also for this purpose many configurations have been proposed. The most common implies the use of an extra reference grating [72]. Adding one extra grating consequently increases the complexity of the system.

Also Bragg gratings in microstructured optical fibers have been widely used as a base for sensors. Having the same basic characteristics of solid fibers, but also having the advantages of tailored dispersion and accessibility to the optical field, sensors based on this kind of fibers can cover all the previous applications and find some new ones in the fields of gas and liquids detection and composition determination [30].

2.3.3 Polymer optical fiber Bragg grating sensors

The same way as for silica fiber Bragg gratings, polymer fiber Bragg gratings can be used as base for sensors, cover the same range of applications while taking advantage from the material, and encounter the same systemic problems. Solid POF FBGs have been reported for strain, bend, temperature and humidity detection [73–75].

In structures with low Young's modulus (as for example textiles) it is possible to see an advantage of using FBG sensors based on polymer fibers instead of those based on silica fibers. In fact, the silica fiber would affect the structure itself by stiffening it [76].

2.4 Microstructured polymer optical fiber Bragg grating sensors

MPOFs are very interesting for Bragg grating based sensors because they combine the advantages of POF FBG sensors with the advantages given by the microstructure, in particular the endlessly single mode guidance. Given the only recent ability of writing gratings in microstructured polymer fibers and the handling problems with them, only a limited amount of publications on sensing applications of the mPOF FBG can be found despite the numerous potential applications. In fact, the only demonstration of applicability of mPOF FBG for a sensor previous to this work was reported by Carrol *et al.* [77].

Chapter 3

Thesis contributions

This dissertation is based on journal publications that have been produced during the doctorate. Contributions to the entire process that leads to the realization and characterization of a sensor were reported. This chapter reports a description of the main results and contextualization of the papers and of some unpublished results.

3.1 Polymer optical fibers fabrication

DTU Fotonik has one of the few university based polymer fiber drawing towers in Europe. The possibility of utilizing this facility has been of utmost importance to this project. Fiber fabrication has a fundamental role towards the realization of fiber components and sensors, even if it is not always possible to see it directly from the publications.

3.1.1 The drawing tower

A picture of the drawing tower and a schematic of the main components are shown in Fig. 3.1. Fibers are drawn in a two step process. In the first step a preform generally of 6 cm of diameter and 8 to 10 cm length, in which the desired structure is contained (Fig. 3.2) is drawn to a 4 to 6 mm diameter fiber, termed a "cane". At this stage the fiber has the correct dimensions for waveguiding THz radiation [25]. The cane is

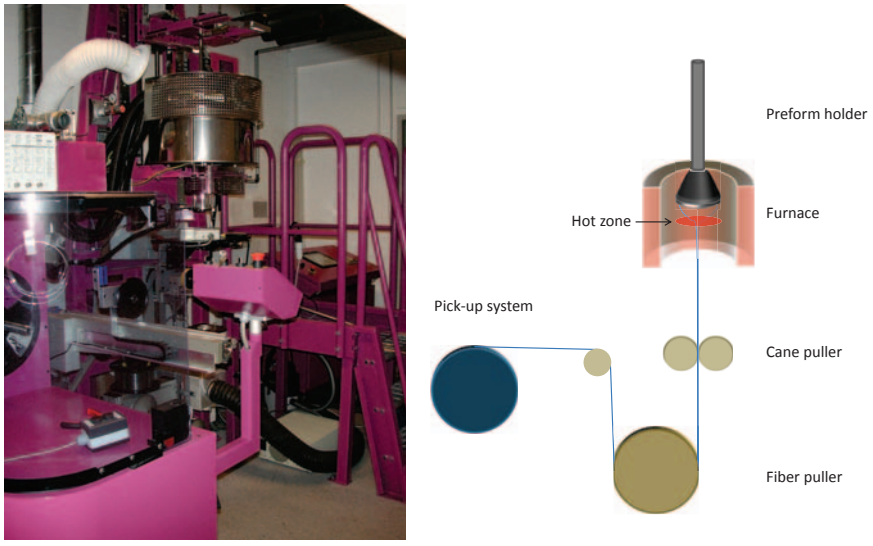

Figure 3.1: DTU Fotonik drawing tower (left) and schematic of the tower main components (right).

sleeved with tubes to create a secondary preform. The outer diameter of the secondary preform depends on the primary preform design, on the cane diameter and on the desired fiber diameter. It is usually between 10 and 40 mm. The secondary preform is then drawn to fiber. The preform is placed in the furnace, where it softens and the bottom part slowly drops out of the furnace due to gravity. The fiber is then pulled with either the cane puller, if the primary preform is drawn, or with the fiber puller, if the secondary preform is drawn. The preform is lowered in the oven during drawing. The feeding speed and the pulling speed determine the final diameter following mass conservation (this is the ideal case in which the neck down area is in a fixed position in the furnace). In the second drawing stage the fiber is collected and spooled with a pick up system.

3.1.2 Fiber design

The structures to be drawn have been designed with the support of numerical simulations. To simulate the guiding properties, such as number of modes, birefringence and guiding loss, a finite element method implemented in the commercial software COMSOL was used. To evaluate confinement loss, the software *Fibre*, part of the package *CUDOS MOF Utilities* [78], which uses a multipole method, was also used.

3.1.3 Preform preparation

The technique used to produce the primary preform is based on drilling holes in a rod of solid material. An example of preforms is shown in Fig. 3.2. The drilling is made by a computer numerically controlled (CNC) drilling machine. This allows the realization of any hole pattern with high precision and repeatability. Due to bending of the drill bit small holes (<2 mm) cannot be drilled sufficiently deep into the preform. For this reason holes with diameter bigger than 2 mm are usually made. The fabrication of a preform is the first step to the production of a fiber. Even seemingly small changes to the procedure at this stage are important to reduce the causes of optical loss in the fiber. Water assisted drilling and the use of different drilling bits are some of the major improvements on this matter that this project benefitted from. Although optical losses are of course very important for any application of an optical fiber, the current losses are not preventing the application of mPOFs for Bragg gratings, especially because of the short length of fiber needed; the loss reduction approaches are therefore not considered in more detail here.

3.1.4 Drawing parameters

The critical parameters during polymer fiber drawing are temperature, tension, feeding speed and pulling speed. An in-depth analysis of these parameters is outside the scope of this dissertation, but they affect the final properties of the fiber and consequently of the sensor. One of them is particulary important and deserves to be mentioned: the fiber ten-

Figure 3.2: Example of PMMA and TOPAS preforms.

sion. Tension is not an active parameter, because it can't be changed directly, but depends on the other parameters and can therefore be indirectly controlled. Tension during drawing determines the alignment of the polymer chains and frozen-in stress. A fiber drawn with high tension has mechanical properties different from one drawn with low tension [7]. The performance of the sensor is therefore indirectly determined by the tension under which the fiber was drawn. A fiber drawn with high tension can be taken to a low stress status through annealing. Annealing is further discussed in section 3.3.1.

3.1.5 Fiber characterization

After drawing, characterization of the fibers is necessary. Apart from the basic visual investigation of the microstructure cross-section in a microscope, to verify that the air-holes have the desired diameter and spacing, the fibers have been characterized for their guiding properties. A first test is made by coupling light into the fiber to verify that

it actually guides. In a second stage cut-back loss measurements are performed to determine the fiber total loss. Loss measurements are reported in **Paper 3**. In particular cases mechanical tests of the fibers are performed, but this will be further discussed in section 3.4.

3.2 Handling of polymer optical fibers

One of the main problems when working with polymer optical fibers is cleaving. The importance of this procedure is that it reflects on any successive result, up to the point of compromising them, nullifying any other technological effort. Various techniques have been proposed and investigated [27, 79, 80]. The technique found to be the most efficient and easiest to use is the hot blade technique. Due to material transition from brittle to ductile, both the fiber and the blade need to be heated to a certain temperature to obtain an optimum cleave [27]. However temperature is not the only parameter to be considered. Moreover the optimum parameters vary from material to material. In **Paper 1** an investigation and optimization on cleaving is made for fibers made of the commonly used POF material, PMMA, and for the first time for fibers made of the cyclic olefin copolymer TOPAS. Supporting the paper and the importance of this process for the entire project an automated cleaver was built. Other than the first time investigation of the hot blade technique for TOPAS fibers, the paper differs from previous contributions by doing a graphical quality analysis of the cleaved fiber end-facet based on an image recognition software in order to identify and reduce the cleaving induced deformation. Particularly important is the identification of the shift of the core, which creates a bend in the initial part of the fiber, and causes coupling loss. In the optimization process the dependence of the quality on the blade thickness is investigated for the first time, resulting in the best result for the thinnest blade available with a flat edge on one side. Investigation on blade and fiber temperature showed that the optimum temperature of both blade and fiber for cleaving PMMA fibers is 77.5 °C, which is in agreement with what is previously reported, and 40 °C for TOPAS fibers. Another relevant result from a practical point of view is the reduced time

needed for cleaving. It was found that only a few seconds are necessary for the whole cleaving process in order to obtain high quality cleaves for thin mPOFs. From a practical point of view the short cleaving time, together with the automation of the process, which increased the reliability of the cleaves to the point of almost not having any bad cleave, gave an important contribution towards the expansion of the polymer fibers field.

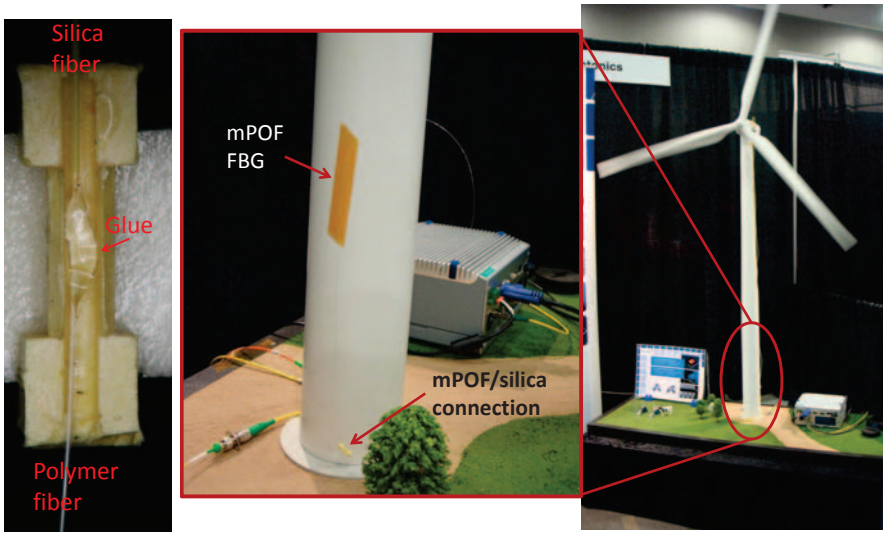

(a) (b)

Figure 3.3: Glued polymer to silica fiber connection on the mechanical support used to strengthen the connection (a) and mPOF FBG installed on a wind mill model in the OFS21 Exhibition in Ottawa to show vibrations detection (b).

A second handling issue that has been investigated is connection of polymer fibers to silica fibers. Splicing has been tried unsuccessfully in collaboration with a group from the National Institute of Telecommunications in Warsaw. The technique that showed the best results is gluing. There are two requirements for the connection: low loss and mechanical stability. In order to satisfy these parameters a two step

gluing process was used. At first, an optical glue with refractive index matching to that of the polymer fiber (*Norland* NOA 78) was used. After alignment the glue was cured. For solid POF the process did not induce significant extra loss compared to just butt-coupling the two fibers and in some cases it actually reduced them. For microstructured fibers the glue infiltrates in the air holes reducing the guiding in the initial section of the fiber, creating extra loss. To reduce this problem a glue with refractive index matching that of silica fibers and with high viscosity has been custom ordered (*My Polymers* MY-145V2000). Unfortunately it hasn't been possible to test this glue yet. Once the optical "bonding" is ensured (with curing the optical glue), the mechanical stability of the bonding has to be checked. The optical glue provides enough mechanical strength for leaving the fibers free standing, but not for moving the fibers around. In order to improve the mechanical strength a second UV curable glue (*Epotek* OG116-31) was applied. This glue does not have good optical properties, but creates a very strong mechanical bond. The strength of the bonding given by the glue was sufficient to carry the fibers around in the lab, but to give extra stability the bonding region has been included in a rigid plastic support. The result is shown in Fig. 3.3 (a). The fiber was taken to Ottawa, where it was installed at the OFS 21 Exhibition in the stand of *Ibsen Photonics A/S*, where the grating was used to show vibration measurements on a wind mill model (Fig. 3.3 (b)). No impact on the grating performance in both transportation and installation was found.

3.3 Polymer optical fiber Bragg gratings writing

Two different techniques for grating writing have been successfully investigated during the project: phase mask UV writing and direct (or point-by-point) IR femtosecond writing. The first technique was already demonstrated for microstructured polymer optical fibers [2], while the second was never used for polymer fibers and only described once for microstructured silica fibers [81]. Other than the implementation of

a grating writing facility and optimization of the process, the work described here involved different fibers, made of different materials, different Bragg wavelengths and grating multiplexing.

3.3.1 Phase mask technique

The system implemented for UV phase mask writing has the same configuration as described in Ref. [2]. The writing technique is mainly presented in **Paper 2**, but also in **Paper 3-5, 8-9**. The set-up used is shown in Fig. 3.4.

The UV light beam from a HeCd laser with emission at 325 nm is first expanded in one direction with a cylindrical lens creating a line beam. The beam is redirected with a periscope and then focused, in the short axis, with a second cylindrical lens. In this way the beam is focused in the core of the fiber. The phase mask is placed in the beam path right on top of the fiber.

Gratings in solid polymer optical fibers

At first gratings have been written in commercial step index polymer optical fibers and with a Bragg wavelength around 1550 nm. Avoiding the microstructure simplifies the writing, since the extra factor of scattering due to the holes is not there. The wavelength choice has been made because of the availability of optical components, because of the possibility of having a better phase mask (the shorter the period, the phase mask becomes more expensive and has lower efficiency towards the ± 1 diffraction orders) and because of the fiber being single mode at this wavelength and not at lower wavelengths. The ability of writing gratings in polymer optical fibers was the first step towards the implementation of working sensors.

Effect of annealing the fibers

Since one of the final goals of the project was to build strain based sensors and to characterize the performance, a first study on how to

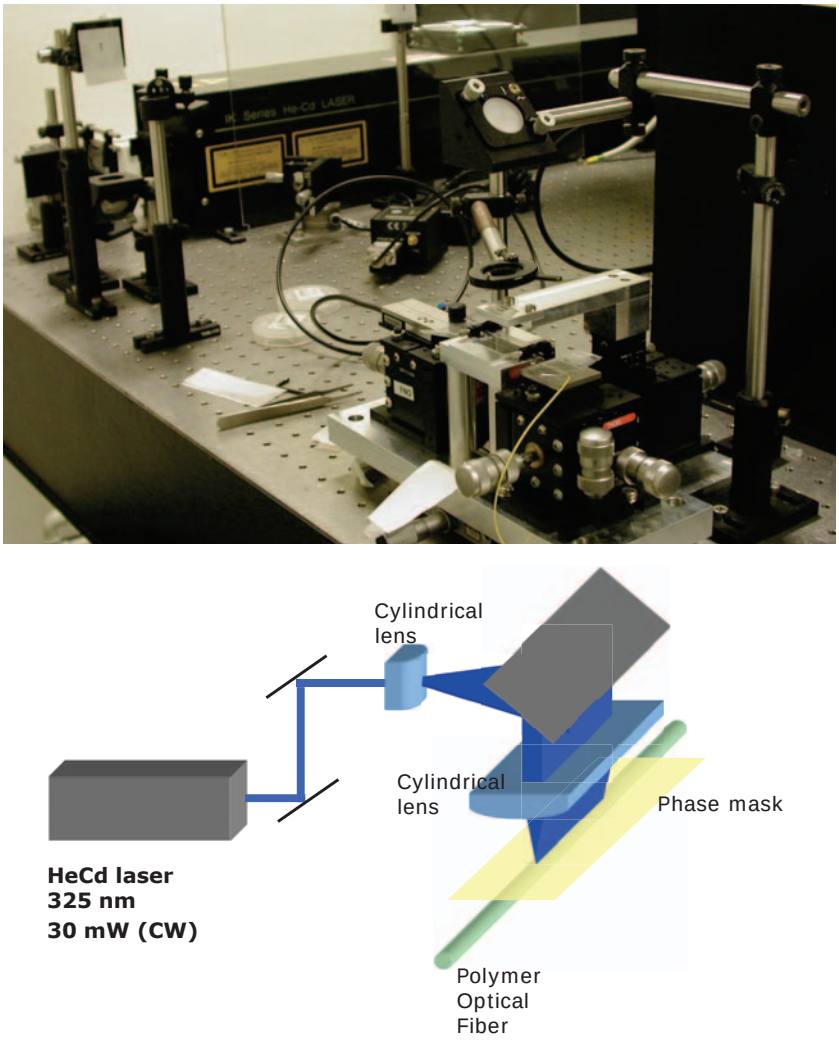

Figure 3.4: UV phase mask writing set-up, picture (top) and schematic (bottom).

improve such performances was done. In **Paper 2** it is shown how annealing affects and in particular improves the performance of the grat-

ings in terms of strain and temperature dependence. The annealing process consists in placing the fiber in the oven at 80 °C for two days. It was found that annealing expanded the linear temperature working range by almost 15 °C (from 60 to 75) and improved strain performance (linear response without hysteresis) from less than 3% to almost 7%. The improved performance and the confirmed linear dependence of wavelength shift on both temperature and strain, demonstrated this POF FBG to be suitable for sensing applications. The characterization of the gratings resulted in measurements of a temperature sensitivity of about $-100\ pm/\,^{\circ}\mathrm{C}$ and of a strain sensitivity of $1.13\ pm/\mu\varepsilon$.

Gratings in PMMA microstructured polymer optical fibers

The commercial step index POF has a very high loss, especially in the 1550 nm region. In order to improve the possibilities and the performance, together with exploiting the fiber drawing facility, grating writing in microstructured fibers was done. Gratings were written first in PMMA mPOFs with a Bragg wavelength around 1550 nm. Some results (mostly in terms of strain sensitivity) using PMMA mPOF gratings at 1550 nm are presented in **Paper 3** and **Paper 8**.

Grating writing at 850 nm

In order to work in a lower loss region and with the advantages of using the electronics window, where fast detectors are available, work was also done on producing gratings at 850 nm. A previous result of grating inscription at this wavelength used a large core multi mode mPOF in order to facilitate the writing. The use of a multi mode fiber leads to a broad reflection spectrum [44]. **Paper 3** presents the results about inscription of gratings in this wavelength window both in POF and mPOFs. The few-mode characteristic of the fibers leads to a narrow grating, more suitable and important for sensing applications. The paper also presents a comparison of strain sensitivities between gratings with wavelengths of 1550 nm and 850 nm. This is relevant when the gratings are intended for strain/elongation based sensors because the choice of a shorter wavelength reduces the FBG strain sensitivity.

Gratings in TOPAS microstructured polymer optical fibers

PMMA has high water affinity. This can be an advantage or a disadvantage depending on the application. If the interest is towards the use of the fiber for a sensor which benefits of water affinity, PMMA is the perfect candidate. If instead water affinity is undesired, as for example in the case of a sensor working in an environment with varying humidity, a material with low water affinity would be desired. For this reason and for the interest in using it also for biosensors, the possibility of writing grating in TOPAS mPOF was also investigated. **Paper 4** reports about grating writing in these fibers. The grating reported here was written with a wavelength of 1568 nm. Subsequently gratings with wavelengths around 850 nm were also written in TOPAS fibers and they were used for the results in **Paper 8**.

Grating multiplexing

The demonstration of multiplexing possibility of mPOF FBGs is shown in **Paper 5**. Multiplexing of FBGs in mPOFs was already shown before [82], but with a different technique. In fact the technique used is an important point presented in the paper. The final grating wavelength was accurately controlled by writing on the fiber in an elongated state. This technique provides the possibility of writing gratings with various well defined wavelengths with a "rigid" technique like the phase mask technique. Moreover the material properties make possible a tunability of the inscribed wavelength as high as 12 nm.

3.3.2 Direct writing technique

Next to the more conventional and commonly used UV phase mask technique, a second approach for grating writing has been investigated. **Paper 6** describes the realization of a Bragg grating in a microstructured polymer optical fiber using direct writing. Direct writing allows more flexibility compared to the phase mask technique in Bragg wavelength and grating profile design. There are also some problems and limitations connected to this technique. The main problem is that, hav-

ing a two-photon absorption process involved, there is a need of high intensity in the core. This factor is limited by the presence of the microstructure and by the material absorption. Not much was possible to be done about the material, while a fiber with a special structure was designed and fabricated in order to create a "scattering free" corridor to the incoming light. This structure together with the optimization of the laser parameters made possible the inscription of a 4th order grating with resonance wavelength around 1520 nm. There are other issues related to this technique, which don't make direct writing look like a valid alternative to phase mask writing. The limitation given by the writing laser spot size requires that high order gratings are written, reducing the efficiency and the ability of writing short wavelength gratings. Another issue is related to the light confinement given by the fiber specially designed microstructure. On the other side this technique gives a huge reduction in grating writing time from minutes or hours, to seconds. One more advantage related to this technique is that it doesn't require photosensitivity. Photosensitivity is an issue for, e.g., perfluorinated fibers. Photosensitivity has been show in the fiber material [83], but no Bragg grating writing has been reported yet in these fibers. In addition these fibers present low loss at 1550 nm not requiring short wavelength gratings.

3.4 Mechanical characterization of polymer optical fibers

One of the intended applications of the polymer fiber Bragg gratings is for sensors such as accelerometers and microphones, where it is required to detect dynamic variations of the parameters to be measured. The viscoelastic nature of polymers limits the possibilities in terms of frequency and strain that can be used. For this reason a characterization of the dynamic mechanical properties of the fibers was done. **Paper 7** reports on the dynamical analysis of polymer fibers in the low strain regime. The choice is related to the potential applications, which do not require large elongations. In the paper a quasi-elastic behaviour,

meaning a frequency independent Young's modulus, is found for low strains and for the investigated range of frequencies (10 to 100 Hz). A closer investigation of the temporal response shows that viscoelastic effects increase with strain and with frequency as expected. It was observed that, when a sinusoidal excitation is applied, the response is a slightly distorted wave which contains high harmonic components. The number and amplitude of these components increase with frequency and strain. These implications are to be kept in mind when designing a sensor working in dynamic conditions. The paper also reports on the stress-relaxation time of the fiber to a constant strain. Time constants of about 5 and 6 seconds are reported for excitation and relaxation, respectively.

3.5 Polymer optical fiber Bragg grating sensors

The final goal of the project was to demonstrate sensors. The feasibility of temperature and strain sensors has already been shown in the previously described papers, with high sensitivities and linear responses.

3.5.1 Temperature compensated strain sensor

One of the problems when working with Bragg grating sensors is the simultaneous sensitivity to more than one parameter, in particular environmental ones. If it is also considered that POF FBGs show a high temperature sensitivity, which is positive in the case of using them as a temperature sensor, but not when temperature fluctuations are not the desired target of the measurement, and if considered that PMMA has high water affinity and consequently humidity sensitivity, which again is an advantage only if the sensor is made to sense humidity, an independent measurement of, for example, strain could become quite complicated in a real situation. In **Paper 5** we show a temperature compensated strain sensor (the sensor compensates also for humidity, since the two gratings are exposed to the same environment, but since no independent humidity compensation is shown, this is not stated). The compensation technique is the use of two gratings written next to

each other, only one of which is subject to strain.

3.5.2 Humidity insensitive strain sensor

As already mentioned, the method described in **Paper 5** should compensate for humidity as well, nevertheless the possibility of having a sensor that is insensitive to humidity would reduce one of the problematic variables of sensors working in unstable environments. For this reason a humidity insensitive strain sensor is reported in **Paper 8**. The insensitivity is achieved through the choice of material, TOPAS. Opposite to PMMA that has a strong and linear dependence to humidity, and is a good candidate for humidity sensors [84], TOPAS presents a 50 times smaller response. Sensitivities of 0.26 pm/% at 850 nm and -0.59 pm/% at 1550 nm were measured, which make it almost insensitive to this factor.

3.5.3 Accelerometer

Some of the bigger advantages of optical sensors over conventional ones are given by their insensitivity to electro-magnetic fields, atmospheric interference and to the capability of multiplexing. These reasons bring interest on optical sensors for covering the areas conventional sensors would not work in [85].

The main application of mPOF FBGs studied and developed during the Ph.D. is an optical accelerometer. Its development was achieved by merging the various techniques described previously in this work. A silica FBG based accelerometer was developed by the partner company *Brüel & Kjær Sound & Vibration Measurement A/S* [86]. In order to improve the performance of the sensor the silica FBG was substituted with an mPOF FBG. The working principle and the results are reported in **Paper 9**. The accelerometer is found to have resonance frequencies of around 3 kHz and flat frequency responses up to more than 1 kHz. Moreover the sensitivity, dependent on the grating wavelength, improved almost 4 times compared to the silica counterpart. A figure of merit is used to characterize accelerometers: it is the product between sensitivity and resonance frequency squared. It was measured

that the reduction of the frequency working range caused by the fiber being more compliant was compensated by the gain in sensitivity. In fact the figure of merit for polymer fiber based accelerometers was found to have a higher value compared to the one of silica based accelerometers. The response of the accelerometers was also measured to be linear for accelerations up to the maximum of the measurement range (15 g).

3.5.4 Microphone

With a similar working principle of the accelerometer, in which the acceleration was transduced by means of a mechanical fork, in elongation of the Bragg grating, an optical microphone was realized. A membrane is placed in contact with the mechanical fork, which transduces the sound pressure into an elongation of the grating. Sound frequency and pressure amplitude can then be detected in the form of a wavelength shift.

The realized microphone is shown in Fig. 3.5. The interrogation system used is the same as for the accelerometer and consists of an I-MON 850-FW (*Ibsen Photonics*). The Bragg grating used was realized with the UV phase mask technique. It was written in a PMMA three rings mPOF. The resonance wavelength is in the 850 nm wavelength window, where the fast electronics allows detection of audio frequencies. The grating length is just above 4 mm.

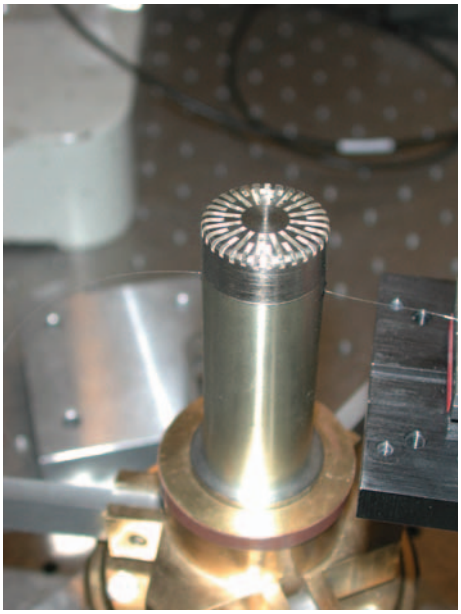

Figure 3.5: Optical microphone based on mPOF FBG.

The microphone was tested as proof of concept with a calibrator. The calibrator produces a sound pressure at a single frequency: 1.01 kHz. The FFT of the wavelength shift was recorded with the calibrator off and on, respectively. The result is shown in Fig. 3.6.

Some noise contributions appear in the situation of no sound pressure applied as well as with sound pressure. They were found to be due to the electronics and to the fitting software. To test the functioning of the optical microphone for detecting and recording a human voice, a simple voice message was recorded. For the test the distance from the microphone was about 30 cm, and a normal conversation voice loudness was used. In Fig. 3.7 the recorded time trace of the wavelength shift for the sentence: “A good weekend to all of you” is reported. The measured wavelength shift can then easily be used to play back the recorded audio using simple software and a speaker.

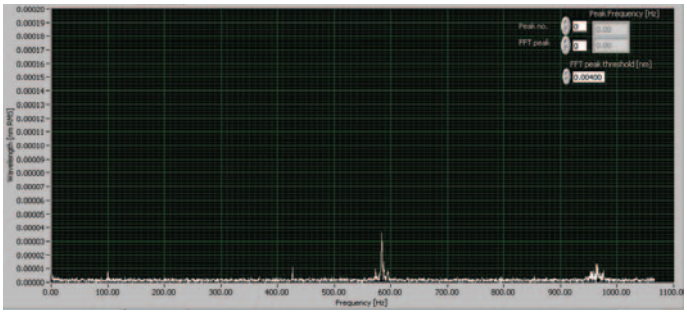

(a) Calibrator off

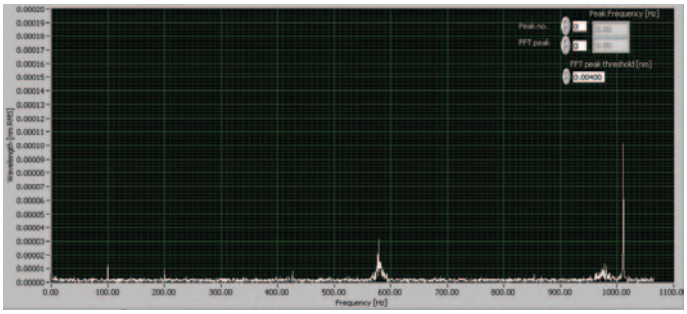

(b) Calibrator on

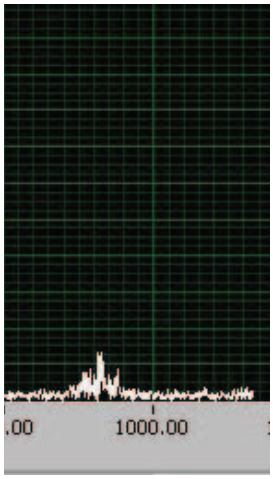

(c) Calibrator off

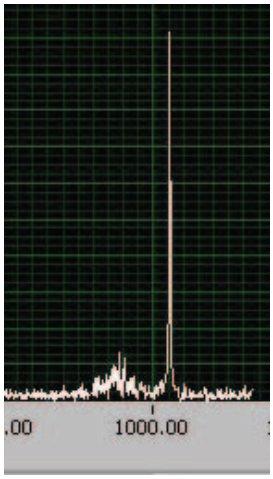

(d) Calibrator on

Figure 3.6: FFT of the FBG wavelength shift before ((a) and (c)) and after ((b) and (d)) turning on the calibrator. Figures (c) and (d) are a zoom of the frequencies around 1 kHz.

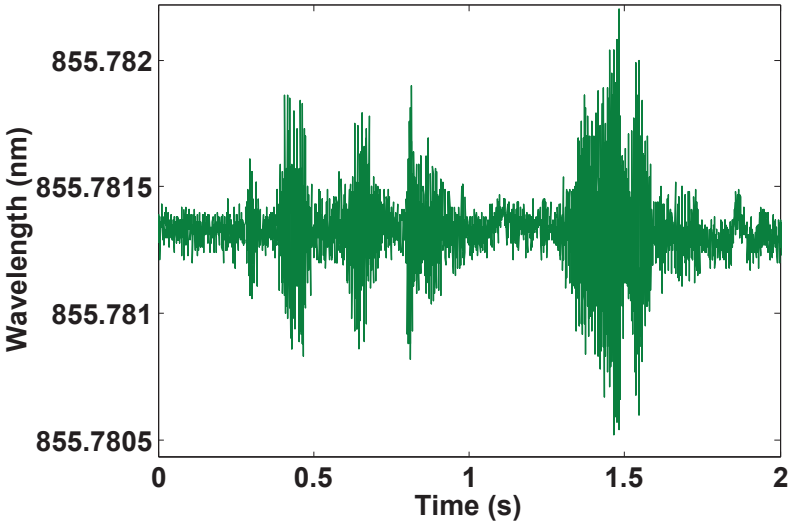

Figure 3.7: Detected wavelength shift for the sentence: "A good weekend to all of you"

Chapter 4

Conclusions

In this thesis the development of fiber Bragg fiber sensors in microstructured polymer optical fibers was investigated and demonstrated from the fiber fabrication to the sensor testing. A discussion on a process that goes from manufacturing the fibers, handling them, writing gratings in different fibers and at different wavelengths, characterizing the fibers and the gratings to realizing and testing the sensors was presented.

More specifically, the optimization of the hot blade cleaving technique for polymer fibers made of PMMA and TOPAS was presented. A fiber cleaver was built. It allows to have repeatable high quality cleaves and within a very short time. A qualitative analysis based on image recognition was presented and used to determine the optimum cleaving parameters by the minimization of the cleaving induced core shift. An optimum temperature of both fiber and blade of 77.5 °C for PMMA and 40 °C for TOPAS was found, respectively. The use of a thin blade with a flat edge showed to improve the quality of the cleaved fibers.

A UV writing facility was implemented. Bragg grating writing with the phase mask technique was done in step index polymer fibers and in microstructured polymer optical fibers made of PMMA and TOPAS. The inscription of Bragg gratings in annealed POF fibers is also reported and the performance of such gratings is compared to that of gratings in non-annealed fibers. An improvement in both thermal and strain performance is reported and in particular an improvement of about 15 °C

of the linear working range with no hysteresis, and with a maximum working temperature of 75 °C is reported. The strain performance has been improved by about 4 percentage points, bringing the hysteresis free regime from 3% to almost 7%.

Bragg grating writing with a bandwidth below 0.3 nm has been achieved in the lower loss region of 850 nm in both step index and microstructured PMMA polymer optical fibers. The strain sensitivity of such fiber Bragg gratings was measured to be 0.71 pm/$\mu\varepsilon$ and it was compared to that of gratings written in the same fibers, but for a resonance wavelength at 1550 nm, and the strain sensitivity was found to be 1.3 pm/$\mu\varepsilon$.

The possibility of writing gratings in TOPAS fibers at both 1550 nm and 850 nm was also demonstrated. The temperature sensitivity of the fiber was measured to be -36.5 pm/°C, which is opposite in sign to what was previously reported for this material [87], indicating a possible error in the previously reported result.

A fabrication technique for tuning the wavelength of the Bragg grating by still using the phase mask technique has been demonstrated. The technique consists in having the fiber in an elongated state during writing, so that when, after writing, the fiber is released the final period will be shorter resulting in a lower Bragg wavelength. The tunability of the gratings was demonstrated up to 12 nm due to the high elasticity of the fiber. This technique was used to controllably inscribe multiplexed gratings on the same fiber. The possibility of having two close gratings in the same fiber was used to demonstrate temperature compensated strain measurements.

Other than the more commonly used UV phase mask technique, grating writing was demonstrated with the direct writing technique. A fiber was designed and fabricated for this purpose. Writing of a 4th order grating at a resonance wavelength of 1520 nm has been reported. This is the first demonstration of this technique in polymer fibers.

Mechanical characterization of polymer fibers from a dynamic strain point of view was performed. The dynamic Young's modulus of PMMA fibers was measured and it was found to be constant at least for frequencies from 10 to more than 100 Hz, showing negligible viscoelasticity for

a strain level of 0.28%. The study of single frequency excitation showed a response of the stress in phase with the applied elongation, again confirming a small loss component due to viscoelasticity for both PMMA and TOPAS. However, high harmonic frequency components can be observed, and they increase in strength with frequency but in particular with strain for both materials. A stress relaxation experiment with a stress of 2.8% was also reported for PMMA and time constants of about 5 and 6 seconds for elongation and release, respectively, were measured.

A TOPAS based Bragg grating was used to demonstrate a humidity insensitive sensor. The humidity sensitivity of TOPAS FBGs was measured with gratings at both 850 and 1550 nm. The measured sensitivity is 0.26±0.12 pm/% in the 850 grating and -0.59±0.02 pm/% in the 1550 nm grating. The results take more value when considering that temperature variation of 0.3 °C could give a higher shift of the maximum variation measured. Moreover if compared to the sensitivity to humidity of PMMA, TOPAS is more than 50 times less sensitive to this factor.

Optical accelerometers were demonstrated and characterized. Accelerometers working with either 850 nm or 1550 nm gratings were reported. For both, a resonance frequency of about 3 kHz is measured and a flat frequency response for frequencies over 1 kHz is shown. The accelerometer has a sensitivity of 19 pm/g when using a 1550 nm grating and 7.6 pm/g when the grating has a resonance wavelength of 850 nm. In both accelerometers the figure of merit (sensitivity times resonance frequency squared) is higher than the corresponding accelerometer based on silica fiber and the same Bragg wavelength.

An optical microphone based on a 850 nm mPOF FBG has also been built. The response to a calibrator and a voice recording have been shown as proof of concept.

4.1 Discussion and outlook

The results achieved and the technological improvements show an increasing possibility for polymer optical fiber sensors and in particular for those using microstructured fibers. Nevertheless polymer fiber op-

tics is still a young field and has important issues to be solved before it can reach full potential and break into the industry market. The first issue is given by the high loss of fibers made of polymers. Even if for sensing applications only a short section of fiber is required, the implications of not being able to have an all-polymer fiber system complicates the picture. The necessity of gluing polymer to silica fibers introduces extra loss and creates stability and robustness issues. Another problem with handling is given by the lack of knowledge and technology for people who don't work with polymer fibers on a regular basis. This factor limits development and interest towards applications that could benefit from using polymer fibers, because the experts in the specific application are not used to handling the fibers. For these reasons, combined with development and improvement on the final result, i.e. the sensors, and with continuous efforts in trying to achieve lower loss, a development of the basic working technology in order to make it effective and accessible to everybody would be necessary. Although fiber design and drawing is at the moment quite reliable and repeatable, the process is still affected by small factors that sometimes compromise a successful drawing. These factors are not of real interest in this discussion, but the possibility of improving this aspect would definitely help to move the production of sensors towards commercialization.

Regarding grating writing, the main issues for the phase mask technique is the time necessary to write gratings, even if doping techniques have already demonstrated time reduction [41]. In order to make POF FBGs ready for mass production the writing time should be reduced even more. Despite this the results are very promising in terms of grating quality. Further improvements on the grating strength could also be important to address, for example for multiplexing (propagation along more fiber is needed) and to increase the performance of dynamic sensors which require short acquisition time to have a larger dynamic range. Benefits could come from writing gratings at wavelengths where the fibers have minimum loss. For this purpose the phase mask technique starts to be inadequate, so considering alternative techniques like interferometer configurations could not only lead to the achievement of this goal but also to the realization of a more flexible technique. Flexibility

is given also from a technique such as direct writing. The technique has several disadvantages compared to the UV writing (e.g., higher order gratings, alignment complexity, limitation in minimum period of the modulation and necessity of a special microstructure) but the few advantages make it unique, interesting and probably worth more investigation: first of all the possibility of writing gratings in non-photosensitive fibers, then the extremely short time necessary for writing and finally the flexibility in grating design.

The viscoelastic nature of polymer poses some limitations in the applications where the bigger advantages of polymer fibers seem to be. However the possibility of tuning mechanical properties (such as Young's modulus, yield strain and failure strain) with the fabrication parameters such as tension and the possibility of designing the applications with these limitations in mind, for example low strain if high dynamic range is required, will still allow to exploit the benefits given by this material.

Although sensors made in polymer fibers are only in a preliminary research stage and they may need extra tests especially on stability and long term life time, the results achieved show a big potential for practical applications. Probably more field tests could give a real idea of the potential. Moreover tests on embedding the sensors in composite materials and research towards polymer fibers made of materials that can withstand higher temperatures and that are already existent could have a big impact on the smart structures sector.

Paper 1

Cleaving of TOPAS and PMMA microstructured polymer optical fibers: Core-shift and statistical quality optimization

A. Stefani, K. Nielsen, H.K. Rasmussen and O. Bang

Optics Communications, vol. 285, pp. 1825-1833 (2012).

Optics Communications 285 (2012) 1825–1833

Contents lists available at SciVerse ScienceDirect

Optics Communications

journal homepage: www.elsevier.com/locate/optcom

Cleaving of TOPAS and PMMA microstructured polymer optical fibers: Core-shift and statistical quality optimization

A. Stefani [a,*], K. Nielsen [a], H.K. Rasmussen [b], O. Bang [a]

[a] Technical University of Denmark, DTU Fotonik, Department of Photonics Engineering, DK-2800 Kgs. Lyngby, Denmark
[b] Technical University of Denmark, DTU Mechanical Engineering, Department of Mechanical Engineering, DK-2800 Kgs. Lyngby, Denmark

ARTICLE INFO

Article history:
Received 19 August 2011
Received in revised form 30 November 2011
Accepted 7 December 2011
Available online 20 December 2011

Keywords:
Cleaving
Microstructured polymer optical fibers
PMMA
TOPAS

ABSTRACT

We fabricated an electronically controlled polymer optical fiber cleaver, which uses a razor-blade guillotine and provides independent control of fiber temperature, blade temperature, and cleaving speed. To determine the optimum cleaving conditions of microstructured polymer optical fibers (mPOFs) with hexagonal hole structures we developed a program for cleaving quality optimization, which reads in a microscope image of the fiber end-facet and determines the core-shift and the statistics of the hole diameter, hole-to-hole pitch, hole ellipticity, and direction of major ellipse axis. For 125 μm in diameter mPOFs of the standard polymer PMMA we found the optimum temperatures to be 77.5 °C for both blade and fiber. For 280 μm in diameter mPOFs of the humidity insensitive polymer TOPAS® (grade 8007) the optimum temperature was 40° for both blade and fiber. A 100 μm thick flat-edge blade was found to minimize the core-shift by the cleaving to only 298 nm or 5% of the pitch for the PMMA mPOF at the optimal temperature.

1. Introduction

The first microstructured Polymer Optical Fiber (mPOF) was fabricated in 2001 by van Eijkelenborg et al. at the Optical Fibre Technology Center (OFTC) in Sydney, Australia [1]. Since then mPOFs with a large variety of hole structures and thus specific optical properties, have been fabricated at the OFTC, including endlessly single-mode mPOFs [2–3], multi-mode graded-index mPOFs (GImPOFs) [2,4], hollow-core photonic bandgap guiding mPOFs [2–3,5], highly birefringent mPOFs [2], twin-core mPOFs, [2], rectangular core mPOFs [4], and solution-doped mPOFs [3,6]. All these mPOFs have been made of conventional PMMA, which is commercially available in optical-grade quality granulates and low industry-grade solid rods.

Multi-material mPOFs with layers of PMMA and polystyrene or polycarbonate, have been used for making bandgap air-guiding mPOFs in the form of hollow polymer Bragg Fibers [7]. Other materials, such as cellulose butyrate, has been used to fabricate multifunctional biodegradable mPOFs [8].

Recently TOPAS® Cyclic Olefin Copolymer (COC) is also increasingly being used [10–14] due to its unique properties for localized biosensing [10–11], humidity insensitive sensing [12–13], and low-loss terahertz (THz) guidance [14]. Unfortunately, like optical-grade PMMA, TOPAS® COC only comes in granulate, which has to be processed. Nevertheless, TOPAS® and PMMA are together now the primary materials for mPOF fabrication.

Applications of mPOFs were initially hoped to be wide-ranging due to a number of advantageous material properties of polymer over silica in biosensing and strain sensing, the shear number of polymers to choose from, and the fact that polymers are drawn at low temperature, typically below 250 °C, making it possible to dope polymer fibers without destroying the dopant [6]. However, the high loss of PMMA (and TOPAS®) outside the visible wavelength regime and issues with splicing and cleaving, have severely hindered their applications. At present the main applications of mPOFs are within biosensing [10–11,15–17] and Fiber Bragg Grating (FBG) based strain sensing [12–13,18–23], even though early work has been done on Long Period Gratings (LPGs) in mPOFs also [24–25]. Polymers, such as PMMA and TOPAS®, are intrinsically photosensitive and thus mPOFs require no doping before an FBG can be UV-written into them, typically around 325 nm [12,18]. In contrast, silica fibers typically require Ge-doping and hydrogen loading, before an FBG can be UV-written into them. For an excellent review of polymer fiber FBGs we refer to [20] and for an excellent overview on the mPOF technology we refer to [26–27].

The advantage of mPOFs in biosensing depends on the material. PMMA is for example highly biocompatible and thus biomolecules may be immobilized directly onto PMMA [19], in contrast to silica, which requires definition of several intermediate layers [28–29]. TOPAS® does not allow direct binding of biomolecules to it, but it enables one to use special UV-activated linker molecules to define localized biosensing capture layers in well-defined sections along the fiber [10–11]. Common to all polymers is that they remain flexible and do not produce shards when damaged, which makes them suitable also for *in vivo* applications.

* Corresponding author.
E-mail address: alste@fotonik.dtu.dk (A. Stefani).

0030-4018/$ – see front matter © 2011 Elsevier B.V. All rights reserved.
doi:10.1016/j.optcom.2011.12.033

Within strain sensing polymer fibers have a clear advantage over silica fibers because of their low Young's modulus and their ability to be stretched much more than silica without breaking [20,27–28]. PMMA mPOFs have for example a Young's modulus of 2–3 GPa, depending on the drawing conditions [30,9], in contrast to the about 72 GPa of silica [26]. This means that much higher sensitivities can be achieved with mPOFs, if one can live with their lower operating temperature and higher loss [20]. Exactly due to the high loss of PMMA around 1550 nm there has been a strong push towards writing FBGs for operation around 850 nm [21,23], where CMOS components are available.

One of the major issues with mPOFs is their handling, such as cleaving and connectorization to silica fibers and other polymer fibers. Today, gluing is typically used to connect polymer fibers to a low-loss silica fiber in sensor applications, but care has to be taken when using mPOFs, in order to avoid too much glue going into the holes.

Canning et al. were the first to report on mPOF cleaving in 2002, where they used a 193 nm ArF laser to cleave 200 μm in diameter PMMA mPOFs, which had multiple cores distributed in a random air–polymer structure with thin bridges, surrounded by a thick solid region [31]. They found that ideally the rep. rate should be below 2 Hz to avoid damaging the fiber end-facet due to thermal build-up because of too long exposure to UV light. However, the cleaving time scales with the rep. rate and it was found that 4 Hz and an intensity of 1.6 J/cm^2 gave satisfactory cleaves in a reasonable time [31]. UV laser cleaving was again used several years later to cleave 400–500 μm in diameter highly porous PMMA mPOFs with high air-fill fraction and no outer solid region [32]. This study confirmed that UV laser cleaving gave clean end-facets and it showed that rotating the mPOFs by 3.6°/s during the cleaving process significantly improved the end-facet [32]. In this later study a 20 Hz rep. rate was used to shorten the cleaving time to about 270 s, but as expected this high rep. rate leads to thermal build-up and degrading of the fiber end-facet [32].

In view of the results of [31–32] it appears that UV laser cleaving consistently gives good cleaves of PMMA mPOFs with even the most complicated hole structures. Focussed Ion Beam (FIB) milling can also be used to cleave PMMA mPOFs [32] and solid single-mode PMMA fibers [33] and provides even better end-facets. However, FIB milling is very expensive and time-consuming, with reported cleaving times of 17.5 h [32].

Clearly price, portability, and cleaving time speak against UV laser cleaving and FIB milling, as was realized early on by Law et al., who instead developed the hot razor-blade/hot-fiber cleaving technique in a series of papers in 2006 [34,30,9]. In all these investigations the studied fiber was a PMMA GImPOF, typically with a diameter of around 400 μm and a thick solid layer around the hole structure. The GImPOF has a range of hole sizes, which makes it ideal for the testing of cleaves.

In the first work of Law et al. they found that the PMMA used in their GImPOF, had a brittle-to-ductile phase-transition close to 60 °C, which prevented good cleaves to be obtained above 60 °C [34]. The brittleness of PMMA is known to depend strongly on its viscosity molecular mass (M_v) with brittle behaviour occurring for $M_v < 10^4$ and ductile behaviour for $M_v > 10^5$, where the particular grade of PMMA used by Law et al. had $M_v = 7.2 \times 10^4$ [34]. The cleaving dynamics of PMMA is quite different in the brittle and ductile regions, with crack front propagation providing the cleaving in the brittle region and interfacial shearing by the blade itself providing the cleaving in the ductile region. Given that the mPOF hole structure forms a crack-stopping structure, it is not surprising that good cleaving could not be obtained above 60 °C.

Law et al. first used a very simple hand-operated cleaver to cleave 580 μm in diameter GImPOFs and found that above 60 °C acceptable cleaves could be obtained with the best and most consistent results being for a fiber temperature of 85–95 °C and a blade temperature of 50–80 °C [34]. Another cleaver was then built, which had independent control of the cleaving speed, the position of the blade, and the fiber and blade temperature. A subsequent study of a different 400 μm in diameter GImPOFs (drawn at 220 °C and 45 g tension) with a blade temperature of 60 °C showed that the optimum fiber temperature had now increased to 70–80 °C [34]. It was also found that an equilibration time of at least 40 s should be used between placing the fiber on the plate and cleaving it, with 60 s being used in the study [34]. The condition of the blade was found to be extremely important, with the optimum being to move the blade between each cut to use a clean pristine section for each cleave [34]. Finally the best cleaving speed was found to be below 0.5 mm/s, with the necessary speed increasing with temperature due to the softening of the fiber [34].

Further studies of identical PMMA GImPOFs showed in more detail the nature of the damage done by the cleaving and considered the correlation between the drawing conditions, the mechanical properties, and the optimum cleaving temperature [9,30]. Measurements on solid fibers of the same PMMA showed that the room temperature Young's modulus increased with increasing draw tension (decreasing temperature) and that the loss modulus had peaks at two characteristic temperatures, which both increased with increasing tension (decreasing temperature) [9,30]. The medium tension GImPOF was shown to have an optimum cleaving temperature close to the first peak in the loss modulus and it was conjectured that this correlation was in fact a general phenomenon [9,30].

The hot-blade/fiber cleaving technique was also used for the cleaving of 110 μm in diameter commercial single-mode solid step-index polymer fibers of PMMA with a slight doping of polystyrene in the core. From visual inspection of the roughness of 1275 cleaves it was found that in addition to the optimum about 80 °C of both blade and fiber found by Law et al., a region of even better cleaves existed for fiber temperatures decreased to 30–40 °C [33]. Whether this different optimum region is due to the fiber being doped with polystyrene, due to the fiber being made from a different PMMA or drawn at different conditions, or due to the fiber being all-solid, thereby only allowing end-facet roughness as a measure of the quality of a cleave, is uncertain.

Not all mPOF hole structures allow cleaving with the hot-blade/fiber technique. It has for example been reported that highly porous mPOFs with a high air-fill fraction and almost no solid material around the microstructure, cannot be cleaved satisfactorily with the hot-blade/fiber technique [32]. These exotic fibers are, however, only of interest for THz guiding and not for fiber-optical sensing or optical transmission fibers. Other failed cleaving attempts of these highly porous THz fibers include using a semiconductor dicing saw [32].

The conclusion to make from the studies of PMMA mPOF cleaving with the hot-blade/fiber technique is that the optimum cleaving parameters depend significantly on the material properties of the drawn fiber, and thus also on the specific drawing conditions and the final hole structure. In PMMA mPOFs the optimum cleaving temperature was thus just above the brittle-to-ductile phase transition. However, what are the optimum cleaving parameters of the emerging TOPAS® mPOFs for example and can one further optimize the blade?

Only one study has so far been published on the cleaving of TOPAS® mPOFs, which was on the highly porous mPOFs for THz guiding [32]. The authors find that neither the hot-blade/fiber technique, nor FIB milling or the semiconductor dicing saw, allows good cleaving of 400–500 μm in diameter highly porous TOPAS® mPOFs [32]. They further argue that this is due to the low glass transition temperature (T_g) of TOPAS®. We would like to note that the TOPAS® used in [32] is in fact grade 8007 with $T_g = 80$ °C, whereas other grades have glass transition temperatures higher than that of standard PMMA, such as TOPAS® grade 6017 with $T_g = 180$ °C.

Here we present a thorough study of the cleaving of TOPAS® mPOFs with a triangular hole structure surrounded by a thick solid region. Such mPOFs can easily be made single-mode and even endlessly single-mode, which is why they have the best prospects for application in, e.g., fiber-optical sensing. The cleaving of such TOPAS® mPOFs has not been considered before. We further study the cleaving of in-house fabricated mPOFs made of industry-grade PMMA, in particular considering how the blade can be improved.

All studies of mPOF cleaving have so far relied on visual inspection. In order to have a repeatable process and minimizing the impact of the human eye, we developed a program for cleaving quality optimization, which reads in a microscope image of the fiber end-facet and determines the statistics of the hole diameter, hole-to-hole pitch, hole ellipticity, and direction of major ellipse axis. The program also calculates the core-shift relative to the fiber center imposed by the cleaving, which is an important parameter for minimizing the coupling and splicing/gluing loss.

For repeatable cleaving we fabricated the electronically controlled cleaver shown in Fig. 1, which provides independent control of fiber temperature, blade temperature, and cleaving speed, just as the cleaver originally used by Law et al. [9,30,34].

Investigating several different blades of different thicknesses and shapes, we find the optimum blade to be a custom-made flat-edge blade with a thickness of 100 μm, which was the smallest thickness we had available.

For 125 μm in diameter mPOFs of the standard polymer PMMA our results show that the optimum cleaving temperature is 77.5 °C for both blade and fiber, thereby confirming that the temperatures found by Law et al. also hold for mPOFs made of industry-grade PMMA with the standard telecom diameter 125 μm. With the 100 μm thick flat-edge blade the core-shift due to the cleaving had also its minimum at the optimum temperature, which was only 298 nm, or 5% of the pitch.

For 280 μm in diameter TOPAS® mPOFs (grade 8007) we found the optimum cleaving temperatures to be 40 °C for both blade and fiber.

2. mPOFs under investigation

In our investigation we use the two mPOFs with hexagonal hole structures shown in Fig. 2: a PMMA 3-ring fiber and a TOPAS® 2-ring fiber. The PMMA fiber has been drawn in a two-step process from a D = 6 cm in diameter preform, with 3 rings of holes with a hole-to-hole spacing, or pitch, of Λ = 6 mm and a hole diameter of d = 3 mm drilled into it. The preform was drawn to a 5 mm in diameter cane. The cane was then sleeved with two PMMA tubes, achieving a secondary preform with a 2 cm outer diameter. The secondary preform was drawn to a 125 μm fiber (standard telecom diameter)

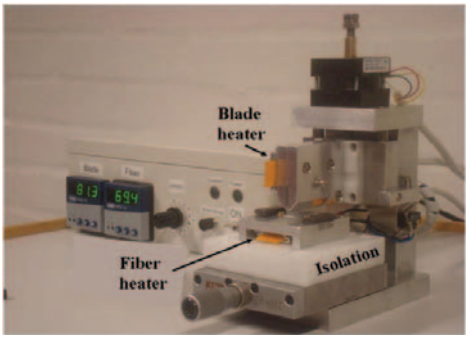

Fig. 1. Polymer fiber cleaver with independent electronic control of cleaving speed and temperature of blade and fiber.

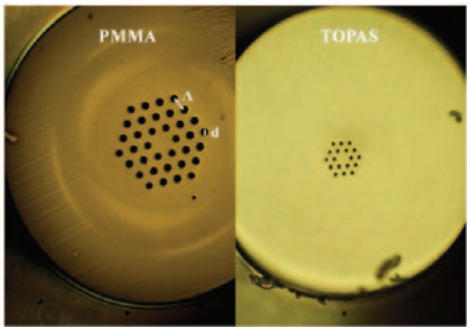

Fig. 2. Fibers under investigation: (left) PMMA 125 μm mPOF with 3 rings of holes with average pitch Λ = 5.92 μm and average hole diameter d = 2.76 μm; (right) TOPAS® 280 μm mPOF with 2 rings of holes with average pitch Λ = 8.4 μm and average hole diameter d = 2.9 μm (right).

with average hole diameter d = 2.76 μm and average pitch Λ = 5.92 μm (see Fig. 5).

The fiber has been drawn at 30 m/min with a set-temperature of 290 °C and a tension of about 24 g. According to the definition of low (5–8 g), medium (65 g), and high tension (130–150 g) used in [9] this places our fiber in the mid-low regime and thus it should have a lower Young's modulus and require a higher cleaving speed and lower cleaving temperature than the 0.5 mm/s and 80 °C found for the medium tension GImPOF used in [9,30,34].

The TOPAS® mPOF has been drawn with the same procedure, but starting from a 2 ring preform (D = 6 cm, d/Λ = 3/6 mm) of grade 8007 TOPAS® and using a 3 cm secondary preform. The secondary preform was drawn to a 280 μm fiber with 8.4 μm average pitch and 2.9 μm average hole diameter.

The TOPAS® mPOF has a hole diameter to pitch ratio of $d/\Lambda \approx 0.35$, which is well below the threshold of 0.42 that ensures endlessly single-mode operation of microstructured optical fibers of arbitrary base material [35]. The PMMA mPOF has a hole diameter to pitch ratio of $d/\Lambda \approx 0.47$, which is just above the cut-off and thus it becomes multi-moded below a short wavelengths cut-off, which for $d/\Lambda \approx 0.47$ is approximately $\lambda_{\text{cut-off}} \approx 0.2\Lambda = 1180$ nm [36].

3. Cleaving parameters

All cleaves presented here have been made with a blade speed of 5.6 mm/s and with an equilibrium time (time allowed to the fiber to reach thermal equilibrium) of about 20 s before cleaving the fiber.

The blade speed is over 10 times higher than the maximum of 0.5 mm/s used for 400 μm GImPOFs in [9,30,34], reflecting the comparably low tension and high temperature used in our drawing, as discussed in Section 2. At low speeds the 5 μm step length of our motor produces steps on the end-facet of the fiber, while this is not a problem at 5.6 mm/s. We note that in fact Law et al. also observed that a high speed was good when cutting at temperatures of 70°C or more [34].

The equilibrium time is 3 times less than the 60 s used in [30,34], which is mainly because our fibers are about 3 times thinner with less holes and thus reach thermal equilibrium faster.

With a fixed cleaving speed and equilibrium time we focus on determining the optimum temperature of fiber and blade for cleaving TOPAS® and PMMA mPOFs. Furthermore we investigate the influence of blade thickness.

In order to judge the quality of a cleave a code for analyzing the end-facet images of the cleaved fibers has been implemented in Matlab, which analyzes the outer fiber shape and the statistics of the hole structure. The program fits the contours of all the holes in

the image with ellipses using the least squares approximation. From the fit we obtain the desired parameters of each ellipse: the length of the major and minor axes (a and b in Fig. 3), the position of the center and the main axis direction with respect to a given direction, which we choose as the cleaving direction (θ in Fig. 3). From now on the main axis direction is also denoted the hole direction.

We define the ellipticity as the ratio between the major and minor axes, a/b. A circular hole will have an ellipticity of 1, whereas an ellipticity larger than 1 implies a deformed hole. The definition of the different parameters is shown in Fig. 3. The hole diameter is calculated as the arithmetic mean of the ellipse axes $(a+b)/2$. The average hole diameter is then calculated as the arithmetic mean of all the hole diameters. The pitch is calculated as the distance between the centers of two adjacent holes. The fiber average pitch is then calculated as the arithmetical average between all the pitches.

The same elliptical fit is also done for the outer circumference of the fiber with the fiber diameter being calculated in the same way as the arithmetic mean of the ellipse axes. With this data we will also be able to calculate the shift of the microstructure (or core-shift) because of the cleaving.

We finally note that the use of the numerical code for cleaving inspection is limited to a parameter regime in which the hole structure is intact after cleaving (no broken bridges), so that it can be analyzed.

4. Cleaving analysis — good cleave

In Fig. 4 we show an example of two good cleaves of the same fiber, but with two different cleaving directions with respect to the hole structure orientation. The cleaving direction is determined by the fine line structure on the bottom left side of the fiber images, where the blade enters, because this is a signature of the blade, as also observed in [34]. Both cleaves have been made with a temperature of 77.5 °C for both blade and base using a standard 130 μm thick wedge-shaped blade (see Fig. 8).

Visually both cleaves seem to be equally good and correspondingly we see that the spread in the pitch (84 counts) and the hole diameter (36 counts) is small. From the ellipticity graph it is found that the holes are almost circular after the cleave, with an average ellipticity of only 1.0421 in cleave A and 1.0602 in cleave B. Given that the holes are almost circular in such a good cleave, the major and minor axes will have almost identical lengths and thus the hole direction is expected to fluctuate quite much and be strongly dependent on the cleaving direction with respect to the hole structure. This is also the case, as seen in the graphs for the hole directions.

For cleave B the hole direction seems to have some correlation along the cleaving direction (zero degrees), with 18 holes out of 36 being in the cleaving direction ±18°. However, given the very small average ellipticity of 1.0602, the tendency is not strong enough to make a definite conclusion.

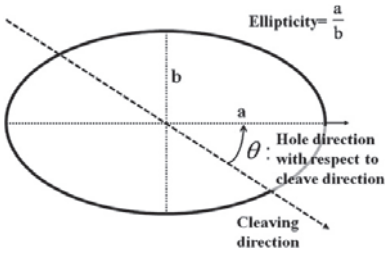

Fig. 3. Definition of elliptical fit: a is the major axis, b the minor axis, the dashed line represents the cleaving direction, and θ is the angle between the main axis (hole direction) and the cleaving direction.

Given these parameters it appears that we can conclude that the cleave A is slightly better than the cleave B, and that both cleaves are very close to ideally preserving the structure.

However, in order for a cleave to be really good, it also has to result in a small separation between the center of the hole structure (the core) and the center of the fiber, which is marked with a white star in the images in Fig. 4. If the separation is too large, this will lead to significant coupling losses when coupling to, e.g., a commercial silica fiber with a nicely centered core. This shift has not been considered in the hitherto published papers on mPOF cleaving [9,30–34]. From Fig. 4 we find that the shift is 3.5308 μm for cleave A and 3.8161 μm for cleave B.

For both cleaves A and B the separation is thus a bit more than half a pitch in the opposite direction to the cleaving direction, which means that neither cleave A, nor cleave B, in reality can be characterized as good, even though their average ellipticity was close to 1.

In Fig. 5 we investigate the dependence of the shift on the cleaving direction by considering cleaves with near optimal temperatures (77.5 °C for both blade and base) made with 4 different directions.

The shifts are measured to be 2.7272 μm, 3.3341 μm, 2.2306 μm, and 3.508 μm, clearly demonstrating that the amount of shift depends on the cleaving direction with respect to the hole structure. We will look more into this shift when considering a "bad cleave" and when optimizing the blade and cleaving parameters in the following.

5. Cleaving analysis — bad cleave

In Fig. 6 we show the result of a bad cleave C of the PMMA mPOF, comparing the statistics of the ellipticity and hole direction with that of the good cleave A. Cleave C has been done with the same parameters as cleave A, except that we have decreased the temperature to 60 °C for the blade and 70 °C of the base.

From the image we clearly see how the microstructure has now been squashed by the blade, with the core (red star) being shifted by 8.3633 μm or about 2 pitches opposite to the cleaving direction (4 times the shift for cleaves A and B). The average ellipticity has increased to about 1.7086, with even the most circular hole of the cleave C being more elliptical than any hole of for cleave A. The holes, are now concentrated around 90° with respect to the cleave direction, which, given the high ellipticity, means that the fiber has been squeezed by the blade. These observations imply a quite big change in the fiber structure itself and leads to the conclusion that the cleaving is "bad".

Let us look a bit closer at the huge shift of the core observed for this bad cleave C. In Fig. 7 we show a microscope image taken from the side of the PMMA mPOF and cleave C. Here we see that the bending of the microstructured region actually starts about 30 μm into the fiber. Due to the two-step sleeving process used in the fiber drawing (5 mm cane sleeved to a 2 cm secondary preform) the central part inside the white regions in Fig. 7 corresponds to the original cane.

From Fig. 7 we see that it is not the whole cane region, but only the air-hole microstructure that is being squeezed. This should mean that the amount of shift is depending on the cleaving direction with respect to the symmetry of the hole structure, which was also what we observed in Fig. 5.

6. Blade thickness and shape

The best cleaving conditions for PMMA mPOFs have been found to be in the temperature regime where the material has a ductile behavior, just above the transition temperature to being brittle [34]. In this situation the blade is continuously in contact with the fiber material and is separating the fiber sides while passing through it. The fiber gets, consequently, moved apart following the blade shape, which gives the fiber end-facet about the same angle as the blade. The continuous contact and friction between blade and fiber is also

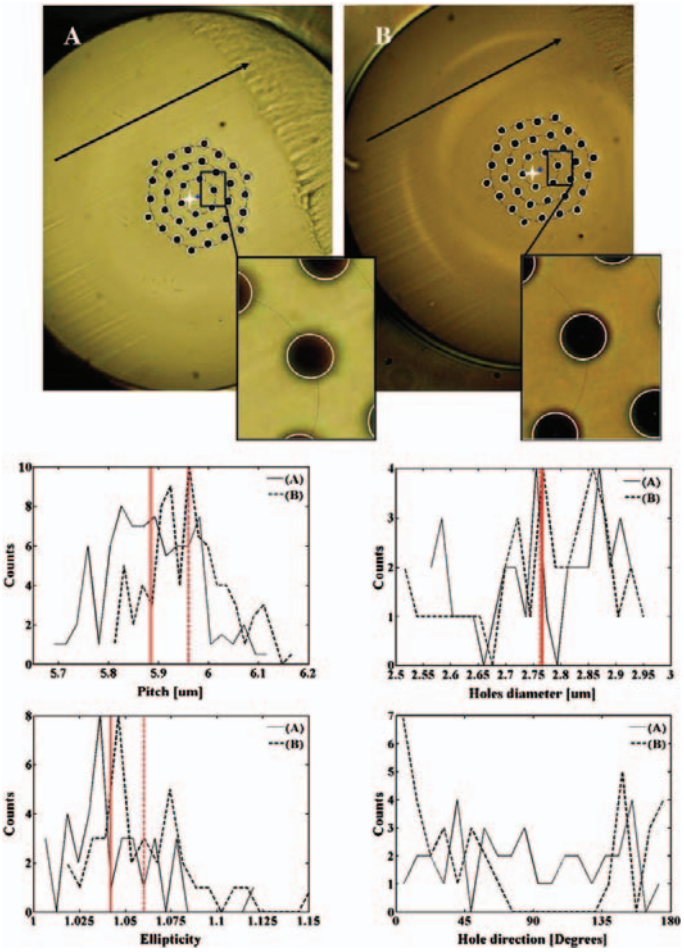

Fig. 4. Two cleaves of the PMMA mPOF made with the same settings (77.5 °C for both blade and base, 130 μm thick wedge-shaped blade) but with a different direction (black arrow) with respect to the hole structure. Cleaves A (left) and B (right) are represented by solid and dashed lines, respectively. The x-axis is divided into bins and the y-axis shows the number of counts with a given parameter value in the bin. The curves are then the center of the bins connected with a line. In the pitch, hole diameter and ellipticity graphs the vertical lines represent average values. The white star on the images marks the center of the fiber.

responsible for inducing the observed shift of the structure in the cleaving direction. In this section we therefore investigate the influence of blade thickness and shape on reducing the contact and friction.

In Fig. 8 we show cleaves of the same piece of an old PMMA mPOF which had too many holes in the cane-sleeving tube interface and was thus never used. We have fixed the cleaving parameters to 80 °C for both blade and base, but used blades of different shape and thickness (130, 200, 250, and 300 μm), given in the respective insets.

The first cleave, shown in Fig. 8(A), is with a 130 μm thick and 470 μm long wedge-shaped blade, which thus has a tip- or wedge-angle of 15.7°. This gave an average ellipticity of 1.28 and a core-shift of 2.42 μm. Increasing the thickness to 200 μm gives an increased wedge angle of 24.0°. As expected this resulted in a worse cleave with a larger average ellipticity of 1.50 and a larger core-shift of 7.60 μm, as shown in Fig. 8(B). The 300 μm thick and 630 μm long blade used for the cleave shown in Fig. 8(D) has the largest wedge angle of 26.8°. Correspondingly, the cleave is very poor.

The cleave shown in Fig. 8(C) is interesting. It is made with a 250 μm thick and 1000 μm long blade, whose wedge angle of 14.3° is about 1° smaller than the wedge angle of the 130 μm blade and should thus result in a slightly better cleave. As expected the average ellipticity of 1.23 is slightly lower than the 1.28 for the 130 μm cleave. However, the shift of 4.66 μm is much larger than the 2.42 μm obtained for the 130 μm blade. The reason for this unexpected result might be that the 250 μm blade is a non-standard blade with a size of only $0.7\times2.5\ \text{cm}=1.7\ \text{cm}^2$, which is much smaller than the $2.2\times3.8\ \text{cm}=8.4\ \text{cm}^2$ of the other three blades and thus much harder to handle in a stable manner.

In general, the tendency is that when the fiber diameter is much smaller than the length of the wedge-shape at the tip of the blade, then the best cleaving quality is obtained with the smallest wedge angle.

We therefore acquired a large quantity of the custom-made blade shown in the inset of Fig. 9, which is only 100 μm thick and has one flat side. The length of the angled region is 700 μm, giving it a wedge angle of only 8.1°. In Fig. 9 we show a cleave of our PMMA

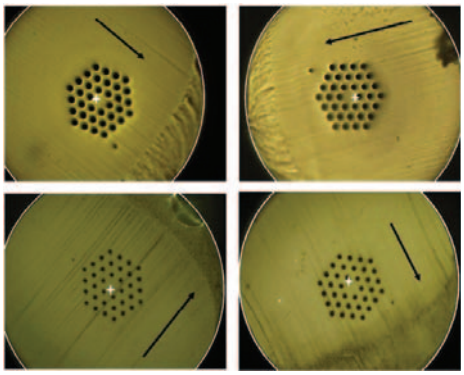

Fig. 5. Four cleaves of the PMMA mPOF made with the same parameters as cleaves A and B (77.5 °C for both blade and base), but different orientations. The white ellipse is the program fit to the contour and the cross is the center of the fitted ellipse.

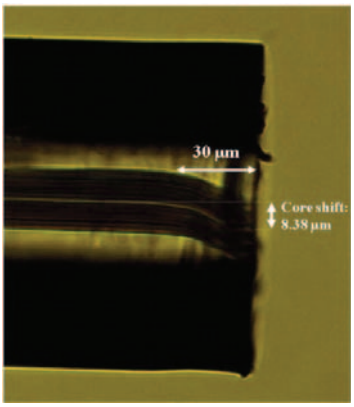

Fig. 7. Microscope image from the side of cleave C of the PMMA mPOF, showing a core-shift of 8.3633 μm starting about 30 μm inside the fiber.

mPOF from Fig. 2, made with the new custom-made blade at the optimum temperature of 77.5 °C for both blade and base (see next section). As expected the cleave is of very high quality, with an average ellipticity of 1.0811 and a core-shift of only 298 nm, corresponding to about 5% of the pitch.

7. PMMA mPOF — optimization

Here we present an optimization of the cleaving temperature of the PMMA mPOF using the fiber end-facet analysis code. We used a cleaving speed of 5.6 mm/s, an equilibration time of 20 s, and the custom-made flat-edge blade presented in Section 6. Only cleaves that have been considered to be acceptable after a quick visual inspection have been processed with the code.

The average hole ellipticity has been used as the quality criterion for judging the cleaves. In particular a threshold of 1.1 in ellipticity has been used to distinguish acceptable from not acceptable cleaves and a level of 1.09 to distinguish between acceptable and optimum cleaves. The results of this investigation are shown in Fig. 10. Acceptable cleaves are generally achieved with a blade temperature between 70 and 77.5 °C and with a base temperature between 75 and 80 °C. The optimum temperature setting is found to be 77.5 °C for both blade and base, which is the only one satisfying the criterion for optimum cleaving.

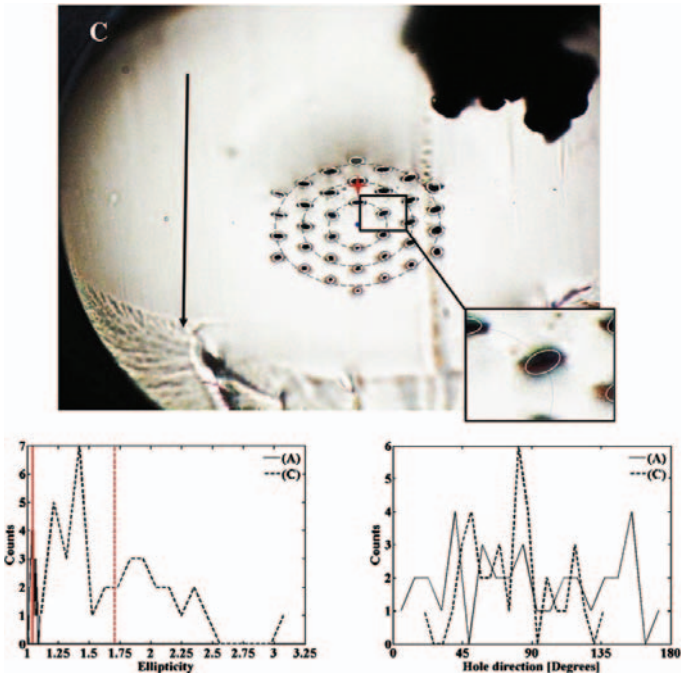

Fig. 6. Cleave of PMMA mPOF with a 60 °C blade and 70 °C base temperature (same 130 μm wedge-shaped blade as for cleaves A and B). Comparison of ellipticity and hole direction between cleaves A (solid) and C (dashed), with curves obtained as in Fig.4. The red star marks the center of the fiber.

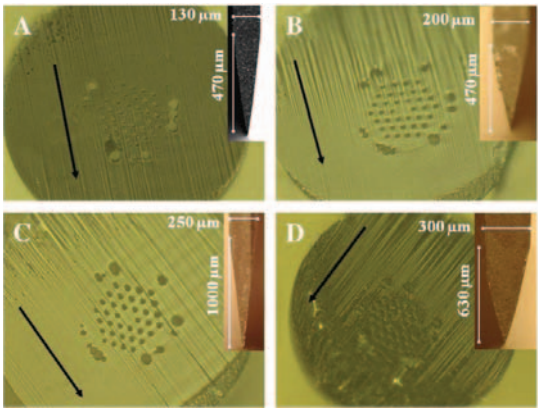

Fig. 8. Microscope images of the "old PMMA mPOF" cleaved with different blades, whose profiles are shown in the insets. The fibers have been cleaved with 80 °C for both the blade and base.

For the optimum temperature setting the cleave and its statistics are shown in Fig. 9, from which we find an average ellipticity of 1.0811. This is actually larger than the average ellipticities of 1.04 and 1.06 observed in Fig. 4 for cleaves A and B with the 130 μm blade with a larger wedge angle than our supposedly better flat-edge 100 μm blade. However, all these ellipticities are so low that the quality of the microscope focusing becomes a determining factor. A bad focus will, e.g., give rise to shades that will be picked up as ellipticity changes by the program. If we inspect closely cleaves A in Fig. 4 and the optimum cleave in Fig. 9, then cleave A indeed seems to be focused better.

What makes the cleaves with the new flat-edge blade used in the optimization better is their very small core-shift. In Fig. 11 we show how the core-shift depends on the base temperature for a fixed blade temperature of 77.5 °C. The graph shows a clear minimum at the optimum cleaving settings of 77.5 °C for both base and blade, where the core-shift is only 298 nm or 5% of the average pitch of 6.0 μm. The existence of a minimum core-shift is also apparent when the temperature is slightly off the optimum, as seen in Fig. 11 for a fixed base temperature of 75 °C. The optimum temperatures of the minimum correspond nicely to the transition from brittle to ductile behavior of PMMA observed in the work of Law et al. [30,34].

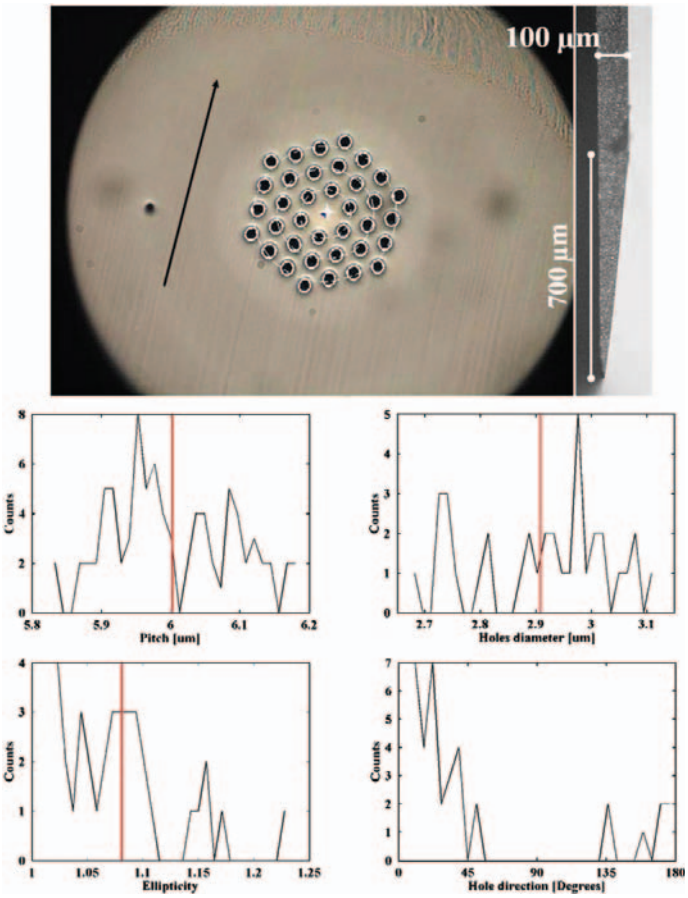

Fig. 9. Microscope image of PMMA mPOF cleaved with a 100 μm thick and 700 μm long flat-edge blade at the optimum temperature of 77.5 °C for both blade and base. The statistical graphs below the image are generated as in Fig. 4. Red vertical lines mark the average pitch 6.00 μm, hole diameter 2.91 μm, and ellipticity 1.0811.

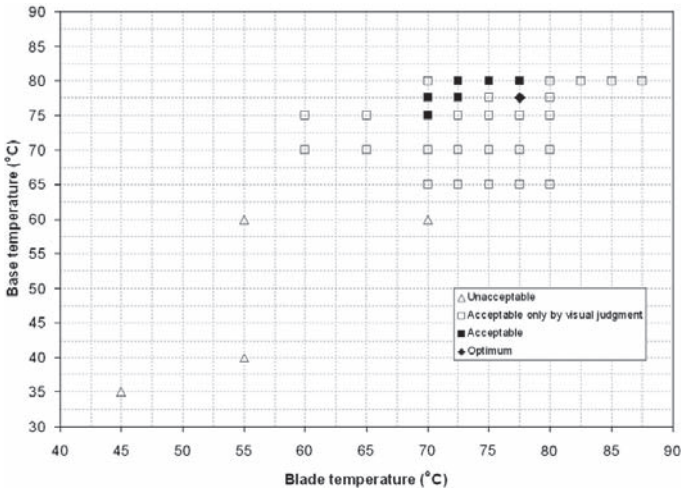

Fig. 10. Cleaving quality versus blade and base temperature for cleaving of the PMMA mPOF with the 100 μm flat-edge blade at a speed of 5.6 mm/s and an equilibration time of 20 s. Optimum cleaves have an average ellipticity below 1.09 and acceptable cleaves have an average ellipticity between 1.09 and 1.10.

8. TOPAS® mPOF — optimization

We now look at the optimum cleaving temperatures of the TOPAS® mPOF using the same blade, cleaving speed, and equilibration time as for the PMMA mPOF. The properties of TOPAS® grade 8007 are much different than PMMA. For example, the glass transition temperature is only $T_g = 80$ °C (see www.ticona.com). It is thus to be expected, that the optimum cleaving temperatures are lower than those for the PMMA mPOF.

The cleaving results are shown in Fig. 12, from which we see that the optimum temperature is 40 °C for both the blade and the base. A range of temperatures between 25 and 40 °C, for both the blade and the base, can be used to obtain acceptable cleaves. For this analysis the ellipticity value, below which a cleave has been considered acceptable, is 1.21, while optimum cleaves have an ellipticity below 1.19. At 40 °C, for both the blade and the base the average ellipticity is the lowest at 1.16. Here the core-shift is 4.288 μm, which is 51% of the average pitch 8.4 μm (see Fig. 2).

One more observation about TOPAS® grade 8007 can be made: being so soft it is really easy to create scratches on the end-facet of the fiber, which makes it more sensitive to blade imperfections and damages. Moreover this is probably the reason for which the hole ellipticity is larger in TOPAS® fibers than in PMMA fibers. Other grades of TOPAS® have higher glass transition temperatures and are thus expected to have higher optimum cleaving temperatures.

In general the same cleaving quality variation applies to TOPAS® grade 8007, as PMMA, which could suggest that a brittle to ductile phase transition also exists for the TOPAS®.

The quality of the cleaves of TOPAS® fibers could be improved by modifying the instrument (for example by using a motor with a different step size). In fact, until now this kind of cleaver has only been implemented for PMMA fibers and then used for TOPAS® fibers.

9. Conclusion

In this article we have studied cleaving of 125 μm thick industry-grade PMMA and 280 μm thick TOPAS® grade 8007 mPOFs with a standard hexagonal hole structure. In the study we have used a statistical numerical tool, which reads in an image of the end-facet of the cleaved fiber, and provides a statistical analysis of the hole structure and, as a novel parameter, the core-shift.

The numerical code and the variation of the core-shift, has allowed us to identify a 100 μm wide and 700 μm long flat-edge blade as the optimum of the blades we considered (conventional razor blades are purely wedge-shaped). With a wedge angle of only 8.1° at the tip, this blade provided very small core-shifts of only 298 nm or 5% of the pitch for the PMMA mPOF and 4.288 μm or 51% of the pitch for the TOPAS® mPOF, at their respective optimum cleaving temperatures.

The optimum cleaving temperature was identified using the code and considering the average hole ellipticity as the quality parameter. With the flat-edge blade the optimum temperature was 77.5 °C for the PMMA mPOF and 40 °C for the TOPAS® mPOF, for both fiber and blade. The settings gave average ellipticities of 1.08 and 1.16 for the PMMA and TOPAS® mPOFs, respectively.

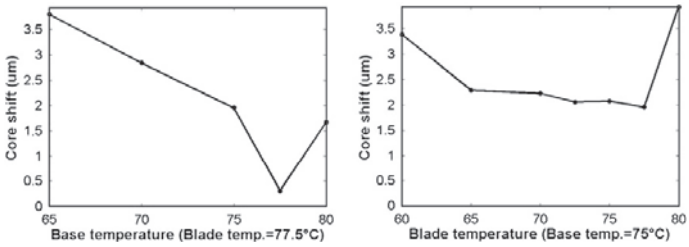

Fig. 11. Core-shift for cleaves in Fig. 10. Left: core-shift vs. base temperature for a fixed blade temperature of 77.5 °C. Right: core-shift vs. blade temperature for a fixed base temperature of 75 °C.

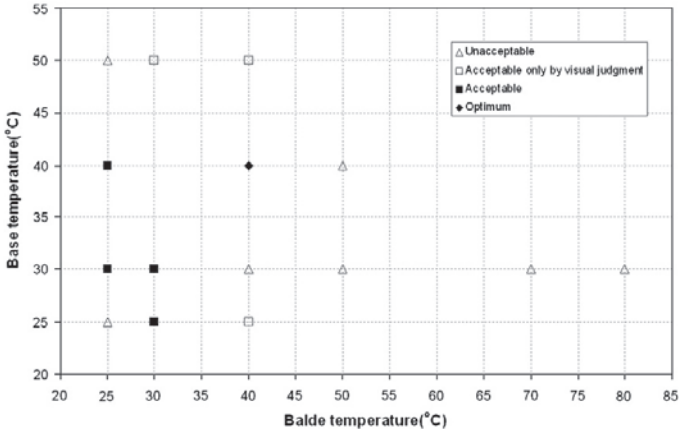

Fig. 12. Cleaving quality versus blade and base temperature for cleaving of the TOPAS® mPOF with the 100 μm flat-edge blade at a speed of 5.6 mm/s and an equilibration time of 20 s. Optimum cleaves have an average ellipticity below 1.19 and acceptable cleaves have an average ellipticity between 1.19 and 1.21.

While the temperatures of 77.5 °C for acceptable cleaves for the PMMA mPOF are within the regimes found in the original work by Law et al. on graded-index mPOFs of optical-grade PMMA [34], we have now found the optimum temperatures for this type of industry-grade PMMA mPOF and quantified its structural statistics. In particular, it was found that the core-shift had a minimum at the optimum setting, clearly relating to the known brittle-to-ductile phase transition of PMMA at these temperatures [34].

The lower cleaving temperature of only 40° of the new type of TOPAS® mPOF grade 8007 reflects the low glass transition temperature of 80° of this particular grade, which is also the reason why the average hole ellipticity was higher than for PMMA. The result emphasizes the fact the different mPOFs of different polymers require different cleaving temperature.

Acknowledgments

We would like to acknowledge support from the Danish National Advanced Technology Foundation.

References

[1] M.A. van Eijkelenborg, M.C.J. Large, A. Argyros, J. Zagari, S. Manos, N.A. Issa, I. Bassett, S. Fleming, R.C. McPhedran, C.M. de Sterke, N.A.P. Nicorovici, Optics Express 9 (7) (2001) 319.
[2] M.A. van Eijkelenborg, A. Argyros, G. Barton, I.M. Bassett, M. Fellew, G. Henry, N.A. Issa, M.C.J. Large, S. Manos, W. Padden, L. Poladian, J. Zagari, Optical Fiber Technology 9 (4) (2003) 199.
[3] M.C.J. Large, A. Argyros, F. Cox, M.A. van Eijkelenborg, S. Ponrathnam, N.S. Pujari, I.M. Bassett, R. Lwin, G.W. Barton, Molecular Crystals and Liquid Crystals 446 (2006) 219.
[4] R. Lwin, G. Barton, L. Harvey, J. Harvey, D. Hirst, S. Manos, M.C.J. Large, L. Poladian, A. Bachmann, H. Poisel, K.-F. Klein, Applied Physics Letters 91 (2007) 191119.
[5] A. Argyros, M. Van Eijkelenborg, M.C.J. Large, I.M. Bassett, Optics Letters 31 (2) (2006) 172.
[6] M.C.J. Large, S. Ponrathnam, A. Argyros, N.S. Pujari, F. Cox, Optics Express 12 (9) (2004) 1966.
[7] E. Pone, C. Dubois, N. Guo, Y. Gao, A. Dupuis, F. Boismenu, S. Lacroix, M. Skorobogatiy, Optics Express 14 (2006) 5838.
[8] A. Dupuis, N. Guo, Y. Gao, N. Godbout, S. Lacroix, C. Dubois, M. Skorobogatiy, Optics Letters 32 (2007) 109.
[9] S. Law, G. Barton, M. van Eijkelenborg, C. Yan, R. Lwin, J. Gan, Proceedings of SPIE The International Society for Optical Engineering 6289 (2006).
[10] G. Emiliyanov, J.B. Jensen, O. Bang, P.E. Hoiby, L.H. Pedersen, E.M. Kjær, L. Lindvold, Optics Letters 32 (2007) 460.
[11] G. Emiliyanov, J.B. Jensen, O. Bang, P.E. Hoiby, L.H. Pedersen, E.M. Kjær, L. Lindvold, Optics Letters 32 (9) (2007) 1059.
[12] I.P. Johnson, W. Yuan, A. Stefani, K. Nielsen, H.K. Rasmussen, L. Khan, D.J. Webb, K. Kalli, O. Bang, Electronics Letters 47 (4) (2011) 271.
[13] W. Yuan, L. Khan, D.J. Webb, K. Kalli, H.K. Rasmussen, A. Stefani, O. Bang, Optics Express 19 (2011) 19731.
[14] K. Nielsen, H.K. Rasmussen, A.J.L. Adam, P.C.M. Planken, O. Bang, P.U. Jepsen, Optics Express 17 (2009) 8592.
[15] J.B. Jensen, P.E. Hoiby, G. Emiliyanov, O. Bang, L.H. Pedersen, A. Bjarklev, Optics Express 13 (2005) 5883.
[16] F.M. Cox, A. Argyros, M.C.J. Large, Optics Express 14 (9) (2006) 4135.
[17] F.M. Cox, A. Argyros, M.C.J. Large, S. Kalluri, Optics Express 15 (2007) 13675.
[18] H. Dobb, D.J. Webb, K. Kalli, A. Argyros, M.C.J. Large, M.A. van Eijkelenborg, Optics Letters 30 (24) (2005) 3296.
[19] K.E. Carroll, C. Zhang, D.J. Webb, K. Kalli, A. Argyros, M.C.L. Large, Optics Express 15 (14) (2007) 8844.
[20] D.J. Webb, K. Kalli, in: A. Cusano, A. Cutolo, J. Albert (Eds.), Fiber Bragg Grating Sensors: Recent Advancements, Industrial Applications and Market Exploitation, Bentham Science Publishers Ltd., 2009, p. 1, (chapter 15).
[21] I.P. Johnson, K. Kalli, D.J. Webb, Electronics Letters 46 (17) (2010) 1217.
[22] W. Yuan, A. Stefani, M. Bache, T. Jacobsen, B. Rose, N. Herholdt-Rasmussen, F.K. Nielsen, S. Andresen, O.B. Sørensen, K.S. Hansen, O. Bang, Optics Communication 284 (2011) 176.
[23] A. Stefani, W. Yuan, C. Markos, O. Bang, IEEE Photonics Technology Letters 23 (10) (2011) 660.
[24] M.A. van Eijkelenborg, W. Padden, J.A. Besley, Optics Communication 236 (2004) 75.
[25] M.P. Hiscocks, M.A. van Eijkelenborg, A. Argyros, M.C.J. Large, Optics Express 14 (11) (2006) 4644.
[26] M.C.J. Large, L. Poladian, G. Barton, M.A. van Eijkelenborg, Microstructured Polymer Optical Fibres, Springer, 2008.
[27] M.C.J. Large, D. Blacket, C.-A. Bunge, IEEE Sensors Journal 10 (7) (2010) 1213.
[28] L. Rindorf, J.B. Jensen, M. Dufva, P.E. Hoiby, L.H. Pedersen, O. Bang, Optics Express 14 (18) (2006) 8224.
[29] L. Rindorf, O. Bang, Journal of the Optical Society of America B: Optical Physics 25 (3) (2008) 310.
[30] S.H. Law, M.A. van Eijkelenborg, G.W. Barton, C. Yan, R. Lwin, J. Gan, Optics Communication 265 (2) (2006-Sep) 513.
[31] J. Canning, E. Buckley, N. Groothoff, B. Luther-Davies, J. Zagari, Optics Communication 202 (2002) 139.
[32] S. Atakaramians, K. Cook, H. Ebendorff-Heidepriem, S. Afshar V., J. Canning, D. Abbott, T.M. Monro, IEEE Photonics Journal 1 (6) (2009) 286.
[33] O. Abdi, K.C. Wong, T. Hassan, K.J. Peters, M.J. Kowalsky, Optics Communication 282 (2009) 856.
[34] S.H. Law, J.D. Harvey, R.J. Kruhlak, M. Song, E. Wu, G.W. Barton, M.A. van Eijkelenborg, M.C.J. Large, Optics Communication 258 (2) (2006-Feb) 193.
[35] N.A. Mortensen, Optics Letters 30 (2005) 1455.
[36] M. Koshiba, K. Saitoh, Optics Letters 29 (2004) 1739.

Paper 2

Improved thermal and strain performance of annealed polymer optical fiber Bragg gratings

W. Yuan, A. Stefani, M. Bache, T. Jacobsen, B. Rose, N. Herholdt-Rasmussen, F.K. Nielsen, S. Andresen, O. Brøsted Sørensen, K. Styhr Hansen and O. Bang

Optics Communications, vol. 284(1), pp. 176-182 (2011).

Optics Communications 284 (2011) 176–182

Contents lists available at ScienceDirect

Optics Communications

journal homepage: www.elsevier.com/locate/optcom

Improved thermal and strain performance of annealed polymer optical fiber Bragg gratings

Wu Yuan [a,*], Alessio Stefani [a], Morten Bache [a], Torben Jacobsen [b], Bjarke Rose [b], Nicolai Herholdt-Rasmussen [b], Finn Kryger Nielsen [c], Søren Andresen [c], Ole Brøsted Sørensen [d], Knud Styhr Hansen [d], Ole Bang [a]

[a] DTU Fotonik, Dept. of Photonics Engineering, Technical University of Denmark, DK-2800 Kgs. Lyngby, Denmark
[b] Ibsen Photonics A/S, Ryttermarken 15-21, DK-3520, Farum, Denmark
[c] Brüel & Kjær Sound & Vibration Measurements A/S, Skodsborgvej 307, DK-2850 Nærum, Denmark
[d] DPA Microphones A/S, Gydevang 42-44, DK-3450 Allerød, Denmark

ARTICLE INFO

Article history:
Received 6 May 2010
Received in revised form 26 August 2010
Accepted 26 August 2010

Keywords:
Fiber Bragg grating
Polymer optical fiber

ABSTRACT

We report on a detailed study of the inscription and characterization of fiber Bragg gratings (FBGs) in commercial step index polymer optical fibers (POFs). Through the growth dynamics of the gratings, we identify the effect of UV-induced heating during the grating inscription. We found that FBGs in annealed commercial POFs can offer more stable short-term performance at both higher temperature and larger strain. Furthermore, the FBGs' operational temperature and strain range without hysteresis was extended by the annealing process. We identified long-term stability problem of even the annealed POF FBGs.

1. Introduction

Fiber Bragg gratings have been written in many types of POFs, for example polymethyl methacrylate (PMMA) POFs [1–14], fluorinated POFs [15,16], and TOPAS POFs [17], by using various methods such as phasemask [1–5], direct writing [6], or a combination of phase mask and interferometry [7–16]. 325 nm has been employed as a mainstream wavelength for writing grating in PMMA POFs [1–5,8–15]. Other wavelength such as 355 nm obtained from a frequency-tripled Nd:YAG laser has been used to write grating in CYTOP fiber developed by Asahi Glass Co. and Keio University [15,16]. On the other hand, 800 nm femtosecond pulses from Ti:Sapphire laser or its double frequency was mainly used for point by point direct writing [6] or grating writing with a phasemask [7].

However, the mechanism of index change does not appear to be fully understood [5,13,18–20]. It is believed that more than one process is involved in the photo-induced refractive index changes and hence in the grating formation dynamics [18–20]. The widely accepted point is that the principle mechanism of index change is an increase due to the photo-induced polymerization of the unreacted monomers [5,18–20], while laser-induced heating in the irradiated region during the inscription may also contribute to the index change [5]. Previous reports indicated that annealing of the POF before FBG inscription can relieve the frozen-in stress induced by the fiber drawing process [21] and increase the linear operation temperature range of FBGs [22]. However, the effect of annealing on the strain sensitivity performance was not yet considered.

Polymer optical FBGs have shown great potential for sensor applications to sense for example temperature and strain with higher sensitivity and wider tunability than its silica counterpart [1–14]. Those advantages are due to the lower Young's modulus and higher thermo-optic coefficient of POFs [23,24]. In addition, polymers are clinically acceptable, which along with the flexible, non-brittle nature of the fibers make these gratings an important candidate for in-vivo biosensing applications [25–28]. Despite of these promises not many commercial applications have been realized yet due to the high material loss of POFs. Here we consider fiber-optical accelerometers and microphones from a commercial point of view. In our applications we need a short length of POF to increase the sensitivity-frequency range product of the transducer and we opt for a commercial single mode POF to potentially have a reliable supply. This means that we are interested in both the strain sensitivity and the temperature stability of POF FBG and how to improve the operation regime.

In this paper we report on an investigation into UV-written FBGs in commercial step-index POFs. The formation dynamics, the temperature response, the thermal stability, and the tensile strain features of the gratings in both annealed and non-annealed POFs are studied and compared. We show that the FBGs in the annealed POFs can offer more stable short-term performance at both higher temperature and larger strain. Furthermore their operational temperature and tensile

* Corresponding author.
E-mail address: wyuan@fotonik.dtu.dk (W. Yuan).

0030-4018/$ – see front matter © 2010 Elsevier B.V. All rights reserved.
doi:10.1016/j.optcom.2010.08.069

strain range without hysteresis can be extended using the annealing process. We also reveal the thermal effect of UV-induced heating during the grating formation. Finally the temperature stability measurements show that even the annealed POF FBGs have the long-term stability problem, when operated at high temperature.

2. Experiments

2.1. POFs and FBGs writing

The gratings in this study were fabricated in PMMA single mode POF with a core doped with Polystyrene (MORPOF02 from Paradigm Optics). The fiber has an outside diameter of 115 μm and an average core diameter of 4 μm. The numerical aperture (NA) of this POF at 1300 nm is about 0.27 according to the specs. The annealing is carried out by placing the POF in an oven at 80 °C for two days. The fiber length decreased to (98.7 ± 0.5) % of its original value over the 48 h period and the diameter of the fiber increased to (104.3 ± 1) % of its original value. So its V value at 1300 nm changed from 2.2 to 2.3 by the annealing.

The gratings were inscribed using a 30 mW CW HeCd laser operating at 325 nm (IK5751I-G, Kimmon). The fiber was supported by v-grooves on both sides with a gap in between to avoid reflection, and it was appropriately stretched to ensure that the fiber did not sag. A circular gauss laser beam was expanded from diameter 1.2 mm to 1.2 cm in one direction along the fiber by a cylindrical lens. The laser beam was then focused vertically downwards into the fiber core using another cylindrical lens to expose the fiber through a phasemask customized for 325 nm writing with a uniform period of 1048.7 nm chosen for 1550 nm grating inscription (Ibsen Photonics). A grating length of 3 mm was defined by a pinhole underneath the focus lens to control the beam width. The laser irradiance at the fiber was about 10 W cm^{-2} and the exposure time was usually over 60 min. The resulting grating wavelength was around 1553 nm.

The growth of the 3 mm gratings were monitored in reflection during the inscription using a silica fiber circulator, a superK Versa broadband source (NKT Photonics) and an optical spectrum analyzer (Ando AQ6317B). A standard SMF-28 silica fiber was butt-coupled to the POF using an angle cleaved end-facet and a small amount of refractive index matching gel in order to reduce the Fresnel reflections, which manifested themselves as background noise. The ends of the POF were prepared using a homemade hot blade cleaver equipped with flat side blade, which gives a high quality end-facet, e.g., avoiding the problem of fiber core shifting [29]. Short lengths of POF (<10 cm) were used due to the high attenuation of the POF, which is about 3 dB/cm at 1550 nm. The high loss around this operating wavelength makes the monitoring of the gratings in transmission extremely troublesome. The typical reflection spectra of a 3 mm grating fabricated in the annealed POF with different exposure time is shown in Fig. 1(a). The grating reflectivity cannot be very exactly estimated since the material loss and coupling loss between POF and SMF28 cannot be precisely measured. A rough estimation is that the reflectivity of the grating with 70 min exposure is about 70% by taking into account the loss of the fiber and comparing

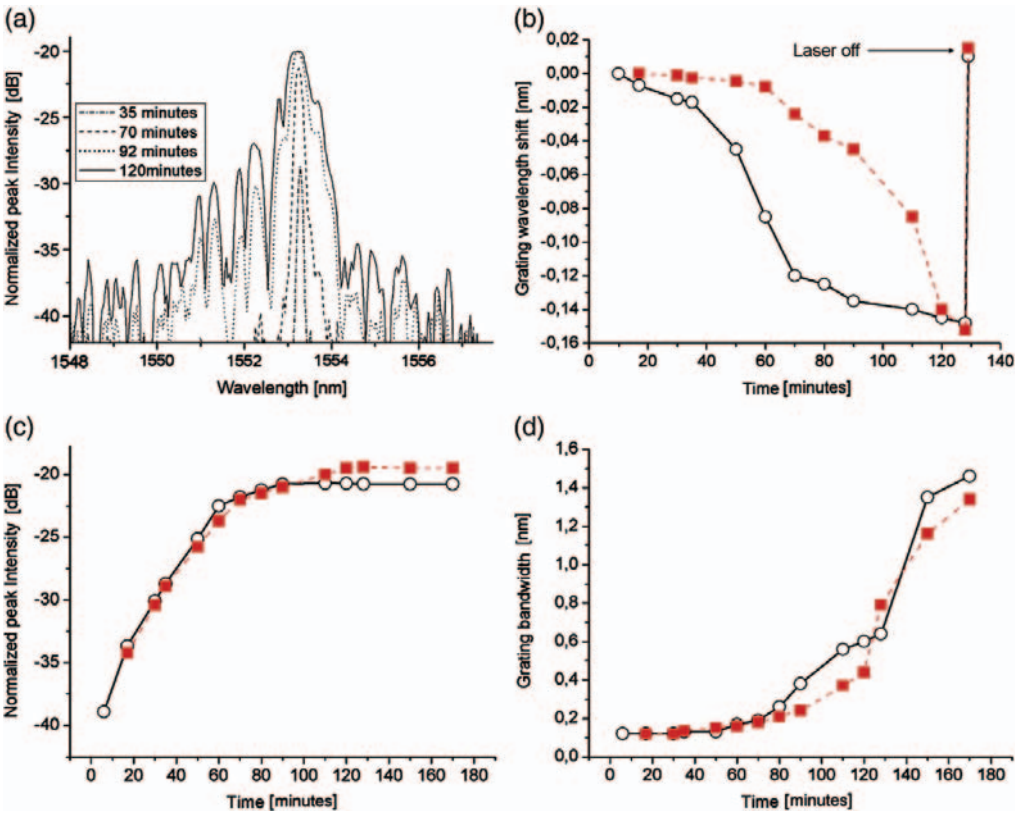

Fig. 1. (a) Reflection spectra of a 3 mm FBG in an annealed POF at different writing time. (b–d) Growth dynamics of the 3 mm FBG in non-annealed POF (squares, dashed line) and annealed POF (circles, solid line). (b) Grating wavelength shift, (c) normalized peak intensity, and (d) grating bandwidth. Measurements preformed in reflection.

the level of the reflected grating peak to the Fresnel reflection from the flat end of the glass fiber. This would give a refractive index modulation of approximately 3×10^{-4} or bigger. It was also found that the side-lobes started to appear in the reflection spectrum at 70 min. This may mean that the grating was partly apodized before 70 min.

The growth dynamics of the gratings, i.e. the time dependent resonance wavelengths, peak intensity, and bandwidth, are shown in Fig. 1(b–d). We found that the gratings inscribed into both the annealed and non-annealed POF follow an almost similar growth procedure. Both gratings begin with a growth in strength accompanied by an almost constant grating bandwidth. After a certain time threshold, which is around 60 min, the grating strength saturates while the grating bandwidth increases rapidly. This would because of a much larger n_{eff} (DC) change than the Δn (AC) change happened and it confirms the known Type-I and Type-II FBG writing regimes [13]. In Ref. [13], Liu and his colleagues indentified that a threshold of exposure exists on growth dynamics of POF gratings, and below which the Δn grows linearly (Type-I); when above the threshold point, bandwidth increases dramatically due to the catastrophic failure of the polymer fiber (Type-II). Simultaneously, the resonance wavelength was shifting to the blue side, until after about 120 min, where a stable resonance wavelength was reached.

The refractive index increase in PMMA induced by a 325 nm laser is mainly due to the material compaction or density increase in the laser-irradiated region, which results from the photo-induced polymerization of unreacted monomers [18–20]. UV-induced heating in the irradiated region during focused laser inscription may contribute to a permanent index increase [5], but this happens only when the local temperature is beyond some shrinking threshold, which is determined by the thermal history of the POF. At the threshold temperature, the length of fiber starts to shrink, which is mainly due to the release of the frozen-in stress induced in the fiber drawing process [22]. This shrinking effect is an irreversible process [22]. Temperature increase below the threshold can only result in a reversible decrease of the refractive index due to the negative thermo-optic coefficient (TOC, -1.1×10^{-4}/°C) of PMMA [24], which can be reversed to the original state once the temperature decreases [22].

Our experiments show that the blue shift of the resonance wavelengths, as shown in Fig. 1(b), were reversible once the writing was stopped. Besides the grating bandwidth didn't change after the laser was turned off. From the grating growth dynamics in both annealed and non-annealed POF, the refractive index increase induced by the material compaction will always be companied by a local temperature increase, which actually decreases the refractive index because of the negative TOC of PMMA. Taking into account the refractive index change by UV-induced polymerization, UV-induced heating should increase the local temperature of POFs by approximately 15 °C in order to have the −0.15 nm blue shift of the resonance wavelength after 120 min of UV irradiation which was observed in Fig. 1(b). This scale of temperature increase is still far below the shrinking threshold [22] and will not result in any irreversible shrinking effect. The lack of further blue shift of the resonance wavelengths after 120 min can be explained by the POF reaching thermal equilibrium. The most significant difference between the POFs is the faster shift in resonance wavelength for the annealed POF. No significant change in photosensitivity of the fiber was observed after the annealing.

2.2. Temperature characterization of FBGs

The temperature response of the gratings was studied with the same monitoring setup as the one used during the grating inscription. The grating section of the polymer fiber was heated up with a resistive hot stage (MC60 + TH60, Linkam). A thermo couple was used to measure the temperature as close to the grating as possible with an uncertainty around 0.3 °C. One end of the POF was clamped and butt-coupled to a silica fiber circulator, and the entire length of the POF with grating was attached to the surface of the heater by several layers of lens papers on the top. All gratings were fabricated with an exposure time of 60 min and they have similar peak intensity of about −25 dB.

Twenty minutes was allowed for the temperature of the grating to stabilize at each new setting before readings of the resonance wavelengths and peak intensity were taken. Firstly the gratings in the normal POF and the non-annealed POF were heated up separately from room temperature to 85 °C stepwisely in a single cycle, as shown in Fig. 2(a) and (b). In both gratings we saw the variation of resonance wavelength and peak intensity, but no obvious bandwidth change was found. To investigate the operational temperature regime without hysteresis, the gratings were cycled 2 times by increasing the temperatures stepwisely up to 55 °C (non-annealed POF) and 75 °C (annealed POF) at the first cycle and to the temperature 85 °C (both) at the second cycle, which was followed by stepwisely cooling down to room temperature after each cycle. The variation of the Bragg wavelength and peak intensity of the gratings with temperature for each cycle is shown in Fig. 3.

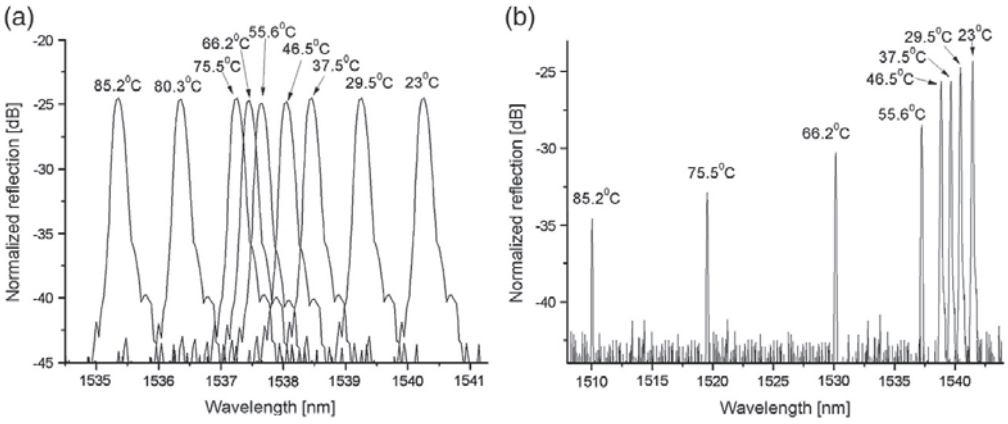

Fig. 2. Reflection spectrum variation of Bragg with a consecutive heating cycle of temperature in the annealed POF (a) and the non-annealed POF (b).

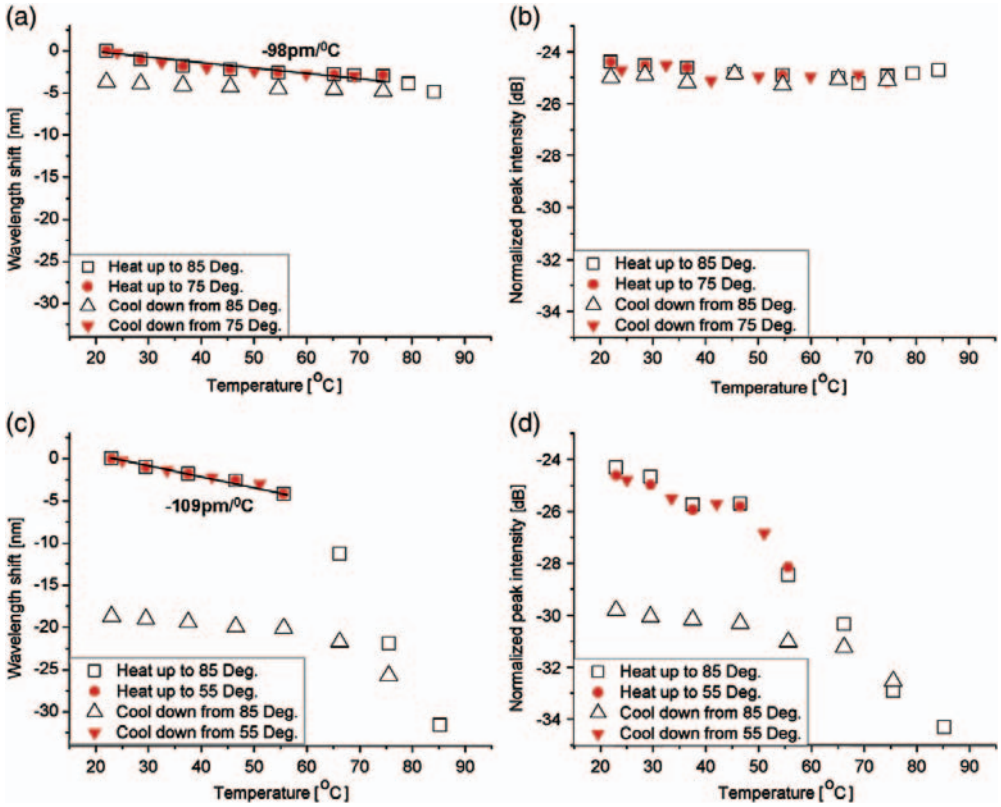

Fig. 3. Bragg wavelength shift and peak intensity variation with temperature for two consecutive heating and cooling cycles in the annealed POF (a–b) and the non-annealed POF (c–d). The temperature response of the Bragg wavelength in (a) and (c) show an approximately linear thermal sensitivity of −98 pm/°C and −109 pm/°C for the annealed and non-annealed POF, respectively.

Hysteresis of the wavelength shift was observed once the temperature was taken to above the threshold, i.e., 75 °C for the annealed POF grating and 55 °C for the non-annealed POF grating. The temperature threshold is largely explained by the fiber shrinking and related to the thermal history of the fiber [10,22]. This hypothesis is supported by the different thermal thresholds of the annealed and non-annealed POF.

When comparing with the non-annealed POF grating, the FBG in the annealed POF showed a higher operational temperature. This improvement is well-known and is mainly due to the releasing of the drawing-induced frozen-in stress by the annealing process [22]. Importantly, the annealed POF grating can provide much more stable peak intensity during the temperature cycle below the threshold temperature, as shown in Fig. 3(b). In contrast, the FBG in the non-annealed POF experienced a constant yet reversible decrease of the peak intensity when the temperature was still lower than the threshold, as shown in Fig. 3(d). The results indicate that in the case of non-annealed POF grating the temperature increase would not only decrease the refractive index of the POF, as indicated by the temperature response of resonance wavelength, but also probably decrease the index modulation of the FBG, which determines the strength of the grating, i.e., the peak intensity of its reflectivity. As shown in Fig. 3(a) and (c), from the fitting of the quasi-linear part of the wavelength shift it can be found that the thermal sensitivity of both FBGs is almost the same. This means that the annealing process does not significantly change the TOC of PMMA.

The fact that the annealing process does not eliminate the threshold totally can be further validated by the thermal stability experiments. As shown in Fig. 4, the grating temperature was increased to and kept at 66 °C and 85 °C for both annealed and non-annealed POF. As demonstrated in Fig. 4(b–d), it was found that both the resonance wavelength and the peak power of the gratings were varying during the monitoring time up to hours once the temperature was beyond the threshold. When the annealed POF grating was subject to 66 °C and after the stable resonance wavelength reached, as shown in Fig. 4(a), no further wavelength shifting and only 2 dB peak power decrease was identified over 5.5 h.

The unavoidable decrease of the peak power seen in Fig. 4 would lead to the gratings being barely observable, especially if the temperature was above the threshold temperature of the gratings, i.e., 75 °C for the annealed POF grating and 55 °C for the non-annealed POF grating. We observed that when the grating was subject to a temperature beyond the threshold for hours its peak power could not recover to the original status after returning to room temperature (results not shown). In contrast, as shown in Fig. 3(b), the annealed POF grating could resume to its original peak power after a short 20 min exposure to a temperature above its threshold 75 °C. This means that the long-term thermal stability of even the annealed POF FBGs is still a problem at high temperature.

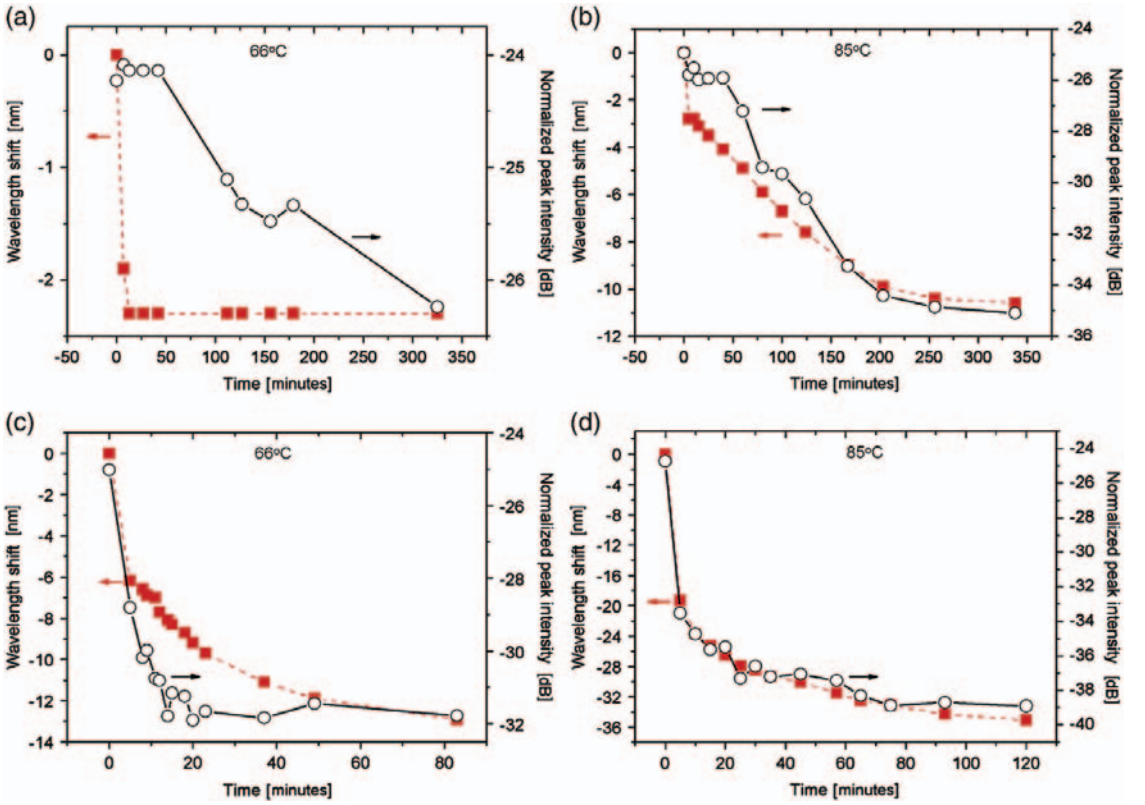

Fig. 4. (a), (b) are thermal stability tests of FBG in annealed POF at 66 °C and 85 °C. (c) and (d) show thermal stability of the FBG in non-annealed POF at the same temperature. Square-dash line represents the relative resonance wavelength of FBG, circle-solid line represents the normalized peak intensity of FBG.

2.3. Tensile strain characterization of FBGs

It is well-known that the annealing process would give a higher operational temperature of the POF FBGs. We are interested in accelerometers and fiber-optical microphones based on POF FBG strain sensor. This means that any improvement of the operational strain regime by annealing would be very important. The strain tuning of the polymer fiber Bragg gratings was investigated by mechanical stretching, and the strain characteristics of the gratings in both annealed and non-annealed POF were compared. The two ends of the POF were clamped to two micro-translation stages, with one of them fixed and used to butt-couple the POF to a silica fiber, and the other stage can move longitudinally to apply the axial strain to the grating manually with a very low loading speed. The axial strain values were determined by dividing the fiber longitudinal elongation by the length of fiber between the two clamping points. The longitudinal displacement accuracy of the moving translation stage is 0.01 mm. All gratings were fabricated with a same exposure time, i.e., 60 min, which give them a similar peak intensity of about −25 dB.

The gratings were left to stabilize for about 10 min each time the tensile strain was changed before reading the reflection spectrum. A single strain loading cycle experiment was carried out firstly to study the strain tuning responses of the two kinds of gratings, as shown in Fig. 5. As shown in Fig. 5(b) and (d), for the non-annealed POF grating, a strong decrease of peak intensity was found when the strain loading was taken over 2.5%, and almost 7 dB peak intensity loss was introduced by the 3.75% strain loading, which was also accompanied by peak splitting [9], which made the grating peak very difficult to identify. As shown in Fig. 5(a) and (c), the strain tuning response of the annealed POF grating also showed a peak intensity decrease when the strain was over 2.81%, but interestingly, the peak intensity only decreases 3 dB even when the applied strain was 6.55%, which is more than twice the strain the non-annealed POF grating can hold. Furthermore, no peak splitting was found in the annealed POF grating even at strain up to 6.55%.

Both gratings showed a quasi-linear response of the wavelength shift over the whole strain loading range. From the data fitting, it was found that the strain sensitivity of both gratings is similar, i.e., about 1.3 pm/με for the non-annealed POF and about 1.37 pm/με for the annealed POF. This is reasonable since the strain sensitivity only depends on the Young's modulus and geometric factors of the POF gratings. We think that the small difference of the strain sensitivity between two gratings is probably due to the small difference of the fiber diameter which has been induced by the shrinking effect of the annealing process.

The recoverability of the grating has been examined through the strain loading and unloading process, as shown in Fig. 6. In the experiments, the strain was gradually applied to both gratings up to 2.81% and 3.75% separately and then gradually unloaded to zero strain. Judging from the variation of the resonance wavelengths and the peak intensities of the gratings during the loading–unloading experiment, as shown in Fig. 6(d), an observable hysteresis in the

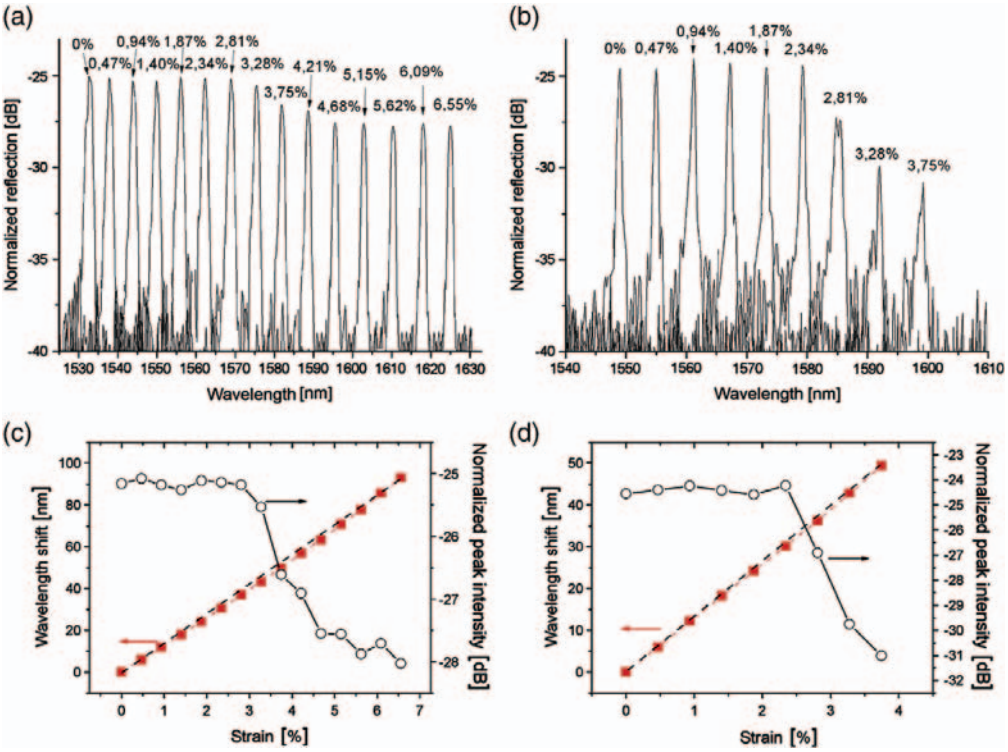

Fig. 5. Single strain loading cycle of FBG in the annealed POF (a, c) and non-annealed POF (b, d). (a, b): strained tuned reflection spectra, (c, d): the dash lines are the fitting of the Bragg wavelength shift. Squares-dashed line represents the relative resonance wavelength shift of FBG, and circles-solid line represents the normalized peak intensity variation of FBG.

resonance wavelength appeared at a strain of 3.75% for the grating in non-annealed POF. For the annealed POF, in contrast, the grating was recoverable also at 3.75% strain, as shown in Fig. 6(c). If we define the operational strain regime of POF FBG as up to where the peak intensity has decreased by 3 dB and the resonance wavelength is still recoverable, the experimental results showed that the operational strain range should be up to about 2.8% for the non-annealed POF grating and at least up to about 3.8% for the annealed POF grating.

Our experiments also showed that once the fibers were strained over threshold, for example, when strain was taken over 2.8% for the non-annealed POF grating or over 3.8% for the annealed POF grating, it took longer time for the gratings to stabilize and return to the original state when the strain was unloaded. The gratings did not return to their original states when the applied strain was over 3.75% for the non-annealed POF grating and over 6.55% for the annealed POF gratings even over 24 h. This could be explained by that the gratings have been strained over their elastic limits.

The comparison of the two kinds of gratings through the strain tuning experiment showed that for the annealed POF there was a significant improvement in the stability of the peak intensity, no peak splitting at high loading strain was found and much higher strain can be applied to the fiber. As we mentioned before, the index modulation of the grating determines the grating strength, so the constant peak intensity means a much more stable modulation of index in the annealed POF grating under strain tuning. The unavoidable peak intensity decrease might be due to the increase of the mode propagation loss when the core of the fiber became smaller under the high longitudinal strain.

3. Conclusions

A detailed characterization of FBGs in commercial step-index POFs was presented. Through a study of the growth dynamics of the grating, the thermal effect of the UV-induced heating was shown to result in a reversible 0.15 nm blue shift in the resonance wavelength, which disappeared after the laser was turned off. We estimated the UV-induced increase in the temperature to be approximately 15 °C. This is below the damage temperature, which is why the blue shift was reversible. Furthermore, no significant change in the photosensitivity of the POF was observed due to the annealing process before the grating writing.

The thermal tuning experiments showed that hysteresis in the wavelength shift and peak intensity was observed once the temperature was taken to above a threshold, which was 75 °C for the grating in the annealed POF and 55 °C for the grating in the non-annealed POF. Comparing with the non-annealed POF grating, the grating in the annealed POF can offer much more stable peak intensity during the temperature cycling below the threshold temperature. The similar thermal sensitivity of both gratings means that the annealing process does not change the TOC of the material significantly. The existence of a temperature threshold even after the annealing process was further validated by thermal stability experiments which showed a 10 dB drop in the reflected peak intensity over 6 h at 85 °C, and it shows that the long-term stability of even the annealed POF FBGs is still a problem.

The strain tuning of the POF FBGs by mechanical stretching demonstrated that the operational strain limits without any

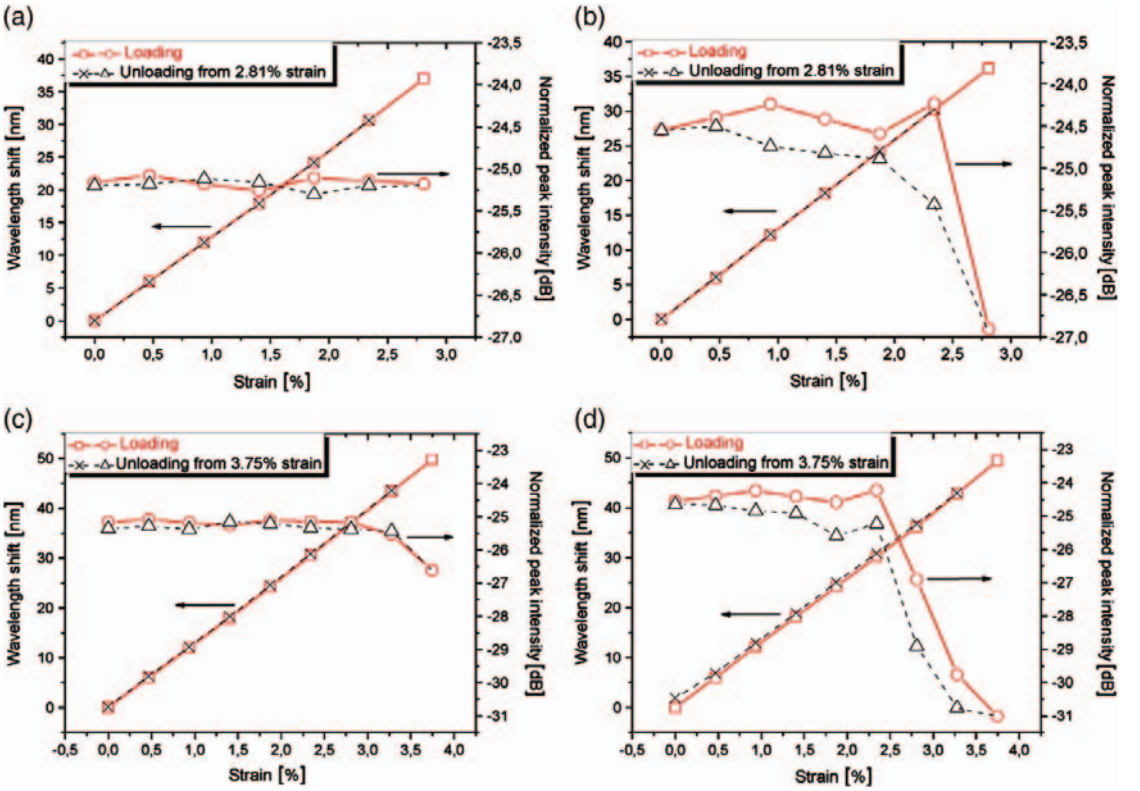

Fig. 6. Strain tuning of FBG in the annealed POF (a, c) and non-annealed POF (b, d). Strain loading and unloading experiments at a maximum loading strain of 2.81% (a–b) and 3.75% (c–d). Squares-dashed line represents the relative resonance wavelength shift of FBG, and circles-solid line represents the normalized peak intensity variation of FBG.

hysteresis is 2.8% for the non-annealed POF grating and 3.8% for the annealed POF grating. The strain sensitivity of both the annealed and the non-annealed POF gratings is similar, which is about 1.37 pm/με and about 1.3 pm/με, respectively. There was a significant improvement of the peak intensity stability, no peak splitting at high loading strain was found, and much higher strain can be applied to the annealed POF grating.

Acknowledgements

We would like to acknowledge support from the Danish National Advanced Technology Foundation.

References

[1] M. Silva-Lopez, A. Fender, W.N. MacPherson, J.S. Barton, J.D.C. Jones, D. Zhao, H. Dobb, L. Zhang, I. Bennion, Opt. Lett. 30 (2005) 3129.
[2] K. Kalli, H.L. Dobb, D.J. Webb, K. Carroll, M. Komodromos, C. Themistos, G.D. Peng, Q. Fang, I.W. Boyd, Opt. Lett. 32 (2007) 214.
[3] H. Dobb, K. Carroll, D.J. Webb, K. Kalli, M. Komodromos, C. Themistos, G.D. Peng, A. Argyros, M.C.J. Large, M.A. van Eijkelenborg, Q. Fang, I.W. Boyd, Proc. SPIE 6189 (2006) 1.
[4] J.M. Yu, X.M. Tao, H.Y. Tam, Opt. Lett. 29 (2004) 156.
[5] K. Kalli, H.L. Dobb, D.J. Webb, K. Carroll, C. Themistos, M. Komodromos, G.D. Peng, Q. Fang, I.W. Boyd, Meas. Sci. Technol. 18 (2007) 3155.
[6] M. Stecher, R.J. Williams, O. Bang, G.D. Marshall, M.J. Withford, G.E. Town, Proc. POF2009- The 18th international conference on plastic optical fibers, 2009.
[7] A. Baum, W. Perrie, P.J. Scully, M. Basanta, C.L.P. Thomas, N.J. Goddard, P.R. Fielden, P.R. Chalker, OFS, , 2006.
[8] Z. Xiong, G.D. Peng, B. Wu, P.L. Chu, IEEE Photon. Technol. Lett. 11 (1999) 352.
[9] H.Y. Liu, H.B. Liu, G.D. Peng, Opt. Commun. 251 (2005) 37.
[10] H.Y. Liu, G.D. Peng, P.L. Chu, IEEE Photon. Technol. Lett. 13 (2001) 824.
[11] H.B. Liu, H.Y. Liu, G.D. Peng, P.L. Chu, Opt. Commun. 219 (2003) 139.
[12] H.Y. Liu, G.D. Peng, P.L. Chu, IEEE Photon. Technol. Lett. 14 (2002) 935.
[13] H.Y. Liu, H.B. Liu, G.D. Peng, P.L. Chu, Opt. Commun. 220 (2003) 337.
[14] G.D. Peng, P.L. Chu, X. Lou, R.A. Chaplin, J. Electr. Electron. Eng. Aust. (1995) 289.
[15] H.Y. Liu, G.D. Peng, P.L. Chu, Opt. Commun. 204 (2002) 151.
[16] H.Y. Liu, G.D. Peng, P.L. Chu, Y. Koike, Y. Watanabe, Electron. Lett 37 (2001) 347.
[17] D.J. Webb, K. Kalli, C. Zhang, M. Komodromos, A. Argyros, M. Large, G. Emiliyanov, O. Bang, E. Kjaer, Proc. SPIE 6990 (2008) L9900.
[18] E.E. Shafee, Polym. Degrad. Stabil. 53 (1996) 57.
[19] W.J. Tomlinson, I.P. Kaminow, E.A. Chandross, R.L. Forkland, W.T. Silvfast, Appl. Phys. Lett. 16 (1970) 486.
[20] M.J. Bowden, E.A. Chandross, I.P. Kaminow, Appl. Opt. 13 (1974) 112.
[21] C. Jiang, M.G. Kuzyk, J.L. Ding, W.E. Johns, D.J. Welker, J. Appl. Physiol. 92 (2002) 4.
[22] K. Carroll, C. Zhang, D.J. Webb, K. Kalli, A. Argyros, M.C.J. Large, Opt. Express 15 (2007) 8844.
[23] D. Webb, K. Kalli, in: A. Cusano, A. Cutolo, J. Albert (Eds.), Chapter 15 of Book "Fiber Bragg Grating Sensors: Recent Advancements, Industrial Applications and Market Exploitation", Bentham Science Publishers Ltd., 2009, p. 1.
[24] M.C.J. Large, L. Poladian, G. Barton, M. Eijkelenborg, Microstructured Polymer Optical Fibres, Springer, 2008.
[25] J. Jensen, P. Hoiby, G. Emiliyanov, O. Bang, L. Pedersen, A. Bjarklev, Opt. Express 13 (2005) 5883.
[26] A. Dupuis, N. Guo, Y. Gao, N. Godbout, S. Lacroix, C. Dubois, M. Skorobogatiy, Opt. Lett. 32 (2007) 109.
[27] G. Emiliyanov, J.B. Jensen, O. Bang, P.E. Hoiby, L.H. Pedersen, E.M. Kjær, L. Lindvold, Opt. Lett. 32 (2007) 460.
[28] G. Emiliyanov, J.B. Jensen, O. Bang, P.E. Hoiby, L.H. Pedersen, E.M. Kjaer, L. Lindvold, Opt. Lett. 32 (2007) 1059.
[29] A. Stefani, K. Nielsen, H.K. Rasmussen, O. Bang, "Microstructured polymer optical fibers cutting optimization and analysis", unpublished, (2010).

Paper 3

Narrow Bandwidth 850 nm Fiber Bragg Gratings in Few-Mode Polymer Optical Fibers

A. Stefani, W. Yuan, C. Markos and O. Bang

IEEE Photonics Technology Letters, vol. 23(10), pp. 660-662 (2011).

Narrow Bandwidth 850-nm Fiber Bragg Gratings in Few-Mode Polymer Optical Fibers

Alessio Stefani, Wu Yuan, Christos Markos, and Ole Bang

***Abstract*—We report on the inscription and characterization of narrow bandwidth fiber Bragg gratings (FBGs) with 850-nm resonance wavelength in polymer optical fibers (POFs). We use two fibers: an in-house fabricated microstructured POF (mPOF) with relative hole size of 0.5 and a commercial step-index POF, which supports six modes at 850 nm. The gratings have been written with the phase-mask technique and a 325-nm HeCd laser. The mPOF grating has a full-width at half-maximum (FWHM) bandwidth of 0.29 nm and the step-index POF has a bandwidth of 0.17 nm. For both fibers, the static tensile strain sensitivity is measured to be 0.71 pm/$\mu\varepsilon$ at 850 nm and 1.3 pm/$\mu\varepsilon$ at 1550 nm.**

***Index Terms*—Fiber Bragg grating (FBG), polymer optical fiber, fiber-optic sensors.**

I. Introduction

FIBER-OPTIC sensors based on Fiber Bragg Gratings (FBGs) have many important industrial applications [1], [2]. The fiber material of choice in industrial applications has so far been silica, because of its low loss and resistance to high temperatures. Polymer optical fiber (POF) FBGs have been used for strain and temperature measurements because of the low Young's modulus, high failure strain, and high thermal sensitivity of polymer compared to silica [3]–[8]. The POF FBGs reported until recently had a resonance wavelength around 1550 nm, primarily because of the availability of cheap telecommunications equipment at that wavelength. However, in contrast to silica fibers, POFs made of for example standard poly(methyl methacrylate) (PMMA) [9] and Topas [10], [11] have very high losses of more than 100 dB/m around 1550 nm. This makes it hard to work with POFs at the telecommunication wavelengths, unless using very short sections of fiber.

A considerable decrease in the material loss to about 2 dB/m can be achieved by working at a lower wavelength [7], [9]. In particular, the 2 dB/m target is possible at 850 nm at which CMOS (complementary metal-oxide-semiconductor) technology is available. For this reason there is currently a strong push in the sensor and interrogator community to develop devices at 850 nm. A 962 nm FBG has been written into a POF [12], but at this wavelength the loss of standard PMMA and Topas is still significant and the FBG suffered from a large zeroth-order component of the phase mask used in the writing process.

More importantly, it was recently reported that a 827 nm FBG could be written into a polymer fiber using a 30 mW 325 nm HeCd CW Laser and writing times around 2 hours through a phase-mask with period 557.20 nm [13]. The fiber was a multimode microstructured POF (mPOF) from Kiriama Pty Ltd, Sydney, Australia, with a large core diameter of 50 μm and 3 rings of holes. The loss was not quoted. The authors reported on prior problems with writing FBGs in both POFs and mPOFs, which they solved for the mPOF by adjusting the distance between the fiber and the phase-mask [13]. In the successful 827 nm writing experiment, the mPOF had a quite large core diameter. This makes it easier to write an FBG into the mPOF, which is otherwise very difficult due to the scattering of light at the air-polymer interface at all the holes [4]. However, the large core unfortunately makes the fiber heavily multimoded, which combined with a relatively short grating length of 1.8 mm, made the spectrum broad, with a full-width at half-maximum (FWHM) bandwidth of 2.45 nm.

For sensing applications narrow bandwidth FBGs and single-mode operation is important. This means that the core diameter of the mPOF is small and it is difficult to fabricate an FBG. Here we report the fabrication of narrow bandwidth 850 nm FBGs in both few-mode POFs (bandwidth 0.17 nm) and mPOFs (bandwidth 0.29 nm).

II. Grating Writing and Loss Measurements

The FBGs have been written using a phase-mask and a 30 mW 325 nm CW HeCd laser (IK5751 I-G, Kimmon) as in [13]. We expanded the beam to 1.2 cm with a cylindrical lens along the direction of the fiber axis and focused it in the orthogonal direction with a second cylindrical lens into the core. The pattern imprinted into the fiber was determined by the phase mask (Ibsen Photonics), placed just above the fiber, whose period of 572.4 nm was optimized for polymer fibers to give 850 nm gratings in the CMOS window.

We used two fibers. (1) a PMMA mPOF that we fabricated ourselves, with 3 rings of holes separated with a pitch of 6 μm and a hole size of 3 μm (see Fig. 1). The relative hole size of 0.5 means that the mPOF is few-mode at 850 nm [14]. (2) a commercially available PMMA step-index POF, which has a polystyrene doped PMMA core (MORPOF02, Paradigm Optics). The fiber has a quoted numerical aperture (NA) of 0.27 at 1300 nm and closer inspection shows that the core is not circular, but elliptical, with a diameter of 2 μm along the short axis and 6 μm along the long axis (see Fig. 1). The normalized frequency $V = (2\pi a)/(\lambda)\mathrm{NA}$, where a is the core radius, is then 2.606 at 1300 nm if considering an average core radius of 4 μm.

Manuscript received August 25, 2010; revised November 08, 2010; accepted February 27, 2011. Date of publication March 10, 2011; date of current version May 04, 2011. This work was supported by the Danish National Advanced Technology Foundation.

A. Stefani, W. Yuan, and O. Bang are with DTU Fotonik, Department of Photonics Engineering, Technical University of Denmark, 2800, Kgs. Lyngby, Denmark (e-mail: alste@fotonik.dtu.dk).

C. Markos is with the Department of Computer Engineering and Informatics, University of Patras, 26500, Patra, Greece.

Color versions of one or more of the figures in this letter are available online at http://ieeexplore.ieee.org.

Digital Object Identifier 10.1109/LPT.2011.2125786

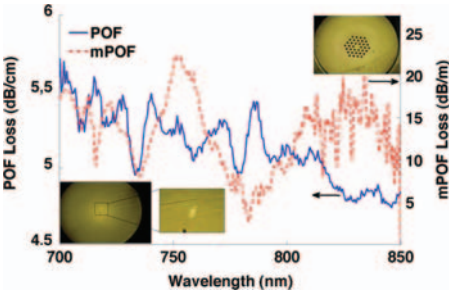

Fig. 1. Loss profile of the mPOF (red dashed line) and the step index POF (blue solid line) with insets showing the fiber end facets.

Scaling for 850 nm the V number becomes 3.98, which indicates that the fiber will support 6 modes at 850 nm. Few-mode POFs and mPOFs have been used successfully before for FBG inscription before, so we anticipate to obtain a reasonably clean reflection spectrum [4].

Before focusing on the FBG writing, we report in Fig. 1 the losses of the two fibers. The loss for the commercial POF has been given by the manufacturer to be 3 dB/cm at 1550 nm, 1 dB/cm at 1000 nm, and less than 0.2 dB/m at 650 nm. Our cutback measurement revealed that the loss was much higher than that. It was so high that we could not use pieces longer than 20 cm and had to settle for only 3 cuts in the cutback measurement. The small number of cuts and the fact that the fiber is multimode at 850 nm means that the loss spectrum has significant oscillations. Nevertheless, we can conclude that the fiber loss is above 100 dB/m even at short wavelength, which explains the fact that nobody were able to write good FBGs in this fiber so far.

The loss of the mPOF, as obtained by a cutback measurement with 14 cuts, is shown in Fig. 1. The mPOF is made from cheap PMMA from Vink with nonoptimal preform fabrication conditions. The measured 10 dB/m loss at 850 nm is thus significantly higher than the record mPOF loss of about 2 dB/m at 850 nm [7]. Nevertheless, 10 dB/m is more than an order of magnitude lower than the loss of the commercial POF. Further optimization in terms of cooling liquid used for preform drilling and proper washing and drying in clean atmosphere after drilling, are underway.

For the characterization of the FBG reflection spectrum we use an 850 nm circulator. The first arm of the circulator was connected to a SuperK Versa broadband source from NKT Photonics A/S. The broadband signal was then butt-coupled to the fiber from the second arm of the circulator. The reflection was collected and measured at the third arm of the circulator with an Optical Spectrum Analyzer (Ando AQ6317B).

The measured reflectance spectra, recorded with -18.5 dBm output power from the SuperK source, are shown in Fig. 2. The spectrum for the mPOF (POF) was recorded before saturation after a writing time of 185 min. (60 min.), where both FBGs show a normalized reflected power of about -40 dB, which includes coupling loss and fiber propagation loss. The longer writing time for the mPOF is due to the strong scattering of light at the holes, which significantly reduces the power reaching the core.

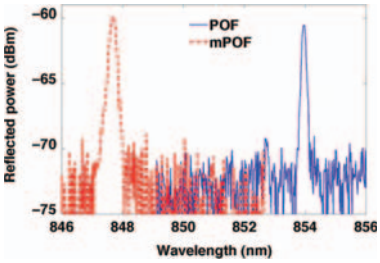

Fig. 2. Reflection spectrum of mPOF (red dashed line) and POF (blue full line) FBGs. The spectrum for the mPOF (POF) was recorded after a writing time of 185 min. (60 min.).

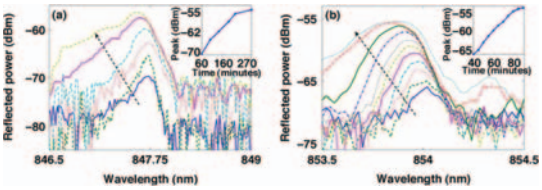

Fig. 3. FBG reflection spectra for increasing writing time for the mPOF (a) and POF (b). Inserts show the peak reflected power versus time.

The reflection spectrum of the mPOF (POF) has a central wavelength of 847.60 nm (853.96 nm) and a FWHM bandwidth of 0.29 nm (0.17 nm). The narrow line width is evidence to the fact that the fibers are few-moded. Both spectra were recorded during the writing process, where the fiber was given a small tension to keep it straight. After the writing, when the tension is released, the peak wavelength will blue shift a couple of nanometers. The noise level is 10 dB lower than the peak power, which means that the FBG resonance can be detected and tracked by conventional interrogators, such as the IMON from Ibsen Photonics.

The growth dynamics of the FBG writing process is shown in Fig. 3. It displays the typical scenario, in which the peak grows faster in the beginning and then saturates [15]. After 185 (60) minutes the spectrum of the mPOF (POF) starts to broaden more and more and side peaks start to appear. This means that the optimum writing time is around 185 min. for the mPOF and 60 min. for the POF. The saturation time, defined as the writing time after which the reflectance saturates, while the FWHM increases rapidly, is around 210 min. for the mPOF and 90 min. for the POF. During the initial rapid growth a standard blue shift of the peak is observed due to laser induced heating, which will disappear after the laser is turned off [6].

III. Strain Sensitivity Measurements

Here we perform strain measurements and check the measured sensitivities of 850 nm and 1550 nm FBGs against each other. The strain sensitivity experiments are particularly relevant due to the applications for which the 850 nm gratings are intended i.e., fiber-optic sensing of acceleration and sound.

The sensitivity of the FBG is defined as [2], [16]

$$\frac{\partial \lambda_B}{\partial \varepsilon} = C\lambda_B,$$
$$C = \frac{2 - n_{\text{eff}}^2[P_{12} - \nu(P_{11} + P_{12})]}{2} \quad (1)$$

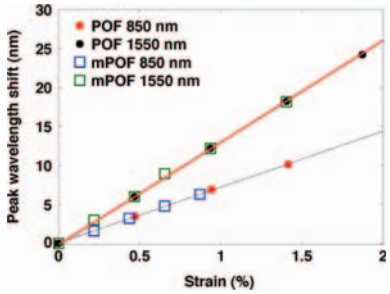

Fig. 4. Strain sensitivity of 1550 nm FBGs in POF (dots) and mPOF (squares), fitted to a straight solid line. Strain sensitivity of 850 nm FBGs in POF (dots) and mPOF (squares), fitted to a straight dashed line.

where $\lambda_B = 2n_{\text{eff}}\Lambda$ is the Bragg wavelength, n_{eff} is the effective index of the fundamental core mode, and Λ is the grating period. The parameter C depends only on the fiber material, with $P_{i,j}$ being the Pockel's (piezo) coefficients of the stress-optic tensor and ν the Poisson's ratio. The change in C over the wavelength range 850–1550 nm can be neglected and thus (1) shows that the ratio between the sensitivity at 1550 nm and at 850 nm of a given fiber is approximately equal to the ratio of the resonance wavelengths, which is 1.82.

Fig. 4 shows the wavelength shift versus applied strain for both 850 nm and 1550 nm gratings in both mPOFs and POFs. Both 850 nm mPOF and POF FBGs respond linearly to the applied strain with an identical sensitivity of 0.71 pm/$\mu\varepsilon$. At 1550 nm both FBGs display a linear response with an identical sensitivity of 1.3 pm/$\mu\varepsilon$, which corresponds to an earlier measurement on this particular 1550 nm POF FBG [6]. The ratio of sensitivities is $1.3/0.71 = 1.83$, which is very close to the theoretically predicted value of 1.82.

We note that the sensitivity can be different from fiber to fiber depending on the material and on the thermal history of the fiber [6] e.g., 1.46 pm/$\mu\varepsilon$ was reported in [18] and 1.13 pm/$\mu\varepsilon$ was reported in [17] around 1550 nm, compared to the 1.3 pm/$\mu\varepsilon$ measured here and in [6]. Thus, even though both our fibers are made of PMMA, the fact that the POF is doped in the core, PMMA can vary from manufacturer to manufacturer, and the drawing conditions have been different, means that our mPOF and POF FBGs should not *a priori* have the same sensitivity. It is thus an interesting result that we find the same sensitivities of these two types of PMMA polymer optical fibers. Since our setup has been the same for the different measurements, this hints at that in fact also the different experimental setups play a role.

IV. Conclusion

In conclusion, we have reported the first narrow bandwidth FBG at 850 nm in two types of few-moded POFs. The 850 nm FBG in our own mPOF has a bandwidth of 0.29 nm, whereas the bandwidth of the FBG in a commercial step-index POF is 0.17 nm. We have measured their strain sensitivities to be identical 0.71 pm/$\mu\varepsilon$ at 850 nm and 1.3 pm/$\mu\varepsilon$ at 1550 nm.

The loss of the commercial PMMA step-index POF is too large for it to be relevant in sensing. However, with a loss of 10 dB/m at 850 nm and a bandwidth of 0.29 nm, the PMMA mPOF FBG is definitely a candidate for future strain sensing devices using CMOS technology, in particular when taking into account that the loss can be further reduced to 1 dB/m by improvement of the fabrication technology.

Acknowledgment

The authors acknowledge fruitful discussions with Prof. G. Town and Prof. D. Webb.

References

[1] D. Webb and K. Kalli, "Polymer fiber Bragg gratings," in *Fiber Bragg Grating Sensors: Recent Advancements, Industrial Applications and Market Exploitation*, A. Cusano, A. Cutolo, and J. Albert, Eds. Oak Park, IL: Bentham eBooks, 2011, pp. 292–312.

[2] A. D. Kersey, M. A. Davis, H. J. Patrick, M. LeBlanc, K. P. Koo, C. G. Askins, M. A. Putnam, and E. J. Friebele, "Fiber grating sensors," *J. Lightw. Technol.*, vol. 15, no. 8, pp. 1442–1463, Aug. 1997.

[3] Z. Xiong, G. D. Peng, B. Wu, and P. L. Chu, "Highly tunable Bragg gratings in single-mode polymer optical fibers," *IEEE Photon. Technol. Lett.*, vol. 11, no. 3, pp. 352–354, Mar. 1999.

[4] H. Dobb, D. J. Webb, K. Kalli, A. Argyros, M. C. J. Large, and M. A. van Eijkelenborg, "Continuous wave ultraviolet light-induced fiber Bragg gratings in few- and single-moded microstructured polymer optical fibers," *Opt. Lett.*, vol. 30, pp. 3296–3298, 2005.

[5] M. Silva-Lopez, A. Fender, W. N. MacPherson, J. S. Barton, J. D. C. Jones, D. Zhao, H. Dobb, L. Zhang, and I. Bennion, "Strain and temperature sensitivity of a single-mode polymer optical fiber," *Opt. Lett.*, vol. 30, pp. 3129–3131, 2005.

[6] W. Yuan, A. Stefani, M. Bache, T. Jacobsen, B. Rose, N. Herholdt-Rasmussen, F. K. Nielsen, S. Andresen, O. B. Sørensen, K. S. Hansen, and O. Bang, "Improved thermal and strain performance of annealed polymer optical fiber Bragg gratings," *Opt. Commun.*, vol. 28, pp. 176–182, 2011.

[7] M. Large, L. Poladian, G. Barton, and M. A. van Eijkelenborg, *Microstructured Polymer Optical Fibres*. New York, : Springer, 2008, pp. 1–20.

[8] I. P. Johnson, W. Yuan, A. Stefani, K. Nielsen, H. K. Rasmussen, L. Khan, D. J. Webb, K. Kalli, and O. Bang, "Optical fibre Bragg grating recorded in TOPAS cyclic olefin copolymer," *Electron. Lett.*, vol. 47, pp. 271–272, 2011.

[9] T. Kaino, "Absorption losses of low-loss plastic optical fibers," *Jpn. J. Appl. Phys. Part 1–Regul. Pap. Short Notes Rev. Pap.*, vol. 24, pp. 1661–1665, 1985.

[10] G. Emiliyanov, J. B. Jensen, O. Bang, P. E. Hoiby, L. H. Pedersen, E. Kjær, and L. Lindvold, "Localized biosensing with Topas microstructured polymer optical fiber," *Opt. Lett.*, vol. 32, pp. 460–462, 2007.

[11] G. Emiliyanov, J. B. Jensen, O. Bang, P. E. Hoiby, L. H. Pedersen, E. Kjær, and L. Lindvold, "Localized biosensing with Topas microstructured polymer optical fiber," *Erratum, Opt. Lett.*, vol. 32, p. 1059, 2007.

[12] Z. F. Zhang, C. Zhang, X. M. Tao, G. F. Wang, and G. D. Peng, "Inscription of polymer optical fiber Bragg grating at 962 nm and its potential in strain sensing," *IEEE Photon. Technol. Lett.*, vol. 22, no. 21, pp. 1562–1564, Nov. 1, 2010.

[13] I. P. Johnson, K. Kalli, and D. J. Webb, "827 nm Bragg grating sensor in multimode microstructured polymer optical fibre," *Electron. Lett.*, vol. 46, pp. 1217–1218, 2010.

[14] B. Kuhlmey, R. C. McPhedran, and C. M. de Sterke, "Modal cutoff in microstructured optical fibers," *Opt. Lett.*, vol. 27, pp. 1684–1686, 2002.

[15] H. Y. Liu, H. B. Liu, G. D. Peng, and P. L. Chu, "Observation of type I and type II gratings behaviour in polymer optical fiber," *Opt. Commun.*, vol. 220, pp. 337–343, 2003.

[16] L. Rindorf and O. Bang, "Sensitivity of photonic crystal fiber grating sensors: Biosensing, refractive index, strain, and temperature sensing," *J. Opt. Soc. Amer. B*, vol. 25, pp. 310–325, 2008.

[17] X. Chen, C. Zhang, D. J. Webb, G. D. Peng, and K. Kalli, "Bragg grating in a polymer optical fibre for strain, bend and temperature sensing," *Meas. Sci. Technol.*, vol. 21, pp. 3155–3164, 2010.

[18] H. Y. Liu, H. B. Liu, and G. D. Peng, "Tensile strain characterization of polymer optical fibre Bragg gratings," *Opt. Commun.*, vol. 251, pp. 37–43, 2005.

Paper 4

Optical fibre Bragg grating recorded in TOPAS cyclic olefin copolymer

I.P. Johnson, W.Yuan , A Stefani, K Nielsen, H.K. Rasmussen, L. Khan, D.J. Webb, K. Kalli and O. Bang

Electronics Letters, vol. 47(4), pp. 271-272 (2011).

Optical fibre Bragg grating recorded in TOPAS cyclic olefin copolymer

I.P. Johnson, W. Yuan, A. Stefani, K. Nielsen, H.K. Rasmussen, L. Khan, D.J. Webb, K. Kalli and O. Bang

A report is presented on the inscription of a fibre Bragg grating into a microstructured polymer optical fibre fabricated from TOPAS cyclic olefin copolymer. This material offers two important advantages over poly (methyl methacrylate), which up to now has formed the basis for polymer fibre Bragg gratings: TOPAS has a much lower water affinity and has useful properties for biosensing. The grating had a Bragg wavelength of 1569 nm and a temperature sensitivity of -36.5 ± 0.3 pm/°C.

Introduction: Over the last twenty years, silica fibre Bragg grating (FBG) sensor technology has been developed to the point where it is now mature enough to find commercial application in a variety of fields, such as structural health monitoring and down-hole sensing for the oil and gas industry. Grating sensors in polymer optical fibre (POF) have been studied for about ten years [1], but remain much less well developed. Nevertheless there appear to be good reasons for pursuing that development owing to the rather different properties of POF compared to silica, especially its much lower Young's modulus [2] and its ability to survive much higher strains [3].

Research to date on POF gratings has essentially involved just one material, poly (methyl methacrylate) (PMMA), with fibres being either fabricated entirely out of this material, in the case of microstructured fibres [4], or based on this material with the addition of dopants in the fibre core, in the case of step index fibres [5]. However there are many other transparent polymers with properties that might be utilised for sensors, if they can be drawn into fibre and if they possess a suitable photosensitivity to permit grating inscription. One example is TOPAS cyclic olefin copolymer. Unlike PMMA, this material is chemically inert, but it has been shown to be possible to fabricate localised biosensors by treatment with antraquinon followed by UV activation [6, 7]. Furthermore, TOPAS has a much reduced affinity for water compared to PMMA [8]. which may prevent the cross-sensitivity to humidity that is an issue for PMMA-based FBGs [9]. Interestingly, TOPAS is also an ideal material for terahertz fibres, because it becomes transparent with strongly reduced material dispersion in the terahertz frequency range [10].

Photosensitivity has been reported in some early TOPAS fibre [11], but the results obtained then were not very reproducible, the grating was visible in transmission but curiously not in reflection, and temperature testing suggested a surprisingly large and positive Bragg wavelength sensitivity. In this Letter, we report on the successful and repeatable inscription of FBGs in microstructured fibre fabricated from TOPAS, and characterise the temperature response of the devices, which we now repeatedly and reliably measure to be negative.

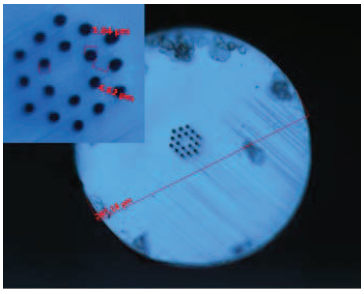

Fig. 1 *Microscope image of cleaved end face of TOPAS fibre of diameter 287 μm*
Inset: Magnified view of core region

Experiment: A solid cylindrical preform of TOPAS 8007-F-04 of 6 cm diameter was drilled with two rings of 3 mm air holes to provide light guidance and drawn down to an all TOPAS fibre in a two stage process. The resulting fibre had a diameter of 270 μm, a hole pitch of 8.5 μm and a hole diameter of 3.8 μm, and was singlemode at 1550 nm; see Fig. 1. Grating inscription was carried out using a 325 nm HeCd laser commonly used for grating fabrication with PMMA based fibre (Kimmon IK3301R-G). The fibre was mounted horizontally in a v-groove for support and the beam focused down from above onto the fibre using a cylindrical lens of focal length 10 cm. The UV light passed through a phase mask of period 1034.2 nm optimised for 325 nm light and supported directly on the fibre. The growth of the grating was monitored by butt coupling an angle cleaved singlemode silica fibre lead from a 2×2 coupler to the TOPAS fibre, which had been cleaved using a razor blade at room temperature. The grating was illuminated using a broadband light source (Thorlabs, Broadband ASE light source) and monitored on an optical spectrum analyser (HP86142A). A small amount of index matching gel was used to reduce Fresnel reflections from the end of the silica fibre. With a beam power of 30 mW approximately 45 minutes were required for the gratings to reach saturation, see Fig. 2. The reflection spectrum from the 1.8 mm-long grating is shown in Fig. 3; the Bragg wavelength is 1567.9 nm and the bandwidth (full width at half maximum) is 0.75 nm.

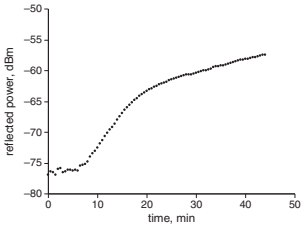

Fig. 2 *Growth in reflectivity against time during grating inscription*
Background noise level is around −77 dBm

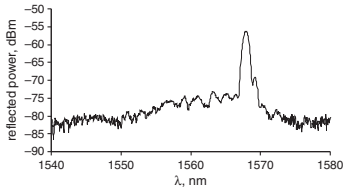

Fig. 3 *Reflection spectrum from FBG in TOPAS fibre*

TOPAS has the same high attenuation as PMMA in the 1550 nm spectral region, which limits practical fibre lengths to around 10 cm. Consequently, following inscription, the grating was glued to the end of a singlemode silica fibre lead to facilitate temperature testing. The grating was placed in an environmental chamber (Sanyo Gallenkamp) with the humidity held at 55% to remove any possibility of this influencing the measurements. The temperature was varied in the range 20 to 35°C and the results are shown in Fig. 4. From the data, the temperature sensitivity is obtained as -36.5 ± 0.3 pm/°C. This value is not very different from that obtained with PMMA-based FBGs at a similar wavelength (−43 pm/°C [12]) and confirms that the preliminary data obtained from the first TOPAS FBG showing a positive wavelength shift was in error [11]. Whilst the data presented in this Letter come from one grating, several were fabricated in the TOPAS fibre, with all exhibiting similar behaviour.

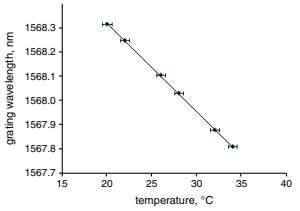

Fig. 4 *Thermal response of TOPAS FBG*

One disadvantage of TOPAS compared to PMMA is its glass transition temperature of 78°C [8], which is almost 30°C less than that of typical PMMA. This provides an upper limit on the usable temperature range.

Conclusion: We have proven definitively that fibre Bragg grating sensors can be reliably recorded in fibres fabricated from TOPAS cyclic olefin copolymer. For the first time this permits the development of POF-based strain sensors that should not suffer from significant cross-sensitivity to humidity and also aids the development of novel grating-based polymer fibre biosensors.

22 November 2010
doi: 10.1049/el.2010.7347
One or more of the Figures in this Letter are available in colour online.

I.P. Johnson, L. Khan and D.J. Webb (*Photonics Research Group, Aston University, Birmingham, B4 7ET, United Kingdom*)

E-mail: d.j.webb@aston.ac.uk

W. Yuan, A. Stefani, K. Nielsen and O. Bang (*DTU Fotonik, Department of Photonics Engineering, Technical University of Denmark, DK-2800 Kgs., Lyngby, Denmark*)

H.K. Rasmussen (*DTU Mekanik, Department of Mechanical Engineering, Technical University of Denmark, DK-2800 Kgs., Lyngby, Denmark*)

K. Kalli (*Nanophotonics Research Laboratory, Cyprus University of Technology, Limassol, 3036, Cyprus*)

References

1 Xiong, Z., Peng, G., Wu, B., and Chu, P.: 'Highly tunable Bragg gratings in single-mode polymer optical fibers', *IEEE Photonics Technol. Lett.*, 1999, **11**, (3), pp. 352–354
2 Brandrup, J.: 'Polymer handbook' (Wiley, 1999)
3 Aressy, M.: 'Manufacturing optimisation and mechanical properties of polymer optical fibre', M.Phil., 2006, Birmingham University
4 Dobb, H., Webb, D.J., Kalli, K., Argyros, A., Large, M.C.J., and van Eijkelenborg, M.A.: 'Continuous wave ultraviolet light-induced fiber Bragg gratings in few- and single-mode microstructured polymer optical fibers', *Opt. Lett.*, 2005, **30**, (24), pp. 3296–3298
5 Peng, G.D., and Chu, P.L.: 'Polymer optical fiber photosensitivities and highly tunable fiber gratings', *Fiber Integr. Opt.*, 2000, **19**, pp. 277–293
6 Emiliyanov, G., Jensen, J.B., Bang, O., Hoiby, P.E., Pedersen, L.H., Kjaer, E.M., and Lindvold, L.: 'Localized biosensing with Topas microstructured polymer optical fiber', *Opt. Lett.*, 2007, **32**, (5), pp. 460–462
7 Emiliyanov, G., Jensen, J.B., Bang, O., Hoiby, P.E., Pedersen, L.H., Kjaer, E.M., and Lindvold, L.: 'Localized biosensing with Topas microstructured polymer optical fiber: Erratum', *Opt. Lett.*, 2007, **32**, (9), p. 1059
8 www.topas.com
9 Zhang, C., Zhang, W., Webb, D.J., and Peng, G.D.: 'Optical fibre temperature and humidity sensor', *Electron. Lett.*, 2010, **46**, (9), pp. 643–644
10 Nielsen, K., Rasmussen, H.K., Adam, A.J.L., Planken, P.C.M., Bang, O., and Jepsen, P.U.: 'Bendable, low-loss Topas fibers for the terahertz frequency range', *Opt. Express*, 2009, **17**, (10), pp. 8592–8601
11 Webb, D.J., Kalli, K., Zhang, C., Komodromos, M., Argyros, A., Large, M., Emiliyanov, G., Bang, O., and Kjaer, E.: 'Temperature sensitivity of Bragg gratings in PMMA and TOPAS microstructured polymer optical fibres'. Photonic Crystal Fibers II2008, pp. L9900–L9900, art. no. 69900L
12 Webb, D.J., and Kalli, K.: 'Polymer fibre Bragg gratings', *in* Cusano, A. (Ed.): 'Fiber Bragg grating sensors: Thirty years from research to market' (Bentham eBooks, 2010)

Paper 5

Tunable Polymer Fiber Bragg Grating (FBG) Inscription: Fabrication of Dual-FBG Temperature Compensated Polymer Optical Fiber Strain Sensors

W. Yuan, A. Stefani, and O. Bang

IEEE Photonics Technology Letters, vol. 24(5), pp. 401-403 (2012).

Tunable Polymer Fiber Bragg Grating (FBG) Inscription: Fabrication of Dual-FBG Temperature Compensated Polymer Optical Fiber Strain Sensors

Wu Yuan, Alessio Stefani, and Ole Bang

***Abstract*— We demonstrate stable wavelength tunable inscription of polymer optical fiber Bragg gratings (FBGs). By straining the fiber during FBG inscription, we linearly tune the center wavelength over 7 nm with less than 1% strain. Above 1% strain, the tuning curve saturates and we show a maximum tuning of 12 nm with 2.25% strain. We use this inscription method to fabricate a dual-FBG strain sensor in a poly (methyl methacrylate) single-mode microstructured polymer optical fiber and demonstrate temperature compensated strain sensing around 850 nm.**

***Index Terms*— Fiber Bragg grating, polymer optical fiber, strain sensing, temperature compensation.**

DUE to the low Young's modulus (about 25 times lower than silica) and high elastic limit of over 10% (about 10 times higher than silica), fiber Bragg gratings (FBGs) in polymer optical fibers (POFs) are attractive for fiber-optical strain sensing [1-2]. POFs are also clinically acceptable, flexible and non-brittle, which makes the POF FBG a candidate for in-vivo biomedical applications [3-6]. FBGs have been reported in both step index POFs [2,7-9] and microstructured POFs (mPOFs) [9-13].

To date the majority of POFs and microstructured POFs (mPOFs) are made of poly (methyl methacrylate) (PMMA), which has a high thermo-optic coefficient and strongly absorbs water. PMMA FBG strain sensors therefore have a large cross-sensitivity to humidity and temperature [1,8,13]. The problem of humidity is strongly reduced by using POF FBGs made of the polymer TOPAS [4,5], which has a humidity sensitivity of less than 38.4 pm/%rH @1565nm [13]. This is more than 50 times less than POF FBGs made of PMMA [10,13]. However, both TOPAS and PMMA POF FBGs are still sensitive to temperature with similar sensitivities [1,13]. This is a major problem for POF (and silica) FBG strain sensors in practical applications, in particular in static strain sensing, where temperature variations occur on the same timescale as the variations in strain.

A simple solution is to use a second closely spaced and strain free FBG with a different resonance wavelength to provide an independent control of the temperature. The difference in resonance frequency between the two FBGs will then still measure the strain, but be independent of temperature, as was demonstrated for silica FBGs [14].

In this letter we demonstrate the concept of dual-FBG temperature compensated strain sensing for POF FBGs. To fabricate two (or more) POF FBGs with closely spaced resonance wavelengths we further demonstrate a simple technique for highly controlled tuning of the resonance wavelength of a POF FBG written with the standard phase-mask technique using the *same phase-mask*. By straining the POF during writing we can linearly tune the wavelength by 7 nm using only 1% strain. Going into the saturated regime we show 12 nm tuning with 2.25 % strain using a force of only 0.5 N due to the low Young's modulus of PMMA. This tuning range is about 5 times higher than for silica fibers [15] and can prove useful for future multiplexed sensor applications of POFs.

In an earlier experiment, two broadband FBGs were inscribed in a large-core multi-mode mPOF at 1562nm and 1545nm using also a single phase-mask, by thermally annealing the first grating before writing the next [16]. Our method differs from the annealing technique, in that it is much more controllable and works with POFs regardless of their drawing conditions and whether they have been annealed or not. Furthermore, we are here able to apply it to narrow-band single-mode POFs to demonstrate closely packed FBGs ideal for future multiplexed POF FBG strain sensors. Most importantly, we use the technique to present the first demonstration of temperature compensated FBG strain sensing in POFs.

In our experiments we use an endlessly single-mode PMMA mPOF fabricated by the drill-and-draw technique. The mPOF has a diameter of 180 μm and a solid core surrounded by three rings of air holes arranged in a hexagonal lattice. The air-hole diameter is on average 2$\pm$0.2 μm and the inter-hole pitch is on average 4.8$\pm$0.2 μm (see inset of Fig. 1(a)). The hole diameter to pitch ratio is thus d/Λ $\approx$0.41, which is below the threshold value of 0.42 that ensures endlessly single-mode operation [9].

We use a 325 nm HeCd CW laser (IK5751I-G, Kimmon) and a phase-mask with a uniform period of 572.4 nm (Ibsen Photonics) customized for 325 nm writing of mPOF FBGs with a resonance wavelength of $\lambda_B = 850$ nm. The fiber was supported by v-grooves on both sides of a gap to avoid reflection, and strain was applied to control the wavelength and keep the fiber straight during writing. Two hours of exposure time was used and the resulting gratings have a length of 10 mm. The applied strain was measured with a v-groove axial force

Manuscript received October 14, 2011; revised December 3, 2011; accepted December 9, 2011. Date of publication December 16, 2011; date of current version February 15, 2012.

The authors are with the Department of Photonics Engineering, DTU Fotonik, Technical University of Denmark, Kongens Lyngby DK-2800, Denmark (e-mail: wyuan@fotonik.dtu.dk; alste@fotonik.dtu.dk; oban@fotonik.dtu.dk).

Color versions of one or more of the figures in this letter are available online at http://ieeexplore.ieee.org.

Digital Object Identifier 10.1109/LPT.2011.2179927

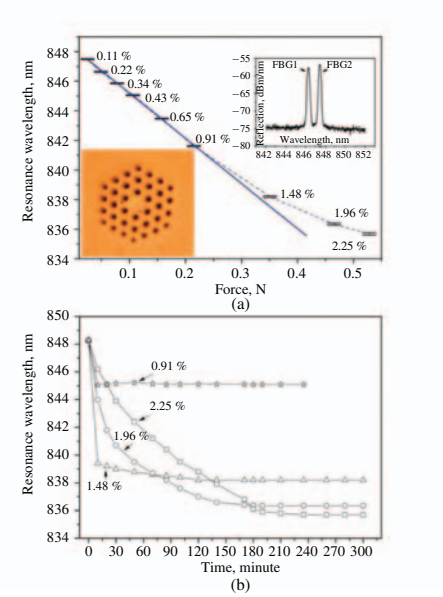

Fig. 1. (a) Resulting FBG resonance wavelength versus force. The corresponding strain is given at the measurement points. Inset shows the mPOF used for grating writing and the reflection spectrum of a fabricated dual-FBG. (b) Relaxation of the resonance wavelength (848.3 nm while strained) after release for different applied strains.

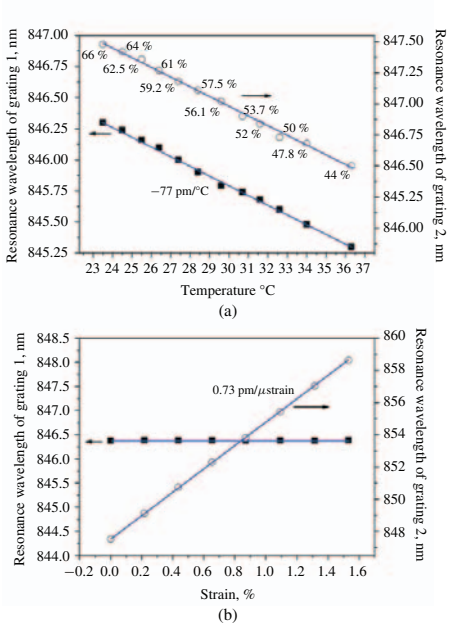

Fig. 2. Resonance wavelength of FBGs 1 and 2 (a) versus temperature/humidity with no strain and (b) versus strain applied to only FBG 2 at a fixed temperature (humidity) of 25 °C (63%).

sensor (FSC102, Thorlabs) and the FBG reflection spectrum was measured in reflection with a spectral resolution of 10 pm using an 850 nm silica fiber circulator, a SuperK Versa broadband source (NKT Photonics), and an optical spectrum analyzer (Ando AQ6317B). A standard single-mode silica fiber was butt-coupled to the mPOF using an angle cleaved end-facet and a small amount of refractive index matching gel in order to reduce Fresnel reflections.

In Fig. 1(a) we show that λ_B depends linearly on the applied force and strain for strains up to 1%, with a total tunability of 7 nm. In this regime λ_B relaxes rapidly to its stationary value, after which it remains stable, as seen in Fig. 1(b). For strains above 1 % the tuning curve saturates and the relaxation time increases significantly. This is a reflection of the visco-elastic properties of the PMMA, which become particularly apparent when the fiber is exposed to high strain for long times [1].

In the inset of Fig. 1(a) we show two FBGs with λ_B = 846.28 nm (FBG1) and 847.44 nm (FBG2) inscribed in the same fiber with 1 cm separation. Both FBGs were unchanged after storage for more than 24 hours. We now use this dual-FBG as a strain sensor to demonstrate temperature compensated strain sensing. We control the temperature of both gratings and mechanically stretch FBG2, while FBG1 remains unstretched. The two ends of FBG2 are glued to micro-translation stages with a UV curable glue (OG116+31, Epotek), which is mechanically much stiffer than the PMMA mPOF, so that it does not influence the strain. One stage was kept fixed, while the other moved to apply axial strain to FBG2 manually with a low loading speed. The axial strain was determined by dividing the fiber longitudinal elongation by the length of fiber between the two gluing points. The longitudinal displacement accuracy of the translation stage is 0.01 mm. The strain-free FBG1, was taped on the fixed stage. Another micro-translation stage was used to butt-couple the mPOF to a single-mode silica fiber (SM800, Thorlabs). The FBGs were heated up with a resistive heater (TH60, Linkam) placed on top of them. A thermocouple was used to measure the temperature as close to the gratings as possible with an uncertainty around 0.3 °C. A humidity sensor (C210, Lufft) was used to monitor the humidity near the two gratings with an uncertainty of 0.5 %rH.

The gratings were heated up from room temperature to 36.3 °C stepwise in a single cycle with the temperature allowed to stabilize for twenty minutes at each new set temperature before the reflection spectra were measured. The relative humidity decreased correspondingly from 66 %rH to 44 %rH. In Fig. 2(a) we show the measured dependence of the resonance wavelength of FBG1 and FBG2 on the temperature, with the corresponding humidity indicated on the curve. A nearly identical blue shift of both resonance wavelengths is observed, while there was no obvious change in the bandwidth (not shown). A temperature sensitivity of -77 ± 7 pm/°C was found for both gratings by a linear fit, which corresponds well with earlier measurements [1].

A strain loading experiment of FBG2 was carried out with a fix temperature of 25 °C (constant humidity of 63%rH).

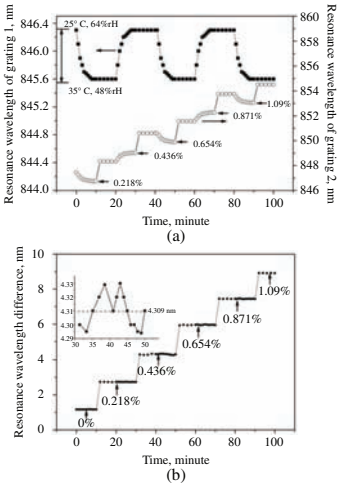

Fig. 3. (a) Resonance wavelength of FBG1 and FBG2 subject to a temperature cycle alternating between 25 °C and 35 °C every 20 min (corresponding humidity 64% and 38% rH) while the strain applied to FBG2 only was increased every 20 min starting after 10 min. (b) Difference in resonance wavelength of FBG2 and FBG1, showing temperature compensation. Inset shows a zoom.

The grating was left to stabilize for about ten minutes each time the tensile strain was changed before reading the reflection spectrum. As seen in Fig. 2(b), FBG2 shows a linear response of the center wavelength over the whole strain loading range up to 1.53% strain, with a linear fit giving a sensitivity of 0.73±0.02 pm/μstrain as also found in [9]. The resonance wavelength of the unstrained FBG1 is stable as expected.

In order to emulate a practical situation and further confirm the temperature (humidity) compensation capability of our dual-FBG strain sensor, a strain-sensing experiment with a periodic temperature (humidity) change was carried out. As shown in Fig. 3(a), strain was gradually applied to FBG2 every 20 min., while the temperature (humidity) experienced by both gratings was cycled between 25 °C (64%rH) and 35 °C (48%rH) every 20 min. with a 10 min. offset from the strain increase. In Fig. 3(a) we see how the strain recorded by FBG2 is strongly affected by the changing temperature (humidity), leading to the expected slow change in center wavelength of 770 pm with every 10 °C change. The temperature dependence is effectively compensated by instead monitoring the difference in center wavelength between FBG2 and FBG1, as demonstrated in Fig. 3(b). In fact one cannot talk about a cross-sensitivity to temperature of this sensor, because the fluctuations observed in the zoom in Fig. 3(b) are so small that they are within the limits of the mechanical stability of the set-up. If we instead analyse the plateaus or periods with fixed strain, then the maximum standard deviation from the mean of 12 pm is found for the third plateau from 30 to 50 min. shown in the zoom. If we then divide the 12 pm with the change in average wavelength of 1687 pm going to the plateau 3 from plateau 2, then we get a measure for the maximum noise of 0.71%. This is obviously a very low degree of noise given that the temperature is increased suddenly by 10 °C during this 20 min. period.

In summary, we have demonstrated a temperature and humidity compensated POF FBG strain sensor, which is based on a dual-FBG architecture in a single-mode PMMA mPOF and operates at the low-loss wavelength 850 nm. We have also demonstrated a simple technique to UV-write POF FBGs with a highly controlled tunable resonance wavelength, still using only a single phase-mask. Applying strain to the POF during writing we linearly tune the resonance by 7 nm using only 1% strain and show that going into the saturation regime allows to tune the FBG resonance by 12 nm with 2.25 % strain.

The strain tuning technique has been applied to silica fibers before but with a limited tunability of only 2.5 nm due to the high Young's modulus of silica. The 12 nm we demonstrated here is thus by far the highest ever achieved with this technique.

REFERENCES

[1] D. J. Webb and K. Kalli, "Polymer fiber Bragg gratings," in *Fiber Bragg Grating Sensors: Recent Advancements, Industrial Applications Market Exploitation*, A. Cusano, A. Cutolo, and J. Albert, Eds. Oak Park, IL: Bentham Science Publishers, 2009, pp. 1–20, ch. 15.

[2] W. Yuan, *et al.*, "Improved thermal and strain performance of annealed polymer optical fiber Bragg gratings," *Opt. Commun.*, vol. 284, no. 1, pp. 176–182, 2010.

[3] J. Jensen, P. Hoiby, G. Emiliyanov, O. Bang, L. Pedersen, and A. Bjarklev, "Selective detection of antibodies in microstructured polymer optical fibers," *Opt. Express*, vol. 13, no. 15, pp. 5883–5889, 2005.

[4] G. Emiliyanov, *et al.*, "Localized biosensing with TOPAS microstructured polymer optical fiber," *Opt. Lett.*, vol. 32, no. 5, pp. 460–462, 2007.

[5] G. Emiliyanov, *et al.*, "Localized biosensing with TOPAS microstructured polymer optical fiber: Erratum," *Opt. Lett.*, vol. 32, no. 9, p. 1059, 2007.

[6] C. Markos, W. Yuan, K. Vlachos, G. E. Town, and O. Bang, "Label-free biosensing with high sensitivity in dual-core microstructured polymer optical fibers," *Opt. Express*, vol. 19, no. 8, pp. 7790–7798, 2011.

[7] Z. Xiong, G. D. Peng, B. Wu, and P. L. Chu, "Highly tunable Bragg gratings in single-mode polymer optical fibers," *IEEE Photon. Technol. Lett.*, vol. 11, no. 3, pp. 352–354, Mar. 1999.

[8] C. Zhang, W. Zhang, D. J. Webb, and G. D. Peng, "Optical fibre temperature and humidity sensor," *Electron. Lett.*, vol. 46, no. 9, pp. 643–644, 2010.

[9] A. Stefani, W. Yuan, C. Markos, and O. Bang, "Narrow bandwidth 850 nm fiber Bragg gratings in few-mode polymer optical fibers," *IEEE Photon. Technol. Lett.*, vol. 23, no. 10, pp. 660–662, May 15, 2011.

[10] H. Dobb, D. J. Webb, K. Kalli, A. Argyros, M. C. J. Large, and M. A. van Eijkelenborg, "Continous wave ultraviolet light-induced fiber Bragg gratings in few and single mode microstructured polymer optical fibers," *Opt. Lett.*, vol. 30, no. 24, pp. 3296–3298, 2005.

[11] I. P. Johnson, K. Kalli, and D. J. Webb, "827 nm Bragg grating sensor in multimode microstructured polymer optical fiber," *Electron. Lett.*, vol. 46, no. 17, pp. 1217–1218, 2010.

[12] I. P. Johnson, *et al.*, "Optical fibre Bragg grating recorded in TOPAS cyclic olefin copolymer," *Electron. Lett.*, vol. 47, no. 4, pp. 271–272, 2011.

[13] W. Yuan, *et al.*, "Humidity insensitive TOPAS polymer fiber Bragg grating sensor," *Opt. Express*, vol. 19, no. 20, pp. 19731–19739, 2011.

[14] F. M. Haran, J. K. Rew, and P. D. Foote, "A strain-isolated fibre Bragg grating sensor for temperature compensation of fibre Bragg grating strain sensors," *Meas. Sci. Technol.*, vol. 9, no. 8, pp. 1163–1166, 1998.

[15] Q. Zhang, D. A. Brown, L. Reinhart, T. F. Morse, J. Q. Wang, and G. Xiao, "Tuning Bragg wavelength by writing gratings on prestrained fibers," *IEEE Photon. Technol. Lett.*, vol. 6, no. 7, pp. 839–841, Jul. 1994.

[16] I. P. Johnson, D. J. Webb, K. Kalli, M. C. J. Large, and A. Argyros, "Multiplexed FBG sensor recorded in multimode microstructured polymer optical fibre," *Proc. SPIE*, vol. 7714, pp. 77140D-1–77140D-10, 2010.

Paper 6

Direct Writing of Fiber Bragg Grating in Microstructured Polymer Optical Fiber

A. Stefani, M. Stecher, G.E. Town and O. Bang

IEEE Photonics Technology Letters doi: 10.1109/LPT.2012.2197194.

Direct Writing of Fiber Bragg Grating in Microstructured Polymer Optical Fiber

Alessio Stefani, Matthias Stecher, Graham E. Town *(Senior Member)* and Ole Bang

***Abstract*—We report point-by-point laser direct-writing of a 1520 nm fiber Bragg grating in a microstructured polymer optical fiber (mPOF). The mPOF was specially designed such that the microstructure did not obstruct the writing beam when properly aligned. A 4th order grating was inscribed in the mPOF with only a 2.5 seconds writing time.**

***Index Terms*—Fiber Bragg grating, polymer optical fiber, microstructured fiber, laser direct writing.**

I. Introduction

Fiber-optic sensors based on fiber Bragg gratings (FBGs) have many important industrial applications [1], [2]. The fiber material of choice in industrial applications has so far been silica, because of its low loss and resistance to high temperatures. However, polymer optical fiber (POF) FBGs are better suited for strain sensing because of the low Young's modulus and high failure strain of polymer compared to silica [1], [3].

Fiber Bragg gratings have been written into both step index POFs and microstructured POFs (mPOFs) using continuous wave (CW) UV illumination in a ring interferometer configuration [4] or with a phase-mask [5]–[12]. Writing times of 30-100 minutes for step index fibers [5], [6] and 60-270 minutes for mPOF [7]–[11] are usually necessary. A specially photosensitized fiber from University of New South Wales (UNSW) has allowed to reduce the writing time to 7.5 minutes [12]. Moreover in the mPOFs the resulting gratings are also relatively weak. The long inscription time is a result of the relatively weak photosensitivity of polymers (except for the UNSW fiber). In mPOFs the obstruction of the core by the high-contrast air-hole microstructure contributes to the increase in writing time, compared to solid POFs, and leads to relatively weak gratings [13]–[15]. Long writing times is a serious problem for applications requiring mass production.

A technique previously used to overcome the low photosensitivity of polymer waveguides is point-by-point grating writing with high intensity ultrashort laser pulses [16]–[18]. This direct writing approach has been demonstrated also in step index silica fibers [19], [20], and in silica waveguides [21]. Laser direct-writing also allows flexibility in the grating design [22], and avoids the expense of the phase mask and use of dopants or hydrogenation to increase the photosensitivity. However, the problem of obstruction by the microstructure still needs to be overcome.

One approach used to overcome scattering by the microstructure is to fill the holes with a material with similar index to the host. However filling the holes can be difficult to achieve in practice and significantly reduces the strong confinement achievable in air-filled microstructures [23] and it would be difficult to get the liquid out of the fiber.

Recently Geernaert *et al.* [24] demonstrated the first grating point-by-point written in a simple silica microstructured fiber in which two layers of air holes defined a rectangular core. The use of only one layer of holes minimized scattering and diffraction of the writing beam. However there is still a tradeoff between confinement of the guided mode and access to the core by the grating writing beam.

In this letter we report femtosecond laser direct-writing of a 4th order Bragg grating at 1518.67 nm with a 2.5 seconds writing time in an mPOF specifically designed for point-by-point side-writing.

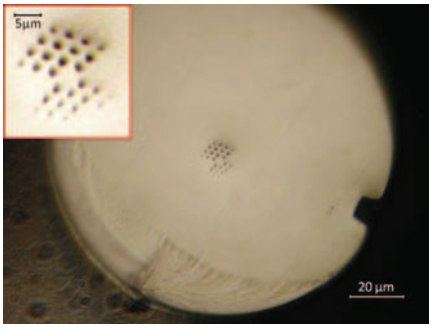

Fig. 1. Cross section of the mPOF designed for direct writing. Inset: zoom on the microstructure.

II. Fiber design and fabrication

The fiber was designed so that the laser beam used for writing would, ideally, pass between the air-holes and encounter minimal scattering before reaching the fiber core. For this reason an "opening" in the 3 ring hexagonal microstructure was created by removing 3 holes; 2 in the outer ring and one in the second ring (see Figs. 1-2). As the fiber was symmetric, 6 holes in total were removed. In this way access for the focused

A. Stefani and O. Bang are with DTU Fotonik, Department of Photonics Engineering, Technical University of Denmark, Ørsteds Plads, 2800 Kgs. Lyngby, Denmark (e-mail: alste@fotonik.dtu.dk).

M. Stecher is with the Philipps University Marburg, 35032 Marburg, Germany. At the time of this work he was supported by a Macquarie University postgraduate scholarship.

G.E. Town is with the Department of Electronic Engineering, Macquarie University, North Ryde NSW 2109, Australia.

We would like to acknowledge support from the Danish National Advanced Technology Foundation and the Australian National Fabrication Facility.

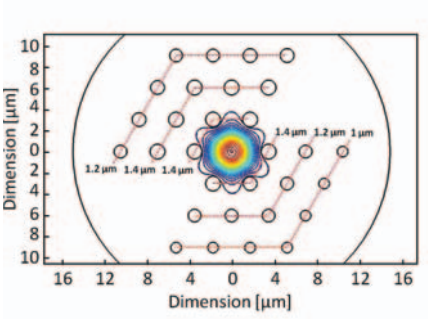

Fig. 2. COMSOL simulation of the guided mode in the fiber. The simulated structure has a pitch of 3.5 μm and hole diameters varying from 1 to 1.4 μm in order to match as much as possible the real structure.

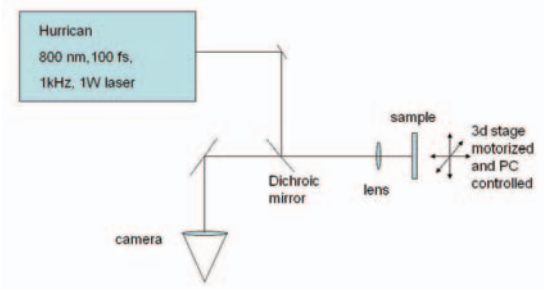

Fig. 3. Schematic of the set-up used for point by point writing.

800 nm laser beam was created through the microstructure on both sides. The pitch of the microstructure was designed so that the beam could also pass the first ring of holes without facing any interface. The focused beam was estimated to have a spot size just above 1 μm and, as we aim for a hole to pitch ratio of 0.42, a minimum pitch of 2 μm was required. The relative hole size of 0.42 was chosen because it would make the mPOF endlessly single mode with all holes present in the cladding [25]. The fiber with all holes was previously used for UV-writing of FBGs, which required over 60 minutes of writing time [10], [11].

The fabricated fiber is shown in Fig. 1 and a zoom on the microstructure can be seen in the inset. From the figure it is possible to notice a design feature on the fiber: an alignment slot in the outer part of the fiber was added in order to facilitate the alignment of the microstructure. The produced fiber, made in poly(methyl methacrylate) (PMMA), has an outer diameter of 130 μm and a resulting microstructure that was slightly asymmetric with hole diameters between 1 and 1.5 μm. The pitch is 3.5 μm, resulting in a hole to pitch ratio between 0.29 and 0.43.

The novel fiber design was simulated with the commercial software COMSOL in order to estimate the guiding properties. A pitch of 3.5 μm and hole diameters varying from 1 to 1.4 μm were used (as shown in Fig. 2) in order to match as much as possible the real structure. The fundamental mode for a wavelength of 1.52 μm is shown in Fig. 2. The simulated fundamental mode has an effective refractive index of n_{eff}=1.48037 (using 1.49 as material refractive index) and from the imaginary part a confinement loss of 0.67 dB/m is calculated, which is negligible compared to the material loss [3].

III. Grating writing

The grating writing set-up [26] is shown in Fig. 3. A regeneratively amplified, low-repetition rate, Ti:sapphire femtosecond laser system (Hurricane, Spectra-Physics) was used to produce the refractive index change. The output of the laser has 100 fs pulses with a central wavelength of 800 nm, repetition rate of 1 kHz and average output power of 1 W. A series of neutral density filters at the output of the laser was used to reduce and control the pulse energy. The beam was then reflected by a dichroic mirror, which allowed to observe the writing process with a CCD camera. After the dichroic mirror the light beam was focused with a 40x objective lens into the fiber. The fiber was held with fiber rotators, which were mounted on a computer controlled 3 axes translation stage (Aerotech FA-130, Aerotech ABL200) that can move with 200 nm resolution. The alignment was done visually with a CCD camera to first find the alignment slot on the fiber, then rotating the fiber 150 degrees in order to align the microstructure, moving the fiber towards the objective for half of the fiber thickness and adjusting the in-plane position by placing the laser beam position in the center of the microstructure. The position was then recorded and the same procedure was repeated at a distance from the first point corresponding to the desired grating length. During the writing the stage is moved with a linear trajectory from one point to the other. A pulse energy of 75 nJ (corresponding

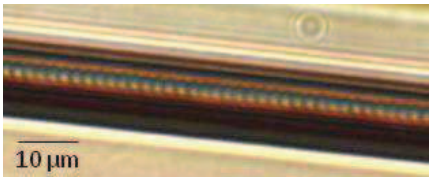

Fig. 4. DIC microscope image of the FBG. The image was taken with a 40x magnification lens. A modulation with about 2 μm period can be seen at the center of the fiber and in particular at the center of the microstructure.

to a fluence of about 1 Jcm^{-2} which gives a refractive index change of about 5×10^{-4} in a PMMA slab [16]) was used and a 4th order grating was written. This grating order was the minimum for which two consecutive spots (with diameter around 1 μm) would not overlap and thereby produce a continuous index change instead of a grating. We aim at a grating at λ_B = 1520 nm, so using n_{eff} = 1.48037, we find a grating period of $\Lambda = \frac{4\lambda_B}{2n_{eff}} = 2.053$ μm. Then, because we want to have a single pulse per spot, we find a necessary translation speed of 2.053 μm $\times$ 1kHz = 2.053 mm/s. Thus, in order to produce a 5 mm long grating a direct writing time of about 2.5 s is needed.

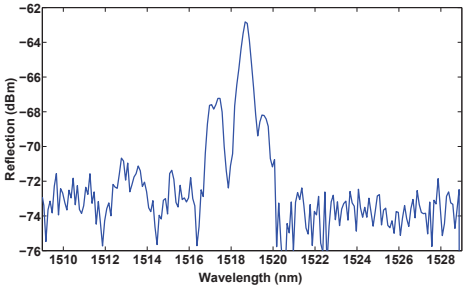

Fig. 5. Measured reflection spectrum of the 4th order grating (OSA resolution 0.2 nm). The main peak central wavelength is 1518.67 nm.

The fiber was examined afterwards under a differential interference contrast (DIC) microscope (Olympus). The resulting image is shown in Fig. 4. From the image a clear modulation of the refractive index is visible. The modulation period is around 2 μm, which is in agreement with the design spacing.

The grating has been characterized by measuring the reflection spectrum using a fiber circulator operating at 1550 nm. The first arm of the circulator is connected to a SuperK Versa broadband source from NKT Photonics A/S. The broadband signal is then butt-coupled to the fiber from the second arm of the circulator. The reflection is collected and measured at the third arm of the circulator with an Optical Spectrum Analyzer (Ando AQ6317B). The measured reflectance spectrum is shown in Fig. 5. The central wavelength is 1518.67 nm and more than one peak can be observed (possibly due to birefringence or the fiber not being single mode).

IV. Conclusion

In conclusion we have shown a new fiber structure to allow direct writing of FBGs in microstructured optical fibers in only 2.5 s. The fiber design is investigated and the fiber is drawn. A fourth order grating resulting in a resonance wavelength of 1518.67 nm is written using the point-by-point technique for the first time into a microstructured polymer optical fiber. The spectrum shown in Fig. 5 is the first reported directly written FBG spectrum in any POF or mPOF.

The proof that the direct writing technique can work for mPOFs could solve one of the crucial problems of mPOF FBG fabrication, i.e. the long writing time, which is generally above 60 minutes for mPOFs [1].

We note that direct writing could allow grating writing in fibers made with non-photosensitive materials, such as low loss perfluorinated POFs [3].

References

[1] D. Webb and K. Kalli, "Polymer fiber Bragg gratings", in *Fiber Bragg Grating Sensors: Recent Advancements, Industrial Applications and Market Exploitation*, 2009, pp. 1-20, A. Cusano, A. Cutolo, and J. Albert, eds. (2009 Bentham Science Publishers Ltd).

[2] A.D. Kersey, M.A. Davis, H.J. Patrick, M. LeBlanc, K.P. Koo, C.G. Askins, M.A. Putnam, and E.J. Friebele, "Fiber grating sensors", J. Lightwave Technol., vol. 15, 1442, 1997.

[3] M. Large, L. Poladian, G. Barton, and M.A. van Eijkelenborg, *Microstructured Polymer Optical Fibres*, (Springer, 2008), pp. 1-20.

[4] Z. Xiong, G.D. Peng, B. Wu, and P.L. Chu, "Highly tunable Bragg Gratings in single-mode polymer optical fibers", IEEE Photon. Technol. Lett., vol. 11, pp. 352-354, 1999.

[5] W. Yuan, A. Stefani, M. Bache, T. Jacobsen, B. Rose, N. Herholdt-Rasmussen, F.K. Nielsen, S. Andresen, O.B. Sørensen, K.S. Hansen, and O. Bang, "Improved thermal and strain performance of annealed polymer optical fiber Bragg gratings", Opt. Commun., Vol. 28, pp. 176-182, 2011.

[6] H.Y. Liu, G.D. Peng, and P.L. Chu, "Polymer fiber Bragg gratings with 28-dB transmission rejection", IEEE Photon. Technol. Lett. 14, 935-937, 2002.

[7] H. Dobb, D.J. Webb, K. Kalli, A. Argyros, M.C.J. Large, and M.A. van Eijkelenborg, "Continuous wave ultraviolet light-induced fiber Bragg gratings in few- and single- moded microstructured polymer optical fibers", Opt. Lett., vol. 30, 3296, 2005.

[8] I.P. Johnson, W. Yuan, A. Stefani, K. Nielsen, H.K. Rasmussen, L. Khan, D.J. Webb, K. Kalli, O. Bang, "Optical fibre Bragg grating recorded in TOPAS cyclic olefin copolymer", Electron. Lett., vol. 47, 271-272, 2011.

[9] W. Yuan, L. Khan, D.J. Webb, K. Kalli, H.K. Rasmussen, A. Stefani, O. Bang, "Humidity insenssitive TOPAS polymer fiber Bragg grating sensor", Opt. Express, vol. 19, 19731-19739, 2011.

[10] A. Stefani, W. Yuan, C. Markos, O. Bang, "Narrow bandwidth 850 nm fiber Bragg gratings in few-mode polymer optical fibers", IEEE Photon. Technol. Lett., vol. 23, 660-662, 2011.

[11] W. Yuan, A. Stefani, O. Bang, "Tunable polymer fiber Bragg grating (FBG) inscription: fabrication of dual-FBG temperature compensated polymer optical fiber strain sensors", IEEE Photon. Technol. Lett, accepted.

[12] C. Zhang, K. Carroll, D.J. Webb, I. Bennion, K. Kalli, G. Emiliyanov, O. Bang, E. Kjær, and G.D. Peng, "Recent progress in polymer optical fibre gratings", Proc. of SPIE, 70044G, 2008.

[13] G.D. Marshall. D.J. Kan, A.A. Asatryan, L.C. Botten, M.J. Withford, "Transverse coupling to the core of a photonic crystal fiber: the photo-inscription of gratings, Opt. Express, vol. 15, 7876-7887, 2007.

[14] T. Baghdasaryan, T. Geernaert, F. Berghmans, and H. Thienpont, "Geometrical study of a hexagonal lattice photonic crystal fiber for efficient femtosecond laser grating inscription", Opt. Express, 7705-7716, 2011.

[15] T. Baghdasaryan, T. Geernaert, M. Becker, K. Schuster, H. Bartelt, M. Makara, P. Mergo, F. Berghmans, H. Thienpont, "Influence of Fiber Orientation on Femtosecond Bragg Grating Inscription in Pure Silica Microstructured Optical Fibers", IEEE Photon. Technol. Lett., vol. 23, 1832-1834, 2011.

[16] P.J. Scully, D. Jones, D.A. Jaroszynski, "Femtosecond laser irradiation of polymethylmethacrylate for refractive index gratings", J. Opt. A: Pure Appl. Opt., vol. 5, S92-S96, 2003.

[17] C. Wochnowski, Y. Cheng, K. Meteva, K. Sugioka, K. Midorikawa, S. Metev, "Femtosecond-laser induced formation of grating structures in planar polymer substrates", J. Opt. A: Pure Appl. Optics, vol. 7, 493-501, 2005.

[18] A.J. Lee, A. Rahmani, J.M. Dawes, G.D. Marshall, M.J. Withford, "Point-by-point inscription of narrow-band gratings in polymer ridge waveguides", Appl. Physics A, 90, 273-276, 2008.

[19] A. Martinez, I.Y. Khrushchev, I. Bennion, "Direct inscription of Bragg gratings in coated fibers by an infrared femtosecond laser", Opt. Lett., vol. 31, 1603-1605, 2006.

[20] A. Martinez, M. Dubov, I. Khrushchev, I. Bennion, "Direct writing of fiber Bragg gratings by femtosecond laser", Electron. Lett., vol. 40, 2004.

[21] G.D. Marshall, M. Ams, M.J. Withford, "Direct laser written waveguide-Bragg gratings in bulk fused silica", Opt. Lett., vol. 31, 2690-2691, 2006.

[22] G.D. Marshall, R.J. Williams, N. Jovanovic, M.J. Steel, and M.J. Withford, "Point-by-point written fiber-Bragg gratings and their application in complex grating designs", Opt. Express, vol. 18, 19844-19859, 2010.

[23] H.R. Sørensen, J. Canning, J. Lægsgaard, K. Hansen, and P. Varming, "Liquid filling of photonic crystal fibres for grating writing", Opt. Commun., vol. 270, 207-210, 2007.

[24] T. Geernaert, K. Kalli, C. Koutsides, M. Komodromos, T. Nasilowski, W. Urbanczyk, J. Wojcik, F. Berghmans, H. Thienpont, "Point-by-point fiber Bragg grating inscription in free-standing step-index and photonic crystal fibers using near-IR femtosecond laser", Opt. Lett., vol. 35, 1647-1649, 2010.

[25] N.A. Mortensen, "Semianalytical approach to short-wavelength dispersion and modal properties of photonic crystal fibers", Opt. Lett., vol. 30, 1455-1457, 2005.

[26] M. Ams, G.D. Marshall, D.J. Spence, M.J. Withford, "Slit beam shaping method for femtosecond laser direct-write fabrication of symmetric waveguides in bulk glasses", Opt. Express, vol. 13, 5676-5681, 2005.

Paper 7

Dynamic characterization of polymer optical fibres

A. Stefani, S. Andresen, W. Yuan and O. Bang

Submitted to IEEE Sensors Journal.

Dynamic characterization of polymer optical fibers

Alessio Stefani, Søren Andresen, Wu Yuan and Ole Bang

Abstract—**With the increasing interest in fiber sensors based on polymer optical fibers it becomes fundamental to determine the real applicability and reliability of this type of sensor. The viscoelastic nature of polymers gives rise to questions about the mechanical behaviour of the fibers. In particular, concerns on the response in the non-static regime find foundation in the viscoelasticity theory. We investigate the effects of such behaviour by an analysis of the mechanical properties under dynamic excitations. It is shown that for low strain (0.28%) the Young's modulus is constant for frequencies up to the limit set by our measurement system. A more detailed analysis shows that viscoelastic effects are present and that they increase with both applied strain and frequency. However the possibility of developing sensors that measure small dynamic deformations is not compromised. A stress-relaxation experiment for larger deformations (2.8%) is also reported and a relaxation time around 5 seconds is measured, defining a viscosity of 20 GPa·s.**

Index Terms—**Polymer Optical Fibers, Dynamic Mechanical Analysis.**

I. Introduction

Polymer optical fibers (POFs) are more and more used for sensors because of their material advantages over silica. In particular microstructured POFs (mPOFs) have been used for applications like strain sensing [1], [2] exploiting the affinity to organic compounds, and the combined low Young's modulus and high failure strain [3] respectively and biosensing [4]–[6] . Different polymers have been used to make fibers, but the most used are poly(methyl methacrylate) (PMMA) and the cyclic olefin copolymer TOPAS. The exploitation of the mechanical properties is strongly enhanced by the fact that these polymers are also photosensitive and that it is then possible to write fiber Bragg gratings (FBGs) in this kind of fiber [2], [7]–[11]. Moreover increasing interest for the use of mPOF FBGs as strain related sensors is driven by the possibility of reducing the environmental influence, by choosing a humidity insensitive polymer (such as TOPAS) [12] and/or by temperature compensating with a dual grating scheme [13].

POF based strain sensors find applications not only in static measurements but also in dynamic ones. Examples could be for monitoring structural vibrations [14] and for accelerometers [15]. As already mentioned the choice of polymer fibers instead of silica is related to their elasticity. Unfortunately polymers are not elastic, but viscoelastic. Viscoelastic materials do not have a constant response to strain/stress with frequency due to molecular rearrangement, which dissipates part of the accumulated energy, as in a plastic deformation [16]. This implies that the material under stress has the tendency to relax. It also implies that they have a Young's modulus that is not constant in temperature and frequency. It is well known that for bulk polymers this behaviour occurs at really low frequencies (often even less than 1 Hz) [17], [18]. This material property seems to exclude polymer optical fibers from all those sensing applications in which the frequency response of the sensor is one of the main characteristics, e.g. accelerometers, microphones and sensors for fast vibrations detection.

Mechanical characterizations of polymer optical fibers have been made, but most of them in terms of dependence of the mechanical properties on the fabrication parameter [2], [19] and static load [20]–[22]. Kiesel et al. [22] show the influence of the strain rate on the strain/stress curve and consequently Young's modulus. A study on time dependent effects has also been done [23], but it reports only on measurements of the relaxation time. The investigations on polymer fibers reported up to now do not consider cyclic strain excitation, and thus the dynamic Young's modulus. In order to fully understand and characterize the viscoelastic properties of polymer optical fibers and exploit the favorable regimes when making POF based sensors, measurements of the dynamic Young's modulus and of the recovery time are necessary. The most used technique for this kind of measurements is the dynamic mechanical analysis (DMA) [17]. It allows for analysis of frequency and temperature behaviour of viscoelastic materials. We base this study on the principles used in the DMA, but in a different configuration. We report on the investigation on the frequency dependence of the Young's modulus of polymer optical fibers and the effects caused by viscoelasticity in this regime. Moreover we also investigate stress-relaxation of polymer fibers.

II. Experimental set-up

Compared with standard DMA we choose a reciprocal approach, also used in [24], in which elongation is applied and force is measured instead of vice versa. A schematic of the set-up used to characterize the fibers is shown in Fig. 1. A current driven shaker (*Brüel & Kjær Type 4810*) is used to produce the desired elongation. The shaker can provide displacement up to 6 mm peak to peak in a frequency range 0 to 18 kHz. The fiber is fixed on one end to the shaker while on the other end it's fixed to a force gauge (*Brüel & Kjær 8230* or *8230-002*). On the shaker side, underneath the fiber holder an accelerometer (*Brüel & Kjær 4507*) is placed in order to determine the displacement. A waveform generator is used to drive the shaker and a data acquisition card (*Brüel*

A. Stefani, and O. Bang are with DTU Fotonik, Department of Photonics Engineering, Technical University of Denmark, Ørsteds Plads, 2800 Kgs. Lyngby, Denmark (e-mail: alste@fotonik.dtu.dk).

S. Andresen is with Brüel & Kjær Sound & Vibration Measurement A/S, Skodsborgvej 307, 2850 Nærum, Denmark.

W. Yuan is with Singapore Institute of Manufacturing Technology, 71 Nanyang Drive, 638075, Singapore.

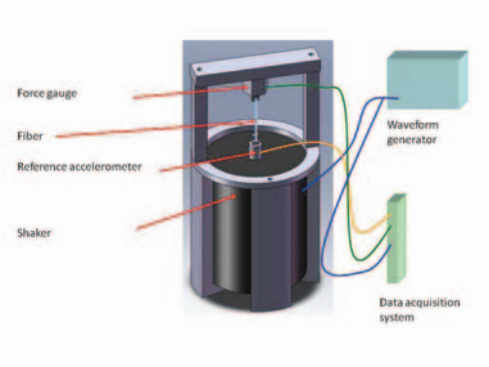

Fig. 1. Schematic of the set-up used for dynamic measurements.

& Kjær LAN-XI module type 3160-B-042) is use to monitor the response of the force gauge, the accelerometer and the shaker input. All the experiments have been conducted at room temperature (about 23°C) in an air conditioned environment.

III. Dynamic Young's modulus measurements

There are different ways to determine the dynamic Young's modulus over a range of frequencies. They only differ in the excitation wave used: it could be by sampling a certain number of sine wave excitations with various frequencies, by sweeping the frequency continuously, by using the free resonance technique or by exciting with a wave with multiple components [17]. We measured the response to a white noise excitation with components from 0.7 Hz to 3.5 kHz. An elongation of 116 μm (RMS value) was applied. Considering that the fiber holders are separated by 4.1 cm, a deformation of 0.28% was produced. The fibers under test are to be used in optical accelerometers [15] for which a 0.02% strain corresponds to an acceleration of already 15g. For this reason we are interested in the small deformation regime and we chose to test the fibers with an about 10 times stronger deformation than what is typically required in our application of fiber-optical accelerometer. The recorded force was divided by the displacement, calculated by double integrating the response of the accelerometer using the software of the data acquisition card. We expected the displacement to be fixed by the input current to the shaker, so that it wouldn't have been necessary to measure the elongation, but we decided to do anyway it in order to make sure that the shaker displacement wasn't influenced by the fiber to the point of not following the specifications. The corresponding Fourier transform (FFT) response gives the frequency dependent spring constant. The Young's modulus was then calculated by multiplying with the fiber length and dividing by the cross sectional area. It was assumed that, for the applied deformation, the variation in cross section and in length was negligible. Three different fibers have been tested this way: a silica SMF-28 fiber with 125 μm diameter; a 115 μm in diameter commercial step index polymer optical fiber made of PMMA with a polystyrene co-doped core (MORPOF02, Paradigm Optics); and a microstructured polymer optical fiber (mPOF) made in PMMA with a diameter of 130 μm. The measured frequency dependent Young's modulus is shown in Fig. 2.

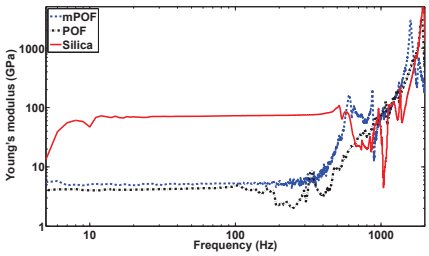

Fig. 2. Dynamic Young's modulus of the PMMA mPOF, the step index POF and of the silica SMF28.

Due to the acquisition system used, the low frequency region, i.e. below 7 Hz, can not be trusted. The whole system presents a mechanical resonance at about 1 kHz which limits the useful high frequency response to just above 100 Hz. In the range of frequencies between 10 to 100 Hz the modulus shows a frequency independent flat response, indicating an elastic like behaviour, and a low viscosity regime for the elongation used. To compare with literature, the value of the modulus was calculated by taking the average value in the flat region. The silica fiber has, as expected, a higher modulus and it's value (71 GPa) *(spanning from 67.8 to 72.8)*, is in agrement with what is reported in the literature [3]. The two polymer fibers have a Young's modulus about a factor of 15 smaller than the silica fiber. The specific values differ slightly, with 4.3 GPa *(spanning from 4 to 4.9)* for the POF and 5.1 GPa *(spanning from 4.9 to 5.3)* for the mPOF. Different values have to be expected, considering that the POF has a core partially composed of a different material, whereas the mPOF is fully made in PMMA. Furthermore, the particular grade of PMMA used for the two fibers could be different (e.g., in terms of molecular weight) and the drawing conditions (in particular the tension) most probably were different for the two fibers [2], [19]. If comparing the result found to what is reported in literature, we notice that the POF has a modulus very similar to what is reported for a fiber made by the same producer and with very similar characteristics [22], while the other results span very much from 1 to 5 GPa [3], [25]. The diversity of the values reported stresses the fact that if it's desired to know accurately the characteristics of a fiber used for a particular application, a measurement of each different batch of fiber is necessary.

IV. Sine wave response

To deeper investigate the effects of viscoelasticity and to have a clearer idea of what can happen when the fiber is used in a dynamic sensor , e.g the accelerometer [15], we investigated the time response to a sine wave excitation, with different frequencies and amplitudes. In order to show the change in behaviour we show the results for two of the investigated frequencies, 1 and 10 Hz, and for two different

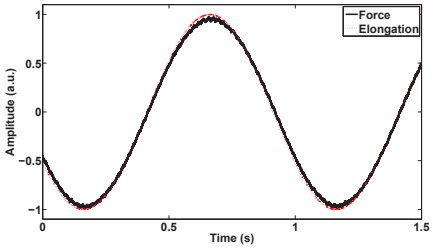

(a) 1 Hz-0.28%

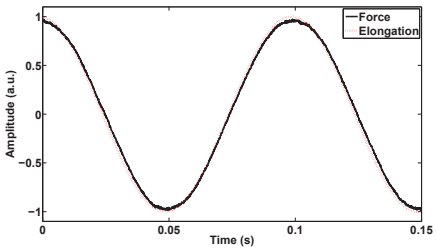

(b) 10 Hz-0.28%

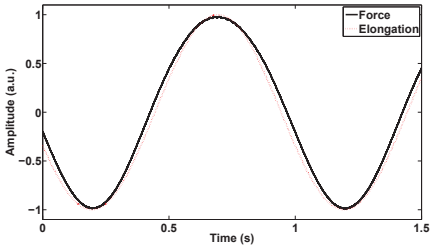

(c) 1 Hz-1.63%

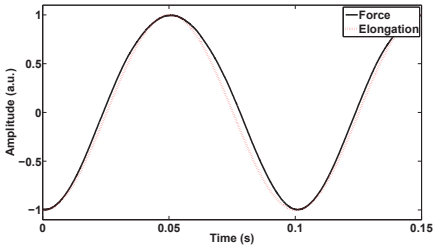

(d) 10 Hz-1.63%

Fig. 3. Measured force (solid black line) and applied sinusoidal elongation (dashed red line) on a PMMA mPOF with frequency of 1 Hz ((a) and (c)) and 10 Hz ((b) and (d)) and RMS elongation of 116 μm (0.28%) ((a) and (b)) and 670 μm (1.63%) ((c) and (d)).

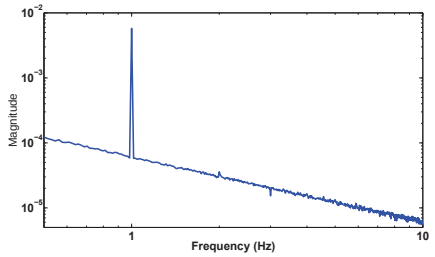

(a) 1 Hz-0.28%

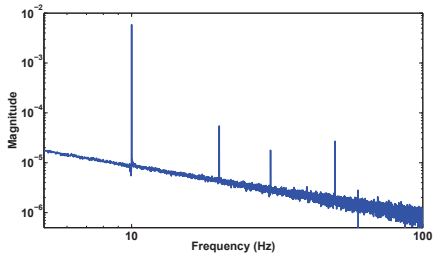

(b) 10 Hz-0.28%

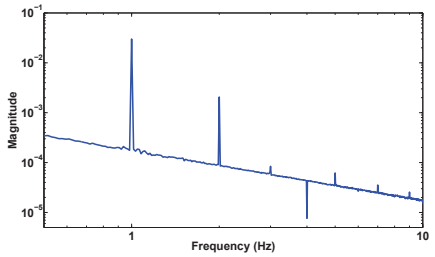

(c) 1 Hz-1.63%

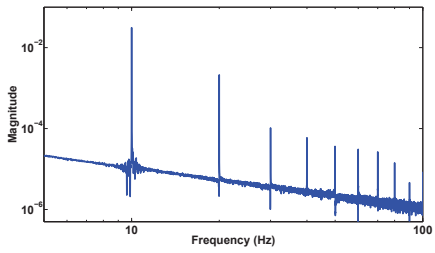

(d) 10 Hz-1.63%

Fig. 4. FFT of the measured force when a sinusoidal elongation is applied on a PMMA mPOF with frequency of 1 Hz ((a) and (c)) and 10 Hz ((b) and (d)) and RMS elongation of 116 μm (0.28%) ((a) and (b)) and 670 μm (1.63%) ((c) and (d)).

elongations (RMS): 116 and 670 μm, corresponding to a strain of 0.28% and 1.63% respectively.

The result is shown in Fig. 3. For a viscoelastic material a phase lag is expected, and it is expected to increase with frequency. It is possible to see that the excitation and response wave have a really small phase difference δ of respectively: 3.1 degrees for the 1 Hz-116 μm excitation; 3.5 degrees for the 10 Hz-116 μm excitation; 0.14 degrees for the 1 Hz-670 μm excitation; 1.6 degrees for the 10 Hz-670 μm excitation. The results show a small increase with frequency and a decrease with amplitude. However the values are very small and, very likely, errors related to the fit and to the noise in the signal (for example the curves for greater elongations have lower noise compared to the ones with low elongation because the signal at the force gauge is stronger) could as well be greater than these differences. The loss component, or damping, (defined as the ratio between the loss to the storage components of the dynamic Young's modulus) can be calculated from the phase difference between excitation and response waves as $\tan(\delta)$. This results in a loss component of: 0.055 for the 1 Hz-116 μm excitation; 0.06 for the 10 Hz-116 μm excitation; 0.002 for the 1 Hz-670 μm excitation; 0.029 for the 10 Hz-670 μm excitation. The dynamic Young's modulus E can be written, in a vectorial representation as:

$$E = E' + iE'' = E_0\cos(\delta) + iE_0\sin(\delta) \qquad (1)$$

where E' is the storage or elastic modulus, E'' is the loss modulus and E_0 is the static Young's modulus. The fraction of the dynamic Young's modulus that is not in the elastic component for such values correspond almost exactly to the loss component ($\sin(\delta) \approx \tan(\delta)$). We can conclude that, as already shown for the dynamic modulus, there is no significant loss component. Even if a behaviour close to elastic can be observed (with response not out of phase), there is a small deviation from it that can be observed. In fact the response waves for the higher amplitude do not perfectly match a perfect sinusoidal wave. A small delay in the response can be seen in Fig. 3 (c) and (d). In order to analyze this particular response a FFT of the response has been made and the result it is shown in Fig. 4. The frequency analysis shows that also the low strain waves have high harmonic components but the number and magnitude (relative to the fundamental frequency) increase both with amplitude and frequency. For the considered frequencies the impact of a strain increase affects more the amplitude of the high order components, while the frequency increase affects the number of high order frequencies detectable. The ratios between the magnitude of the main component and the magnitude of the first harmonic are listed in Tab. 1. It is possible to notice how the effect is higher for the strain increase than for the frequency increase, for the parameter variation here reported.

The same analysis was made for a TOPAS (grade 8007) mPOF. The main differences with PMMA are the lower glass transition temperature, and consequently lower material transition temperatures, e.g. the transition from brittle to ductile required for good fiber cleaving [26], and the lower affinity to water. The first of the two would imply that the material, at room temperature, should have a more viscous behaviour

TABLE I
RATIO BETWEEN THE MAGNITUDES OF THE MAIN COMPONENT AND THE FIRST HARMONIC OF THE FFT OF THE RESPONSE TO SINUSOIDAL EXCITATION FOR BOTH PMMA AND TOPAS MPOFS.

	PMMA		**TOPAS**	
	1 Hz	10 Hz	1 Hz	10 Hz
0.28%	814.3	107.4	172	155.7
1.63%	14.8	14.7	17.3	16

if the two materials would be otherwise the same. The fiber used has a 225 μm diameter. The measured force to the applied sinusoidal elongation is shown in Fig. 5. As for the PMMA fiber, the phase difference does not look significant, even if slightly more evident than in the case of PMMA. The measured values are: 4.2 degrees for the 1 Hz-116 μm excitation; 5.3 degrees for the 10 Hz-116 μm excitation; 3.4 degrees for the 1 Hz-670 μm excitation; 5.2 degrees for the 10 Hz-670 μm excitation. The corresponding loss component are: 0.074 for the 1 Hz-116 μm excitation; 0.093 for the 10 Hz-116 μm excitation; 0.06 for the 1 Hz-670 μm excitation; 0.092 for the 10 Hz-670 μm excitation. The fiber shows the same mechanical behaviour as the PMMA mPOF in this regime. The analysis of the frequency components of the measured response has been also done for this fiber and the result is shown in Fig. 6. Again the result resembles the one found for the fiber made of PMMA. Also for this fiber the values of the ratio between the magnitude of the FFT main peak and the first harmonic are reported in Tab. 1.

From a practical point of view this gives a limitation on the frequency and amplitude of the signals that can be detected correctly. In fact, the harmonics will give an error contribution in the case of detection of signals with multiple frequencies.

V. LOW FREQUENCIES RESPONSE: STRESS RELAXATION

An experiment that is very common for polymer characterization is the creep-recovery experiment. It consist of a step excitation and the observation of the response of the material to it. The excitation is a given force and the measured parameter is the elongation. The reciprocal experiment is the stress-relaxation test. It measures the force response to an elongation step excitation. From this experiment it is possible to obtain information about the low frequency (quasi static) behaviour and it makes also possible to measure the viscosity of the material. Two fibers have been investigated with this technique: the silica fiber and the PMMA mPOF. Their step responses are shown in Fig. 7. The elongation step used in the experiment for the silica fiber is 350 μm while a 1.16 mm step was used for the mPOF. The corresponding strain is respectively 0.85% and 2.8%.

As it is possible to see the silica fiber shows an almost perfect step, implying, as expected, an immediate response and no relaxation, typical of elastic materials. The polymer fiber shows a decay time after the strain was applied and released. This is a typical behaviour of viscoelastic materials. A fit to an exponential curve was made to determine the time constant. The stretching and relaxation processes show two slightly different time constants. In fact, a time constant of

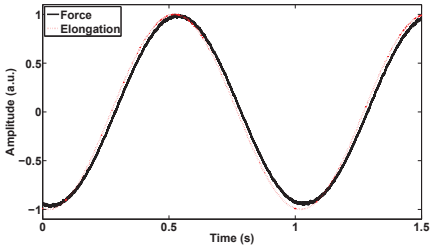

(a) 1 Hz-0.28%

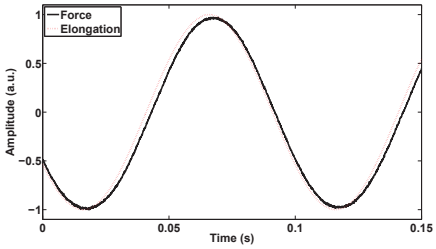

(b) 10 Hz-0.28%

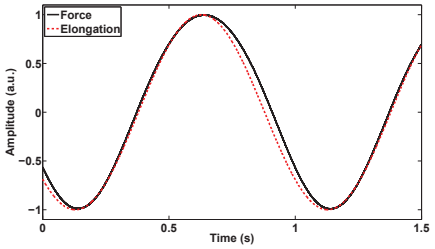

(c) 1 Hz-1.63%

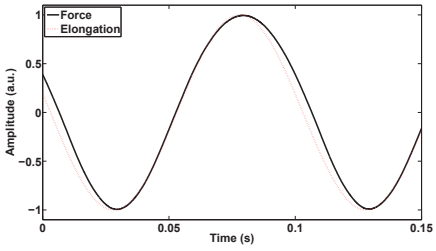

(d) 10 Hz-1.63%

Fig. 5. Measured force (solid black line) and applied sinusoidal elongation (dashed red line) on a TOPAS mPOF with frequency of 1 Hz ((a) and (c)) and 10 Hz ((b) and (d)) and RMS elongation of 116 μm (0.28%) ((a) and (b)) and 670 μm (1.63%) ((c) and (d)).

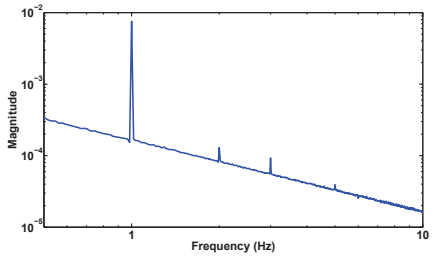

(a) 1 Hz-116 μm

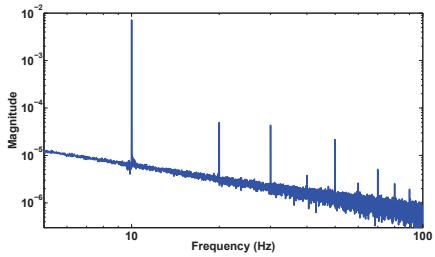

(b) 10 Hz-116 μm

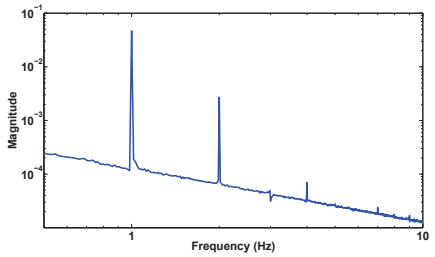

(c) 1 Hz-1.63%

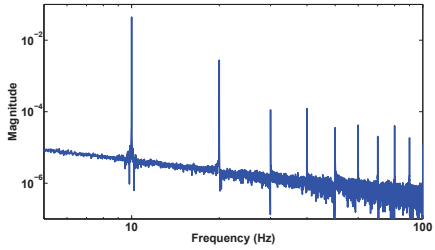

(d) 10 Hz-1.63%

Fig. 6. FFT of the measured force when a sinusoidal elongation is applied on a TOPAS mPOF with frequency of 1 Hz ((a) and (c)) and 10 Hz ((b) and (d)) and RMS elongation of 116 μm (0.28%) ((a) and (b)) and 670 μm (1.63%) ((c) and (d)).

about 4.7 seconds was measured when the fiber was stretched and a time constant of about 5.8 seconds for when the fiber length was brought back to the original state. The fiber had a prestrain applied before being elongated in order to make sure it wasn't loose. From the time constant it's possible to estimate the viscosity of the material [17]. In particular it is possible to use the Maxwell model for viscoelastic materials. This model represents the material as a spring and a dashpot in series. The spring models the elastic response and the dashpot the viscous one. This model is particularly good for stress relaxation experiments, since the strain can be seen as the sum of the strain on the two components and the two components experience the same stress. It has to be noted that an instantaneous strain is required for using the Maxwell model to interpret stress relaxation experiments, but this is to a good approximation the case in our situation where the time scale of the viscoelastic dynamic is a lot longer than the shaker response time. The Maxwell model is a simplification and, a number of spring-dashpot systems in parallel would give a more accurate modeling of the real behavior. Nevertheless the exponential decay that we observe is well explained by this simplified model. Let's consider the strain (ε) as the sum of the two components: $\varepsilon = \varepsilon_{elastic} + \varepsilon_{viscous}$. The variation of the strain in time is:

$$\frac{d\varepsilon}{dt} = \frac{1}{E}\frac{d\sigma}{dt} + \frac{\sigma}{\eta} \tag{2}$$

where E is the Young's modulus, σ is the stress and η is the viscosity. Since the elongation is kept constant $\frac{d\varepsilon}{dt} = 0$, and

$$\frac{d\sigma}{dt} = -E\frac{\sigma}{\eta} \tag{3}$$

which gives

$$\sigma(t) = \sigma_0 \exp\frac{-Et}{\eta}. \tag{4}$$

The time constant is then the ratio between the viscosity and the Young's modulus. In the case of the PMMA mPOF under investigation the resulting viscosity is 20 GPa·s. No calculation of the viscosity in a polymer fiber has been reported previously, so it was not possible to compared the result found here and determine the error given by using a simplified model. The implications of this relaxation in a practical application are quite important. For example, if the fiber is to be used as strain sensor, an error in the measured value is to be expected, especially on variations that have dynamical time scale comparable to that of the time constant.

VI. Conclusion

In conclusion we investigated the behaviour of polymer fibers made of both PMMA and TOPAS under dynamic excitation. The dynamic Young's modulus was measured for two different PMMA fibers when 0.28% strain was applied. Fiber optic acceleration sensing [15] requires strain up to 0.02%, we investigated strain 10 times higher than what is necessary for this application. A frequency independent value was found for all the frequencies the system allowed to measure reliably, i.e. 10 to 100 Hz, confirming an elastic response in this regime. The Young's modulus was measured

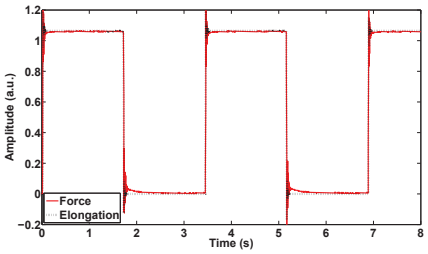

(a) Silica

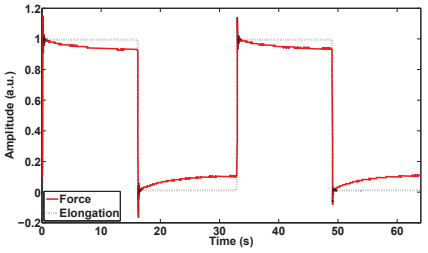

(b) PMMA

Fig. 7. Measured force response (red solid line) to and elongation step (black dashed line) for a silica SMF28 fiber (a) and for a PMMA mPOF fiber (b).

for a PMMA mPOF and was found to be 5.1 GPa. The value for a commercial step-index POF (MORPOF02, Paradigm Optics) was found to be 4.9 GPa, which is in agrement with an earlier measurement [22]. The value for a silica SMF-28 fiber was found to be 71 GPa, also in agreement with what is reported in the literature [3]. The response to a sine wave is also reported for two different values of the applied strain (0.28% and 1.63%) and two different frequencies (1 Hz and 10 Hz). No important phase difference between excitation and response wave was found, determining a weak viscoelastic behaviour, but a relaxation effect appeared. The effect results in the creation of frequency harmonics with the increase of elongation and frequency. From an application point of view, these results imply that polymer fibers can be used for high frequency applications but in the small deformations regime. Moreover it has been demonstrated how the low frequency regime can also be affected by the viscoelastic nature of polymers. The step response of a PMMA mPOF was also investigated and relaxation times of 5 and 6 seconds for elongation and release, respectively, were found when a 2.8% strain was applied.

VII. Acknowledgments

We would like to acknowledge support from the Danish National Advanced Technology Foundation.

References

[1] X. Chen, C. Zhang, D.J. Webb, G.-D. Peng and K. Kalli, Bragg grating in a polymer optical fibre for strain, bend and temperature sensing, Meas. Sci. Technol. 21 (2010) 094005.

[2] D.J. Webb and K. Kalli, Polymer fiber Bragg gratings in *Fiber Bragg Grating Sensors: Recent Advancements, Industrial Applications and Market Exploitation* (Bentham Science Publishers Ltd) (2009).
[3] M.C.J. Large, L. Poladian, G.W. Barton and M.A. van Eijkelenborg *Microstructured Polymer Optical Fibres* (New York: Springer) (2008).
[4] J.B. Jensen, P.E. Hoiby, G. Emilianov, O. Bang, L.H. Pedersen and A. Bjarklev, Selective detection of antibodies in microstructured polymer optical fibers, Opt. Express 13 (2005) 5883.
[5] G. Emiliyanov, J.B. Jensen, O. Bang, P.E. Hoiby, L.H. Pedersen, E. Kjær and L. Lindvold, Localized biosensing with Topas microstructured polymer optical fiber, Opt. Lett. 32 (2007) 460.
[6] G. Emiliyanov, J.B. Jensen, O. Bang, P.E. Hoiby, L.H. Pedersen, E. Kjær and L. Lindvold, Localized biosensing with Topas microstructured polymer optical fiber; erratum, Opt. Lett. 32 (2007) 1059.
[7] G.-D. Peng, Z. Xiong and P.L. Chu, Photosensitivity and gratings in dye-doped polymer optical fibers, Opt. Fiber Technol. 5 (1999) 242-251.
[8] H. Dobb, D.J. Webb, K. Kalli, A. Argyros, M.C.J. Large and M.A. van Eijkelenborg, Continuous wave ultraviolet light-induced fiber Bragg gratings in few- and single-mode microstructured polymer optical fibers, Opt. Lett. 30 (2005) 3296-3298.
[9] W. Yuan, A. Stefani, M. Bache, T. Jacobsen, B. Rose, N. Herholdt-Rasmussen, F.K. Nielsen, S. Andresen, O. B. Sørensen, K.S. Hansen and O. Bang, Improved thermal and strain performance of annealed polymer optical fiber Bragg gratings, Opt. Commun. 28 (2011) 176-182.
[10] A. Stefani, W. Yuan, C. Markos and O. Bang, Narrow Bandwidth 850 nm Fiber Bragg Gratings in Few-Mode Polymer Optical Fibers, IEEE Photon. Technol. Lett. 23 (2011) 660-662.
[11] I.P. Johnson, W. Yuan, A. Stefani, K. Nielsen, H.K. Rasmussen, L. Khan, D.J. Webb, K. Kalli and O. Bang, Optical fibre Bragg grating recorded in TOPAS cyclic olefin copolymer, Electron. Lett. 47 (2011) 271-272.
[12] W. Yuan, L. Khan, D.J. Webb, K. Kalli, H.K. Rasmussen, A. Stefani and O. Bang, Humidity insensitive TOPAS polymer fiber Bragg grating sensor, Opt. Expr. 19 (2011) 19731-19739.
[13] W. Yuan, A. Stefani and O. Bang, Tunable Polymer Fiber Bragg Grating (FBG) Inscription: Fabrication of Dual-FBG Temperature Compensated Polymer Optical Fiber Strain Sensor, IEEE Photon. Technol. Lett. 24 (2012) 401-403.
[14] K.S.C. Kuang and W.J. Cantwell, The use of plastic optical fibre sensors for monitoring the dynamic response of fibre composite beams, Meas. Sci. Technol. 14 (2003) 736-745.
[15] A. Stefani, S. Andresen, W. Yuan and O. Bang, High Sensitivity Polymer Optical Fiber Bragg Grating Based Accelerometer, IEEE Photon. Technol. Lett. (2012) (accepted on April 17th).
[16] J. Rösler, H. Harders and M. Bäker, Mechanical behaviour of polymers in *Mechanical behviour of engineering materials* (Springer) (2007).
[17] K.P. Menard, *Dynamic mechanical analysis: a practical introduction* (CRC Press LLC) (1999).
[18] B.E. Read and J.C. Duncan, Measurement of dynamic properties of polymeric glasses for different modes of deformation, Polym. Test. 2 (1981) 135-150.
[19] S. Law, G.W. Barton, M.A. van Eijkelenborg, C. Yan, R. Lwin and J. Gan, The effect of fabrication parameters on the cleaving of microstructured polymer optical fibers, SPIE Proc. (2006) 6289.
[20] C. Jiang, M.G. Kuzyk, J.-L. Ding, W.E. Johns and D.J. Welker, Fabrication and mechanical behavior of dye-doped polymer optical fiber, J. Appl. Phys. 92 (2002) 4-12.
[21] J.I. McKechnie, R.N. Haward, D. Brown and J.H.R. Clarke, Effects of Chain Configurational Properties on the Stress-Strain Behavior of Glassy Linear Polymers, Macromolecules 26 (1993) 198-202.
[22] S. Kiesel, K. Peters, T. Hassan and M. Kowalsky, Behaviour of intrinsic polymer optical fibre sensor for large-strain applications, Meas. Sci. Technol. 18 (2007) 3144-3154.
[23] M.C.J. Large, J. Moran and L. Ye, The role of viscoelastic properties in strain testing using microstructured polymer optical fibers (mPOF), Meas. Sci. Technol. 20 (2009) 034014.
[24] http://www.bksv.com/doc/technicalreview1970-2.pdf.
[25] L. Thévenaz, *Advanced Fiber Optics, concepts and technology* (EPFL press, distributed by CRC Press) (2011)
[26] A. Stefani, K. Nielsen, H.K. Rasmussen and O. Bang, Cleaving of TOPAS and PMMA microstructured polymer optical fibers: Core-shift and statistical quality optimization, Opt. Commun. 285 (2012) 1825-1833.

Paper 8

Humidity insensitive TOPAS polymer fiber Bragg grating sensor

W. Yuan, L. Khan, D.J. Webb, K. Kalli, H.K. Rasmussen, A. Stefani and O. Bang

Optics Express, vol. 19(20), pp. 19731-19739 (2011).

Humidity insensitive TOPAS polymer fiber Bragg grating sensor

Wu Yuan,[1] Lutful Khan,[2] David J. Webb,[2,*] Kyriacos Kalli,[3] Henrik K. Rasmussen,[4] Alessio Stefani,[1] Ole Bang[1]

[1]*DTU Fotonik, Dept. of Photonics Engineering, Technical University of Denmark, DK-2800 Kgs. Lyngby, Denmark*
[2]*Photonic Research Group, Aston University, Aston Triangle, Birmingham, B4 7ET, UK*
[3]*Nanophotonics Research Laboratory, Cyprus University of Technology, Cyprus*
[4]*Dept. of Mechanical Engineering, Technical University of Denmark DK-2800 Kgs. Lyngby, Denmark*
**d.j.webb@aston.ac.uk*

Abstract: We report the first experimental demonstration of a humidity insensitive polymer optical fiber Bragg grating (FBG), as well as the first FBG recorded in a TOPAS polymer optical fiber in the important low loss 850nm spectral region. For the demonstration we have fabricated FBGs with resonance wavelength around 850 nm and 1550 nm in single-mode microstructured polymer optical fibers made of TOPAS and the conventional poly (methyl methacrylate) (PMMA). Characterization of the FBGs shows that the TOPAS FBG is more than 50 times less sensitive to humidity than the conventional PMMA FBG in both wavelength regimes. This makes the TOPAS FBG very appealing for sensing applications as it appears to solve the humidity sensitivity problem suffered by the PMMA FBG.

OCIS codes: (060.2370) Fiber optics sensors; (060.2270) Fiber characterization; (050.2770) Gratings; (160.5470) Polymers.

References and links

1. H. Dobb, K. Carroll, D. J. Webb, K. Kalli, M. Komodromos, C. Themistos, G. D. Peng, A. Argyros, M. C. J. Large, M. A. van Eijkelenborg, Q. Fang, and I. W. Boyd, "Grating based devices in polymer optical fibre," Proc. SPIE 618901 (2006).
2. W. Yuan, A. Stefani, M. Bache, T. Jacobsen, B. Rose, N. Herholdt-Rasmussen, F. K. Nielsen, S. Andresen, O. B. Sørensen, K. S. Hansen, and O. Bang, "Improved thermal and strain performance of annealed polymer optical fiber Bragg gratings," Opt. Commun. **284**(1), 176–182 (2011).
3. G. Emiliyanov, J. B. Jensen, O. Bang, P. E. Hoiby, L. H. Pedersen, E. M. Kjaer, and L. Lindvold, "Localized biosensing with Topas microstructured polymer optical fiber," Opt. Lett. **32**(5), 460–462 (2007).
4. G. Emiliyanov, J. B. Jensen, O. Bang, P. E. Hoiby, L. H. Pedersen, E. M. Kjaer, and L. Lindvold, "Localized biosensing with TOPAS microstructured polymer optical fiber: Erratum," Opt. Lett. **32**(9), 1059 (2007).
5. G. E. Town, W. Yuan, R. McCosker, and O. Bang, "Microstructured optical fiber refractive index sensor," Opt. Lett. **35**(6), 856–858 (2010).
6. C. Markos, W. Yuan, K. Vlachos, G. E. Town, and O. Bang, "Label-free biosensing with high sensitivity in dual-core microstructured polymer optical fibers," Opt. Express **19**(8), 7790–7798 (2011).
7. W. Yuan, G. E. Town, and O. Bang, "Refractive index sensing in an all-solid twin-core photonic bandgap fiber," IEEE Sens. J. **10**(7), 1192–1199 (2010).
8. F. M. Cox, A. Argyros, and M. C. J. Large, "Liquid-filled hollow core microstructured polymer optical fiber," Opt. Express **14**(9), 4135–4140 (2006).
9. J. Jensen, P. Hoiby, G. Emiliyanov, O. Bang, L. Pedersen, and A. Bjarklev, "Selective detection of antibodies in microstructured polymer optical fibers," Opt. Express **13**(15), 5883–5889 (2005).
10. A. Dupuis, N. Guo, Y. Gao, N. Godbout, S. Lacroix, C. Dubois, and M. Skorobogatiy, "Prospective for biodegradable microstructured optical fibers," Opt. Lett. **32**(2), 109–111 (2007).
11. B. Hadimioglu and B. T. Khuri-Yakub, "Polymer Films as Acoustic Matching Layers," Ultrasonics Symposium, Proceedings IEEE, 3, 1337–1340 (1990).
12. Z. Xiong, G. D. Peng, B. Wu, and P. L. Chu, "Highly tunable Bragg gratings in single-mode polymer optical fibres," IEEE Photon. Technol. Lett. **11**(3), 352–354 (1999).
13. A. Stefani, W. Yuan, C. Markos, and O. Bang, "Narrow bandwidth 850 nm fiber Bragg gratings in few-mode polymer optical fibers," IEEE Photon. Technol. Lett. **23**(10), 660–662 (2011).

#151392 - $15.00 USD Received 19 Jul 2011; revised 5 Sep 2011; accepted 6 Sep 2011; published 23 Sep 2011

14. C. Zhang, W. Zhang, D. J. Webb, and G. D. Peng, "Optical fibre temperature and humidity sensor," Electron. Lett. **46**(9), 643–644 (2010).
15. N. G. Harbach, "Fiber Bragg gratings in polymer optical fibers," PhD Thesis, Lausanne, EPFL (2008).
16. H. Dobb, D. J. Webb, K. Kalli, A. Argyros, M. C. J. Large, and M. A. van Eijkelenborg, "Continuous wave ultraviolet light-induced fiber Bragg gratings in few- and single-mode microstructured polymer optical fibers," Opt. Lett. **30**(24), 3296–3298 (2005).
17. I. P. Johnson, K. Kalli, and D. J. Webb, "827nm Bragg grating sensor in multimode microstructured polymer optical fiber," Electron. Lett. **46**(17), 1217–1218 (2010).
18. I. P. Johnson, W. Yuan, A. Stefani, K. Nielsen, H. K. Rasmussen, L. Khan, D. J. Webb, K. Kalli, and O. Bang, "Optical fibre Bragg grating recorded in TOPAS cyclic olefin copolymer," Electron. Lett. **47**(4), 271–272 (2011).
19. Y. Tsuchida, K. Saitoh, and M. Koshiba, "Design of single-moded holey fibers with large-mode-area and low bending losses: the significance of the ring-core region," Opt. Express **15**(4), 1794–1803 (2007).
20. D. J. Webb, K. Kalli, K. Carroll, C. Zhang, M. Komodromos, A. Argyros, M. Large, G. Emiliyanov, O. Bang, and E. Kjaer, "Recent developments of Bragg gratings in PMMA and TOPAS polymer optical fibers," Advanced Sensor Systems and Applications III, Proc. of SPIE **6830**, 683002 (2007).
21. D. J. Webb, K. Kalli, C. Zhang, M. Komodromos, A. Argyros, M. Large, G. Emiliyanov, and O. Bang, "E, Kjaer, "Temperature sensitivity of Bragg gratings in PMMA and TOPAS microstructured polymer optical fibres," Photonic Crystal Fibers **II**, L9900 (2008).
22. www.topas.com.
23. G. Khanarian and H. Celanese, "Optical properties of cyclic olefin copolymers," Opt. Eng. **40**(6), 1024–1029 (2001).
24. K. Nielsen, H. K. Rasmussen, A. J. L. Adam, P. C. M. Planken, O. Bang, and P. U. Jepsen, "Bendable, low-loss Topas fibers for the terahertz frequency range," Opt. Express **17**(10), 8592–8601 (2009).
25. M. C. J. Large, L. Poladian, G. Barton, and M. A. van Eijkelenborg, "Microstructured polymer optical fibres," Springer, (2008).
26. M. A. van Eijkelenborg, M. C. J. Large, A. Argyros, J. Zagari, S. Manos, N. A. Issa, I. Bassett, S. Fleming, R. C. McPhedran, C. M. de Sterke, and N. A. P. Nicorovici, "Microstructured polymer optical fibre," Opt. Express **9**(7), 319–327 (2001).
27. N. A. Mortensen, "Semianalytical approach to short-wavelength dispersion and modal properties of photonic crystal fibers," Opt. Lett. **30**(12), 1455–1457 (2005).
28. G. D. Marshall, D. J. Kan, A. A. Asatryan, L. C. Botten, and M. J. Withford, "Transverse coupling to the core of a photonic crystal fiber: the photo-inscription of gratings," Opt. Express **15**(12), 7876–7887 (2007).
29. L. Rindorf and O. Bang, "Sensitivity of photonic crystal fiber grating sensors: biosensing, refractive index, strain, and temperature sensing," J. Opt. Soc. Am. B **25**(3), 310 (2008).

1. Introduction

Fiber Bragg gratings (FBGs) in polymer optical fiber (POF) are attractive for optical fiber sensing applications that measure strain and temperature due to their low Young's modulus (25 times lower than silica), their high thermo-optic coefficient, and because they can be stretched far more than silica fibers before breaking (in excess of 10%) [1,2]. In addition, polymer optical fibers (POFs) are clinically acceptable, which along with their flexible and non-brittle nature makes POFs important candidates for in-vivo biosensing applications [3–10]. A recent important application to photo-acoustic imaging has been demonstrated, which takes advantage of the low Young's modulus and the fact that polymers are, in general, much better impedance matched to water than glass fibers [11]. Fiber Bragg gratings have been reported in both step index POFs [2,12–15] and microstructured POFs (mPOFs) [13,16–18]. Microstructured optical fibers have a cladding consisting of a pattern of air holes that extend for the full length of the fiber and the optical properties can be designed by adjusting the relative position, size and shape of the air holes. Such mPOFs have the advantage that they easily can be made endlessly single-mode, i.e., single-mode at all frequencies, even when the core is large [19]. Furthermore, the holes of the mPOF can be used to hold a gas or a biological sample, which can then be studied by evanescent-wave sensing with a strong overlap between the electric field and the holes [3,4,9].

The majority of POFs to date are based on PMMA. Monomer residues inside PMMA, and its aptitude for water absorption often make the drawing process with PMMA preforms problematic, and PMMA based FBG strain sensors have a significant cross-sensitivity to humidity [15,18,20,21]. These problems might be reduced by using other polymer materials, such as TOPAS, which is a cyclic olefin copolymer [22]. TOPAS has no monomers and its moisture absorption is reported to be at least 30 times lower than PMMA [23]. Furthermore, although TOPAS is chemically inert and bio-molecules do not readily bind to its surface,

#151392 - $15.00 USD Received 19 Jul 2011; revised 5 Sep 2011; accepted 6 Sep 2011; published 23 Sep 2011

treatment with antraquinon and subsequent UV activation allows sensing molecules to be deposited in well defined spatial locations [3,4]. When combined with grating technology this provides considerable potential for label-free bio-sensing [18]. In addition, TOPAS is also an ideal material for fabricating low-loss terahertz fibers [24].

Despite their promise, no commercial application of POF FBGs has been realized as yet, primarily due to the high material loss of both PMMA and TOPAS mPOFs in the 1300-1600 nm spectral region. A considerable decrease in the material loss from approximately 100 dB/m to 1 dB/m is achievable by working at a lower wavelength [23,25]. In this paper we therefore address two important problems for the application of POF FBGs: We fabricate and characterize the first FBGs in single-mode TOPAS mPOFs in the lower loss window around 800-900 nm and we use these FBGs to further demonstrate humidity insensitive operation due the properties of the base material TOPAS. The humidity measurements are carried out for both of the important sensing wavelengths 850 nm and 1550 nm.

Specifically, we use the phase-mask technique and a 325 nm HeCd laser to write several FBGs around 800-900 nm in TOPAS mPOFs. The same technique was used previously to fabricate a TOPAS grating with a resonance wavelength of 1567.9 nm [18], The static tensile strain sensitivity and the temperature sensitivity of an 870 nm TOPAS grating have been measured to be 0.64 pm/μstrain and −78 pm/°C, respectively. The relatively low material loss of the fiber at this wavelength, compared to that at longer wavelengths, will considerably enhance the potential utility of the TOPAS FBG, just as for PMMA, in which an FBG was recently written at 827 nm [17] and 850 nm [13]. It is also convenient to work at 850 nm, because CMOS technology can potentially provide interrogation systems that are even cheaper than those at the C and L band. Furthermore, the characterization reported here shows a humidity sensitivity of below 0.7 pm/% for both 850 nm and 1550 nm TOPAS FBGs, the value being actually limited by the 0.3 °C temperature stability of the environmental chamber used for the tests. This is more than 50 times lower than the 38 pm/% reported for a 1565 nm PMMA FBG [14]. The low affinity for water makes TOPAS FBGs very good candidates to address the humidity sensitivity problem suffered by PMMA FBGs, which has so far compromised their suitability for long term strain monitoring.

2. Experiments

2.1 TOPAS mPOFs and FBG writing

The drill-and-draw technique [25,26], was used for the fabrication of the mPOFs. The material used for the TOPAS mPOFs was a TOPAS® cyclic olefin copolymer in the form of granulates of the particular grade 8007, obtained from TOPAS Advanced Polymers, Inc. The TOPAS granulates were cast into 6 cm diameter rods and the desired hexagonal hole structure was drilled into the rod with a 3 mm diameter drill. This structure was preserved throughout the drawing process. The preforms were then drawn to fiber by first drawing a 5 mm cane, which was then sleeved and drawn again. The TOPAS mPOF used in our experiment was drawn without pressure and with low tension. The resulting mPOF has a diameter of 240 μm and a solid core surrounded by two rings of air holes arranged in a hexagonal lattice. The air-hole diameter is on average 2±0.2 μm and the inter-hole pitch is on average 6±0.2 μm, respectively, as shown in Fig. 1. The Topas mPOF has a hole diameter to pitch ratio of $d/\Lambda \approx 0.33$, which is well below the threshold of 0.42 that ensures endlessly single-mode operation of microstructued optical fibers of arbitrary base material [27].

#151392 - $15.00 USD Received 19 Jul 2011; revised 5 Sep 2011; accepted 6 Sep 2011; published 23 Sep 2011

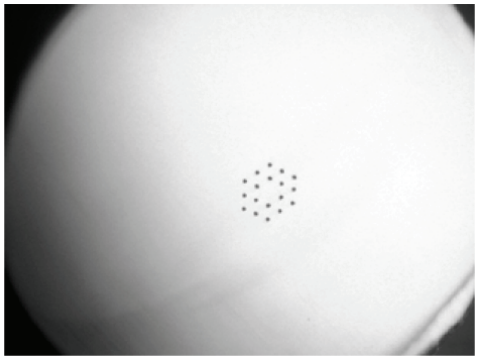

Fig. 1. The microscope image of the end facet of our TOPAS mPOF.

The gratings were inscribed using a 30 mW CW HeCd laser operating at 325 nm (IK5751I-G, Kimmon). The fiber was supported by v-grooves on both sides with a gap in between to avoid reflection, and it was taped down to ensure that the fiber did not sag. A circular Gaussian laser beam was expanded from diameter 1.2 mm to 1.2 cm in one direction along the fiber by a cylindrical lens. The laser beam was then focused vertically downwards into the fiber core using another cylindrical lens to expose the fiber through a phasemask customized for 325 nm writing with a uniform period of 572.4 nm (Ibsen Photonics), which was originally designed for 850 nm grating inscription in PMMA. A grating length of 10 mm was defined by an aperture underneath the focus lens to control the beam width. The laser irradiance at the fiber was about 5 Wcm^{-2}. The resulting grating wavelength was around 870 nm, with the longer resonance wavelength compared to that in PMMA fiber being due to the higher refractive index $n \approx 1.53$ of TOPAS at 800 nm.

The growth of the 10 mm gratings was monitored in reflection with a spectral resolution of 0.01 nm during the inscription using an 850 nm silica fiber circulator, a SuperK Versa broadband source (NKT Photonics) and an optical spectrum analyzer (Ando AQ6317B). A standard single-mode silica fiber was butt-coupled to the mPOF using an angle cleaved end-facet and a small amount of refractive index matching gel in order to reduce Fresnel reflections, which manifested themselves as background noise. The ends of the mPOF were prepared using a homemade hot blade cleaver equipped with flat side blade with a temperature of 50 °C for both the blade and fiber, which gives a high quality end facet. Typical reflection spectra of a 10 mm grating fabricated in the TOPAS mPOF with different exposure times are shown in Fig. 2(a). The necessary exposure time to write a FBG in an mPOF is longer than to write a grating in a solid step-index POF of the same diameter. This is because the holes around the core of the mPOF scatter a significant part of the laser power during the writing process [28], and that is why we only used two rings of air holes in our TOPAS mPOF. We further observed that side-lobes appeared in the reflection spectrum after 236 minutes.

The growth dynamics of the gratings, i.e. the time dependent peak intensity and grating bandwidth, are shown in Fig. 2(b). The grating writing dynamics initially displays a growth in strength accompanied by an almost constant grating bandwidth. After a certain threshold time, which was around 300 minutes, the grating strength begins to saturate. The bandwidth is less than 0.34 nm and thus we do not need to take it into account when we investigate the sensitivity of the FBG [29].

#151392 - $15.00 USD Received 19 Jul 2011; revised 5 Sep 2011; accepted 6 Sep 2011; published 23 Sep 2011

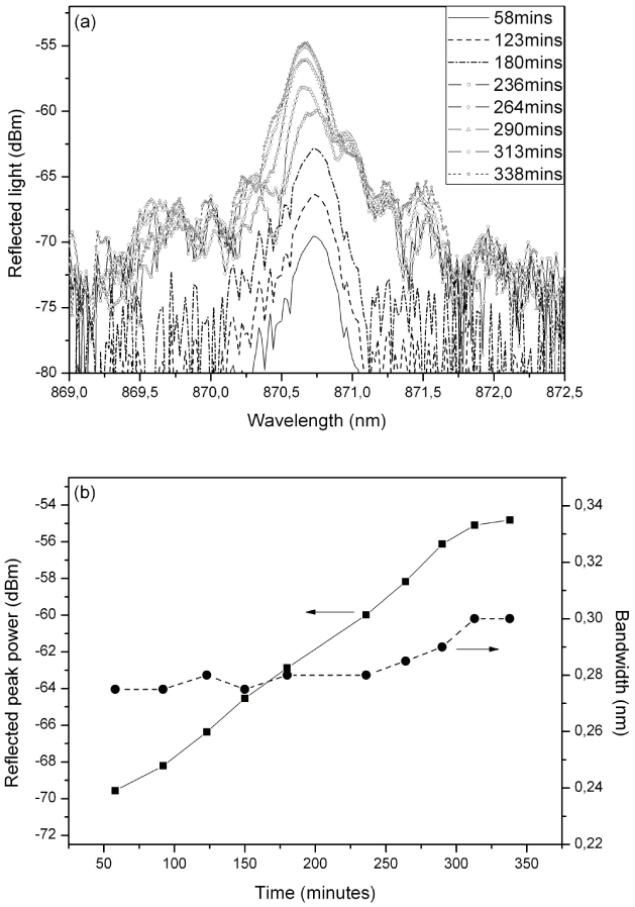

Fig. 2. (a) Reflection spectra (spectral resolution 0.01 nm) of the 10 mm FBG in a TOPAS mPOF at different writing times. (b) Growth dynamic of the peak intensity and bandwidth of the 10 mm FBG during writing.

2.2 Strain and temperature characterization of TOPAS mPOF FBGs

The strain tuning of the 870 nm FBG was investigated by mechanical stretching. The two ends of the mPOF were glued to two micro-translation stages with epoxy glue (Loctite 3430), with one of them fixed and used to butt-couple the mPOF to a silica single mode fiber. The epoxy glue is mechanically much stiffer than the TOPAS mPOF, so that it does not unduly influence the strain. The other stage can move longitudinally to apply axial strain to the grating manually with a low loading speed. The axial strain values were determined by dividing the fiber longitudinal elongation by the length of fiber between the two gluing points. The longitudinal displacement accuracy of the moving translation stage is 0.01 mm. The gratings were left to stabilize for about ten minutes each time the tensile strain was changed

#151392 - $15.00 USD Received 19 Jul 2011; revised 5 Sep 2011; accepted 6 Sep 2011; published 23 Sep 2011

before reading the reflection spectrum. A strain loading experiment was carried out to study the strain tuning response of the grating, as shown in Fig. 3(a). The fiber was gradually stretched to 2.17% strain. The grating shows a linear response of the wavelength shift over the whole strain loading range and a linear fit of the results gives a strain sensitivity of 0.64±0.04 pm/μstrain, which is similar to the reported sensitivities of 0.71 pm/μstrain of PMMA mPOF FBGs at 827nm [17] and 850nm [13].

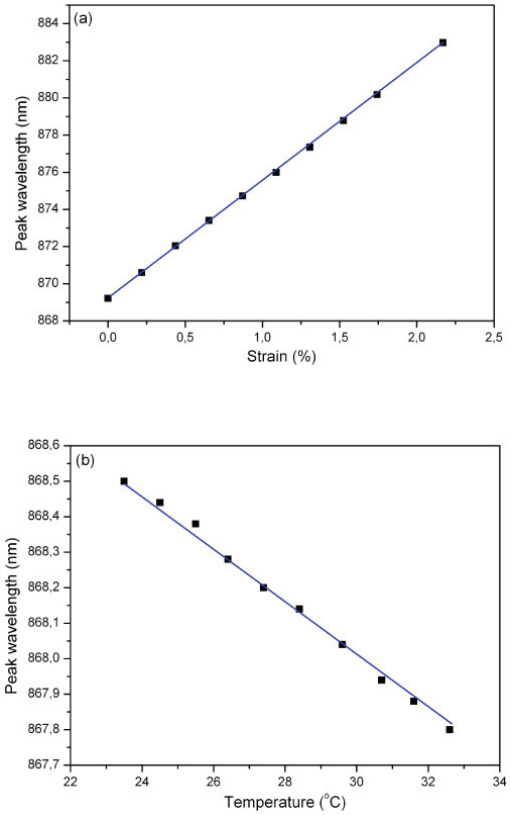

Fig. 3. Strain (a) and temperature (b) response of the 10mm TOPAS mPOF FBG, giving sensitivities of 0.64±0.04 pm/μstrain and −78±1 pm/°C, respectively.

The temperature response of the gratings was also studied with the same monitoring setup as the one used during the grating inscription. The polymer fiber was heated up with a resistive hot stage (MC60+TH60, Linkam). A thermo coupler was used to measure the temperature as close to the grating as possible with an uncertainty around 0.3°C. One end of the mPOF was clamped and butt-coupled to a silica fiber circulator, and the entire length of the mPOF with grating was attached to the surface of the heater by several layers of lens papers on the top. Twenty minutes was allowed for the temperature of the grating to stabilize at each new setting before readings of the resonance wavelengths and peak intensity were taken. The grating was heated up from room temperature to 32.6°C stepwise in a single cycle, as shown in Fig. 3(b). A blue shift of the resonance wavelength was indentified during the

#151392 - $15.00 USD Received 19 Jul 2011; revised 5 Sep 2011; accepted 6 Sep 2011; published 23 Sep 2011

heating up process, but no obvious bandwidth change was found. A temperature sensitivity of −78±1 pm/°C was found for this grating by a linear fit. In contrast, a temperature sensitivity of −36.5 pm/°C was reported for a 1567.9 nm FBG in a 2-ring TOPAS mPOF before [18]. The fiber used in [18] had a slightly larger diameter of 287 μm, larger holes with a diameter of 3.8 μm, and a larger pitch of 8.5 μm. The larger relative hole size of 0.44 (compared to the 0.33 of the fiber we use here) could be what shields against a temperature increase in the core and thereby gives a weaker temperature sensitivity if the fiber is not left to stabilize at each temperature setting. The difference is currently under investigation. The negative temperature sensitivity means that the negative thermo-optic coefficient of approximately -1×10^{-4}/°C [23], dominates the positive thermo-expansion coefficient of approximately $+6\times10^{-5}$/°C [23], in the thermal response of the TOPAS mPOF FBG, which is similar to the case of the PMMA FBG [2]. This corrects earlier preliminary results that showed a strong positive response of a TOPAS FBG [20,21]. The FBG reported here has a clear reflection spectrum, whereas the earlier measurement showed an FBG that could only be measured in transmission [21], which is most probably the explanation of the earlier result.

2.2 Humidity characterization of TOPAS mPOF FBGs

Research to date on POF gratings has essentially involved PMMA, which has an affinity for water. When PMMA FBGs are applied to temperature and strain sensing, an important issue is the cross-sensitivity to humidity. In contrast, TOPAS has a much lower moisture absorption uptake, i.e., <0.01% [23], and this property makes it a very appealing alternative to address the humidity sensitivity problem suffered by PMMA, which has a moisture absorption uptake of 0.3% [23]. After inscribing the 870 nm grating in the TOPAS mPOF, a second phase mask was then used to enable the fabrication of a grating in the same mPOF with a smaller Bragg wavelength that is more compatible with the available light sources and detectors at 850 nm. The same TOPAS mPOF was also used in the inscription of a Bragg grating with a resonance wavelength of ~1568 nm for studying the humidity response of the TOPAS FBG in the L band.

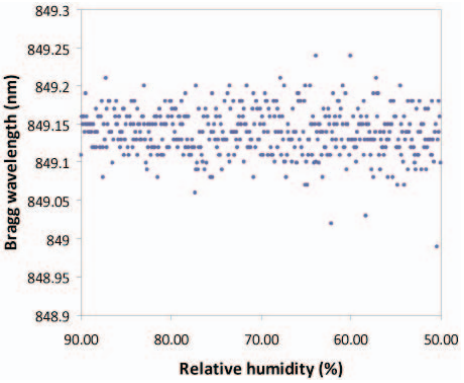

Fig. 4. , Humidity response of an 849 nm TOPAS mPOF FBG. The humidity was continuously decreased from 90% to 50% over a 4 hour time period.

As shown in Fig. 4, a TOPAS mPOF FBG with a resonance peak of ~849 nm has been examined in an environmental chamber (Sanyo Gallenkamp) for 4 hours at 25 °C, where it was subject to a humidity gradually decreasing from 90% to 50% over that period. Linear regression provides a slope of 0.26±0.12 pm/%, which means that over this humidity range a shift of the mean resonance peak of only about −10 pm was found. Caution must however be exercised in interpreting this wavelength shift because the environmental chamber has a

#151392 - $15.00 USD Received 19 Jul 2011; revised 5 Sep 2011; accepted 6 Sep 2011; published 23 Sep 2011

specified temperature stability of 0.3 °C. Given the measured temperature sensitivity of the FBG quoted earlier, a 0.3 °C temperature rise would cause a wavelength shift of −18pm, which is rather larger than the −10pm average shift observed in the data of Fig. 4. Consequently, we cannot conclude that the observed wavelength shift is due to humidity change as it may be simply due to temperature drifts in the chamber. All we can do is to calculate an upper limit on the magnitude of any humidity sensitivity. We do this using a worst-case scenario where we assume that there has been a negative temperature change of 0.3 °C over the course of the experiment, leading to a temperature induced positive wavelength shift of 18pm; the observed net negative wavelength shift of −10pm would therefore require a contribution to wavelength shift from humidity of −28pm over the experiment or 0.7 pm/% relative humidity. We must stress that this is a worst case calculation and the actual sensitivity is likely to be lower. As a comparison, a PMMA based FBG at 1565nm displayed a sensitivity of 38.4±0.4 pm/% relative humidity [14], which is over 50 times more than the maximum possible humidity sensitivity of the TOPAS FBG studied here.

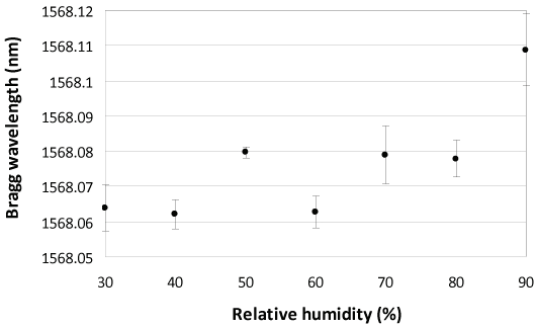

Fig. 5. Variation of the Bragg wavelength of a 1568 nm TOPAS FBG with humidity from 30% to 90%.

Following the humidity test carried out on the 849 nm TOPAS FBG, a second test was run to determine the humidity sensitivity of TOPAS using a 1568 nm FBG. Unlike the previous test, the environmental chamber was this time set to increase humidity stepwise from 30% to 90% at 25°C with 10% increments and a duration of two hours for each step. Spectral data were obtained every 30 seconds at each humidity, following a 30 minute acclimatisation period; the average value and associated error are plotted in Fig. 5. Linear regression of the humidity response gives a sensitivity of −0.59±0.02 pm/% relative humidity, with a shift of 36 pm over the humidity range studied. However, once again the measurement is effectively limited by the 0.3°C stability of the oven as a temperature drift of such magnitude could produce a shift of 33 pm over the course of the experiment. The measured sensitivity is nevertheless already 65 times smaller than for an equivalent FBG in PMMA based fiber [14]. Previous studies already showed that the high and positive humidity sensitivity of the PMMA grating was due to the swelling of the fibre and the increase of refractive index, both of which were caused by the high moisture uptake of the material [14, 15, 23].

3. Conclusions

We have demonstrated for the first time the inscription of FBGs in TOPAS mPOFs with resonance wavelengths within 800-900 nm. The relatively low material loss of the fiber at this wavelength compared to that at longer wavelengths, together with the convenient accessibility of the cost-effective CMOS technology at this wavelength, will considerably enhance the potential utility of the TOPAS FBGs. The static tensile and thermal characterization of an 870 nm TOPAS grating showed the strain sensitivity and the temperature sensitivity to be 0.64

#151392 - $15.00 USD Received 19 Jul 2011; revised 5 Sep 2011; accepted 6 Sep 2011; published 23 Sep 2011

pm/μstrain and −78 pm/°C, respectively. Furthermore, we determined for the first time that the humidity sensitivity of the TOPAS FBG was more than 50 times less than that of PMMA FBGs, which makes TOPAS FBGs better candidates for long-term monitoring of strain and temperature with negligible cross-sensitivity to humidity.

Acknowledgements

We would like to acknowledge support from the Danish National Advanced Technology Foundation.

#151392 - $15.00 USD Received 19 Jul 2011; revised 5 Sep 2011; accepted 6 Sep 2011; published 23 Sep 2011

Paper 9

High Sensitivity Polymer Optical Fiber Bragg Grating Based Accelerometer

A. Stefani, S. Andresen, W. Yuan, N. Herholdt-Rasmussen, and O. Bang

IEEE Photonics Technology Letters, vol. 24(9), pp. 763-765 (2012).

High Sensitivity Polymer Optical Fiber-Bragg-Grating-Based Accelerometer

Alessio Stefani, Søren Andresen, Wu Yuan, Nicolai Herholdt-Rasmussen, and Ole Bang

***Abstract*— We report on the fabrication and characterization of the first accelerometer based on a polymer optical fiber Bragg grating (FBG) for operation at both 850 and 1550 nm. The devices have a flat frequency response over a 1-kHz bandwidth and a resonance frequency of about 3 kHz. The response is linear up to at least 15 g and sensitivities as high as 19 pm/g (shift in resonance wavelength per unit acceleration) have been demonstrated. Given that 15 g corresponds to a strain of less than 0.02% and that polymer fibers have an elastic limit of more than 1%, the polymer FBG accelerometer can measure very strong accelerations. We compare with corresponding silica FBG accelerometers and demonstrate that using polymer FBGs improves the sensitivity by more than a factor of four and increases the figure of merit, defined as the sensitivity times the resonance frequency squared.**

***Index Terms*— Accelerometer, fiber Bragg grating, optical fiber sensor, polymer optical fiber.**

I. Introduction

FIBER Bragg grating (FBG) sensors have attracted a lot of attention in the last decade because of their performance, size, and multiplexing capability [1]–[3]. Traditionally, silica FBGs were used because of their low loss and high operational temperature. However, polymer optical fiber (POF) FBGs have also recently been used in order to exploit the low Young's modulus (2-3 GPa compared to 72 GPa of silica [4]), and high failure strain (up to 10% [3], [4]). FBGs in POF were developed for various resonance wavelengths [3], [5]–[9]. In particular, there has been interest in FBGs with a resonance wavelength (λ_B) of 850 nm [8], [9] where POFs have much lower loss than around 1550 nm and where CMOS components are available. FBGs-based sensors have the advantage of being easy to multiplex, which has now also been demonstrated for POF FBGs [10], [11] thereby enabling temperature compensation [11]. Most POF FBGs are made of Poly(methyl methacrylate) (PMMA) but recently humidity insensitive POF FBGs in TOPAS were also developed [12], [13].

Manuscript received November 4, 2011; revised January 25, 2012; accepted February 5, 2012. Date of publication February 14, 2012; date of current version April 11, 2012. This work was supported in part by the Danish National Advanced Technology Foundation.

A. Stefani and O. Bang are with DTU Fotonik, Department of Photonics Engineering, Technical University of Denmark, Kgs. Lyngby 2800, Denmark (e-mail: alste@fotonik.dtu.dk; oban@fotonik.dtu.dk).

S. Andresen is with Brüel and Kjær Sound and Vibration Measurement A/S, Nærum 2850, Denmark (e-mail: soren.andresen@bksv.com).

W. Yuan is with the Singapore Institute of Manufacturing Technology, 638075, Singapore (e-mail: wyuan@SIMTech.a-star.edu.sg).

N. Herholdt-Rasmussen is with Ibsen Photonics A/S, Farum 3520, Denmark (e-mail: Nicolai.Herholdt-Rasmussen@ibsen.dk).

Color versions of one or more of the figures in this letter are available online at http://ieeexplore.ieee.org.

Digital Object Identifier 10.1109/LPT.2012.2188024

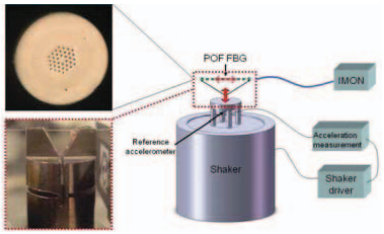

Fig. 1. Schematic of the accelerometer characterization setup. Top inset: mPOF cross section. Bottom inset: mPOF FBG-based accelerometer.

Fiber optic accelerometers [14], which are insensitive to electromagnetic interference and able to withstand harsh environments, can be used where conventional piezoelectric accelerometers would fail [15]. They have been based on interferometric techniques [14], [16]–[18], intensity change detection [19] and FBGs. The first demonstration of an FBG-based accelerometer was made by Berkoff et al. [20] and since then many different designs have been adopted [21], [22] and various performances in terms of sensitivity, frequency response, and signal to noise ratio have been achieved [18].

Here we present the development and characterization of the first POF FBG based accelerometers for operation at both 1550 and 850 nm. Corresponding accelerometers based on silica FBGs are used for a comparative performance evaluation [23].

II. Accelerometer Concept and Realization

The basic construction of the fiber-optical accelerometer is shown in Fig. 1. The acceleration is converted into strain by a mechanical transducer (Brüel & Kjær). The transducer has a fork shape and acceleration causes an increase in the separation between the arms of the fork. The FBG is attached to the fork and is then elongated. In FBGs, elongation produces a wavelength shift ($\Delta\lambda_B$) proportional to the strain (ε): $\Delta\lambda_B = 2n_{eff}\Lambda_B\varepsilon$, where n_{eff} is the effective refractive index and Λ_B is the grating period. The transducer is made so that the strain on the fiber is linearly dependent on acceleration. In this way the Bragg wavelength shift corresponds to acceleration [23]. The POF FBGs were produced by using the phase mask technique and a 30 mW 325 nm CW HeCd laser (IK5751I-G, Kimmon). The phase masks (Ibsen Photonics) have a pitch of 1024.7 nm for the 1550 nm FBGs and a pitch of 572.4 nm for the 850 nm FBGs. The POF in the accelerometer is a three ring microstructured POF (mPOF) made of PMMA with a hole diameter to pitch ratio of about $d/\Lambda = 0.5$ (top inset

Fig. 1). This is above the threshold of $d/\Lambda = 0.42$, which ensures endlessly single-mode operation of microstructured optical fibers of arbitrary base material, and thus our mPOF is few-moded [9].

A 40 cm mPOF with a 5 mm FBG (cleaved at 77.5 °C [24]) was glued onto the 10 mm fork of the Brüel & Kjær designed transducer (lower inset Fig. 1) and then butt coupled to a silica SMF 28 and glued to it for stability. The gluing process is important for the linear operation of the accelerometer. A first bonding (silica-PMMA) with an optical UV curable glue (NOA78-Norland) was made in order to have index matching between the fibers and to avoid Fabry–Perot cavity effects. This glue has poor mechanical strength, so a second UV curable glue was used to make the bonding stable. The mechanically stable glue was also used to fix the FBG onto the transducer. At first the fiber at one end of the grating was fixed on one of the transducer arm. After applying the desired pretension, the fiber at the second end was then glued on the second arm.

The test setup is shown in Fig. 1. A current driven shaker (Brüel & Kjær Type 4810) provides acceleration levels up to 15 g at frequencies up to 18 kHz. The mPOF FBG accelerometer is placed on top of the shaker platform. Underneath we placed a piezoelectric accelerometer with integrated charge preamplifier (Brüel & Kjær 4507) as a feedback reference for the current generator, in order to ensure that the shaker produced the desired acceleration level. The Bragg peak shift is measured with an I-MON 850-FW interrogator for 850 nm operation and an I-MON 80D-R interrogator for 1550 nm operation (both from Ibsen Photonics). The experiments were conducted at about 23 °C in an air conditioned room to limit the Young's modulus temperature dependence. Thus this factor should be taken into consideration by specific mechanical test on the different fibers. Several mPOF FBGs were written with resonance wavelengths around 850 nm and 1550 nm (also different fiber thickness have been used) and FBGs in silica fibers with the same resonance wavelengths were used for comparison. Both the wavelength shift versus acceleration at a fixed frequency and the wavelength shift versus frequency at a fixed acceleration were characterized.

III. Acceleration Measurements

In order to test the sensitivity and operational range of the accelerometer, the response to a sine wave with a fixed frequency of 159.2 Hz was measured. The amplitude of the excitation is proportional to the acceleration and accelerations in the range from 0.1 g to 15 g (RMS) was used for the measurements shown in Fig. 2. In order to analyze the results we first investigate the influence of the fiber diameter on the sensitivity. To do so we compare in Fig. 2 the response of an accelerometer based on an 850 nm FBG in two mPOFs with an outer diameter (OD) of 160 μm (solid red line) and 130 μm (solid blue line), respectively. The sensitivity is, as expected, lowest for the accelerometer using a thick fiber, simply because a larger cross-sectional fiber area translates into a higher spring constant. Here the sensitivity drops from 5.9 pm/g to 4.22 pm/g with the 30 μm increase in OD. With the influence of the

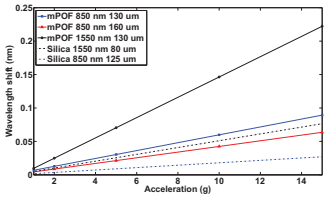

Fig. 2. Bragg wavelength shift versus acceleration for accelerometers based on silica FBGs with resonance wavelength of 1550 nm (80-μm OD, dashed black line) and 850 nm (125-μm OD, dashed blue line) and mPOF FBGs with resonance wavelength of 1550 nm (130-μm OD, solid black line) and 850 nm (solid blue line for 130-μm OD and solid red line for 160-μm OD).

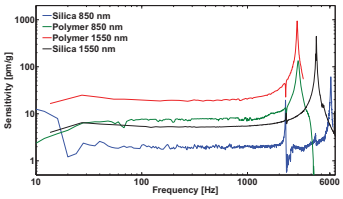

Fig. 3. Frequency response of the accelerometers normalized to the applied acceleration of 1 g. Fiber and accelerometer data are given in Table I.

fiber diameter in mind we can now compare the sensitivities of corresponding polymer and silica FBG accelerometers. The black solid and dashed lines show the response of a 1550 nm FBG accelerometer using a 130 μm OD mPOF and an 80 μm OD silica fiber, respectively. Both show a linear response in the whole measurement range of 0.1-15 g, but the sensitivity of the mPOF accelerometer is about 3 times higher than the corresponding silica fiber accelerometer (15.2 pm/g against 5.1 pm/g), despite that the mPOF has a 50 nm larger diameter. The same improved sensitivity is found for the FBG accelerometer operating at 850 nm, where the 130 μm OD mPOF gives a sensitivity of 5.9 pm/g (solid blue line), which is 3.3 times the sensitivity of 1.8 pm/g obtained with a thinner 125 μm OD silica fiber (dashed blue line).

From Fig. 2 we also observe that the sensitivity decreases when the Bragg wavelength decreases, which is seen for both the mPOF and silica fiber based accelerometers. This is a well-known effect basically due to the fact that the same elongation is transduced to a wavelength shift proportional to the resonance wavelength [9].

The responses shown in Fig. 2 are limited to 15 g because of the shaker limit. It is important to note that this corresponds to a wavelength shift of less than 300 pm and a strain of less than 0.02%. Given that the linear response regime of polymer fibers is much higher, then it is evident that the mPOF FBG accelerometer can measure very high accelerations.

IV. Frequency Response

In Fig. 3 we show the frequency response for a fixed acceleration of 1 g for 1550 nm and 850 nm operated FBG accelerometers based on mPOF and silica FBGs. The response has been normalized to the applied acceleration and FBG and

TABLE I
*MEASURED AT FIXED ACCELERATION, i.e., 1 G, AND CALCULATED AS THE AVERAGE OF THE FLAT PART OF THE FREQUENCY RESPONSE

Material	λ_B [nm]	OD [μm]	Sensitivity* [pm/g]	f_{res} [kHz]	FOM [$10^6 Hz^2 pm/g$]
PMMA	1550	130	19	2.9	159.79
PMMA	850	130	7.6	3	68.4
Silica	1550	80	5.3	4.4	102.608
Silica	850	125	1.8	6.1	66.978

accelerometer data are summarized in Table I. For all the FBGs, the accelerometer shows a flat response for frequencies up to about 1 kHz. When using a silica FBGs the resonance frequency (f_{res}) is higher because of the stiffness of the fiber. A more compliant fiber, such as the mPOF, lowers the system resonance frequency. The resonance frequency is close to 3 kHz for both mPOF based accelerometers, while it is 4.4 kHz when using the 80 μm OD 1550 nm silica FBG and 6.1 kHz for the 125 μm OD 850 nm silica FBG.

The two mPOF FBG based accelerometers have the same resonance since they use the same fiber. while the silica FBGs are written in two different fibers. The thicker fiber shows a higher resonance because of the system being stiffer. The positive side is that a more compliant fiber has a higher sensitivity. In fact it is possible to see that the mPOF based accelerometers have a sensitivity about four times higher than the corresponding silica based ones. In order to take into account both factors a figure of merit is often used when characterizing accelerometers, which is the product of the sensitivity and the square of the resonance frequency. A comparison between silica and polymer fiber based FBG accelerometers is given in Table I, from which we see that the sensitivity gained by using polymer fibers, because of their about 30 times lower Young's modulus, compensates for the decrease in resonance frequency, and gives the polymer FBG accelerometer the highest figure of merit.

It must be considered that for this particular figure of merit, an increase in thickness of the fiber would in fact give an advantage since the gain in resonance frequency counts more than the gain in sensitivity (for example in the 850 nm accelerometers the difference in figure of merit between polymer and silica is lower than for the 1550 nm ones because the fiber is thicker). In any case, the choice of the accelerometer is often given by the particular application for which it is intended. Disregarding the resonance frequency and looking only at frequencies lower than 1 kHz, then the mPOF FBG based accelerometers have better performances than the silica ones for both 850 nm and 1550 nm operation.

In conclusion we demonstrated the first mPOF FBG based accelerometer operating at both 850 nm and 1550 nm. We characterized the accelerometers and demonstrated that they have a linear response (at 159.2 Hz) for accelerations up to 15 g and a flat frequency response up to 1 kHz with a resonance frequency around 3 kHz for a fixed acceleration of 1 g. The polymer FBG accelerometers were compared to identical accelerometers based on silica FBGs. The results showed that the use of polymer FBGs increased the sensitivity by a factor of about 4 and improved the figure of merit, given by the sensitivity times resonance frequency squared.

REFERENCES

[1] S. Yin, P. B. Ruffin, and F. T. S. Yu, *Fiber Optic Sensors*, 2nd ed. Boca Raton, FL: CRC Press, 2008, pp. 109–162.

[2] A. D. Kersey, *et al.*, "Fiber grating sensors," *J. Lightw. Technol.*, vol. 15, no. 8, pp. 1442–1463, Aug. 1997.

[3] D. J. Webb and K. Kalli, "Polymer fiber Bragg gratings," in *Fiber Bragg Grating Sensors: Recent Advancements, Industrial Applications and Market Exploitation*, A. Cusano, A. Cutolo, and J. Albert Eds. Oak Park, IL: Bentham eBooks, 2011, pp. 292–312.

[4] M. C. J. Large, L. Poladian, G. Barton, and M. A. van Eijkelenborg, *Microstructured Polymer Optical Fibres*. New York: Springer-Verlag, 2008.

[5] Z. Xiong, G. D. Peng, B. Wu, and P. L. Chu, "Highly tunable Bragg gratings in single-mode polymer optical fibers," *IEEE Photon. Technol. Lett.*, vol. 11, no. 3, pp. 352–354, Mar. 1999.

[6] H. Dobb, D. J. Webb, K. Kalli, A. Argyros, M. C. J. Large, and M. A. van Eijkelenborg, "Continuous wave ultraviolet light-induced fiber Bragg gratings in few and single-mode microstructured polymer optical fibers," *Opt. Lett.*, vol. 30, no. 24, pp. 3296–3298, 2005.

[7] W. Yuan, *et al.*, "Improved thermal and strain performance of annealed polymer optical fiber Bragg gratings," *Opt. Commun.*, vol. 28, no. 1, pp. 176–182, 2011.

[8] I. P. Johnson, K. Kalli, and D. J. Webb, "827 nm Bragg grating sensor in multimode microstructured polymer optical fibre," *Electron. Lett.*, vol. 46, no. 17, pp. 1217–1218, 2010.

[9] A. Stefani, W. Yuan, C. Markos, and O. Bang, "Narrow bandwidth 850 nm fiber Bragg gratings in few-mode polymer optical fibers," *IEEE Photon. Technol. Lett.*, vol. 23, no. 10, pp. 660–662, May 15, 2011.

[10] I. P. Johnson, D. J. Webb, K. Kalli, M. C. J. Large, and A. Argyros, "Multiplexed FBG sensor recorded in multimode microstructured polymer optical fibre," *Proc. SPIE*, vol. 7714, pp. 77140-1–77140-10, May 2010.

[11] W. Yuan, A. Stefani, and O. Bang, "Tunable polymer fiber Bragg grating (FBG) inscription: Fabrication of dual-FBG temperature compensated polymer optical fiber strain sensor," *IEEE Photon. Technol. Lett.*, vol. 24, no. 5, pp. 401–403, Mar. 1, 2012.

[12] I. P. Johnson, *et al.*, "Optical fibre Bragg grating recorded in TOPAS cyclic olefin copolymer," *Electron. Lett.*, vol. 47, no. 4, pp. 271–272, 2011.

[13] W. Yuan, *et al.*, "Humidity insensitive TOPAS polymer fiber Bragg grating sensor," *Opt. Express*, vol. 19, no. 20, pp. 19731–19739, 2011.

[14] A. B. Tveten, A. Dandridge, C. M. Davis, and T. G. Giallorenzi, "Fiber optic accelerometer," *Electron. Lett.*, vol. 16, no. 22, pp. 854–856, 1980.

[15] *Test of fiber optic transducer system on Vestas V90* [Online]. Available: http://www.bksv.com/doc/bn1039.pdf

[16] A. S. Gerges, T. P. Newson, J. D. C. Jones, and D. A. Jackson, "High-sensitivity fiber-optic accelerometer," *Opt. Lett.*, vol. 14, no. 4, pp. 251–253, 1989.

[17] B. Wu, C. Chen, G. Ding, D. Zhang, and Y. Cui, "Hybrid-integrated michelson fiber optic accelerometer," *Opt. Eng.*, vol. 43 no. 2, pp. 313–318, 2004.

[18] E. A. Moro, M. D. Todd, and A. Puckett, "A performance comparison of transducer designs for interferometric fiber optic accelerometers," *Proc. SPIE*, vol. 7648, pp. 76480G1–76480G12, May 2010.

[19] J. A. Bucaro and N. Lagakos, "Lightweight fiber optic microphones and accelerometers," *Rev. Scientific Inst.*, vol. 72, no. 6, pp. 2816–2821, 2001.

[20] T. A. Berkoff and A. Kersey, "Experimental demonstration of a fiber Bragg grating accelerometer," *IEEE Photon. Technol. Lett.*, vol. 8, no. 12, pp. 1677–1679, Dec. 1996.

[21] H. Y. Au, S. K. Khijwania, and H. Y. Tam, "Fiber Bragg grating based accelerometer," *Proc. SPIE*, vol. 7004, pp. 1–4, Apr. 2008.

[22] P. Antunes, H. Varum, and P. André, "Uniaxial fiber Bragg grating accelerometer system with temperature and cross axis insensitivity," *Measurement*, vol. 44, no. 1, pp. 55–59, 2011.

[23] S. Andresen, F. K. Nielsen, T. R. Licht, M. N. Rasmussen, and M. Kirkelund, "Fibre Bragg grating vibration transducer based on novel mechanical sensing element for monitoring applications," *Proc. SPIE*, vol. 7753, no. 1, pp. 77537-1–77537-4, 2011.

[24] A. Stefani, K. Nielsen, H. K. Rasmussen, and O. Bang, "Cleaving of TOPAS and PMMA microstructured polymer optical fibers: Core-shift and statistical quality optimization," *Opt. Commun.*, vol. 285, no. 7, pp. 1825–1833, 2012.

Bibliography

[1] M.A. van Eijkelenborg, M.C.J. Large, A. Argyros, J. Zagari, S. Manos, N.A. Issa, I. Bassett, S. Fleming, R.C. McPhedran, C.M. de Sterke, and N.A.P. Nicorovici. Microstructured polymer optical fibre. *Optics Express*, 9(7):319–327, 2001.

[2] H. Dobb, D.J. Webb, K. Kalli, A. Argyros, M.C.J. Large, and M.A. van Eijkelenborg. Continuous wave ultraviolet light-induced fiber Bragg gratings in few- and single-mode microstructured polymer optical fibers. *Optics Letters*, 30(24):3296–3298, 2005.

[3] M.C.J. Large, L. Poladian, G. Barton, and M.A. van Eijkelenborg. *Microstructured Polymer Optical Fibres*. Springer, 2008.

[4] T. Kaino, K. Jinguji, and S. Nara. Low loss poly(methylmethacrylate-d8) core optical fibres. *Applied Physics Letters*, 42(7):567–569, 1983.

[5] Y. Koike and T. Ishigure. High-bandwidth plastic optical fiber for fiber to the display. *Journal of Lightwave Technology*, 24(12):4541–4553, 2006.

[6] N. Tanio and Y. Koike. What is the most transparent polymer? *Polymer Journal*, 32(1):43–50, 2000.

[7] D.J. Webb and K. Kalli. *Fiber Bragg Grating Sensors: Recent Advancements, Industrial Applications and Market Exploitation*, chapter Polymer fiber Bragg gratings, pages 1–20. Bentham Science Publishers Ltd., 2009.

[8] M. Murofushi. Low loss perfluorinated POF. In *Proceedings of the International Plastic Optical Fibres conference*, pages 17–23, 1996.

[9] R.J. Bartlett, R. Philip-Chandy, P. Eldridge, D.F. Merchant, R. Morgan, and P.J. Scully. Plastic optical fibre sensors and devices. *Transactions of the Institute of Measurement & Control*, 22(5):431–457, 2000.

[10] J.C. Knight, T.A. Birks, P.St.J. Russell, and D.M. Atkin. All-silica single-mode optical fiber with photonic crystal cladding. *Optics Letters*, 21(19):1547–1549, 1996.

[11] N.A. Mortensen. Semianalytical approach to short-wavelength dispersion and modal properties of photonic crystal fibers. *Optics Letters*, 30:1455–1457, 2005.

[12] N.A. Mortensen, J.R. Folkenberg, M.D. Nielsen, and K.P. Hansen. Modal cutoff and the V parameter in photonic crystal fibers. *Optics Letters*, 28(20):1879–1881, 2003.

[13] T.M. Monro, Y.D. West, D.W. Hewak, N.G.R. Broderick, and D.J. Richardson. Chalcogenide holey fibres. *Electronics Letters*, 36(24):1998–2000, 2000.

[14] R. Lwin, G. Barton, L. Harvey, J. Harvey, D. Hirst, S. Manos, M.C.J. Large, L. Poladian, A. Bachmann, H. Poisel, and K.-F. Klein. Beyond the bandwidth-length product: graded index microstructured polymer optical fiber. *Applied Physics Letters*, 91:191119, 2007.

[15] M.A. van Eijkelenborg, A. Argyros, G. Barton, I.M. Bassett, M. Fellew, G. Henry, N.A. Issa, M.C.J. Large, S. Manos, W. Padden, L. Poladian, and J. Zagari. Recent progress in microstructured polymer optical fibre fabrication and characterisation. *Optical Fiber Technology*, 9(4):199–209, 2003.

[16] A. Argyros, M. van Eijkelenborg, M.C.J. Large, and I.M. Bassett. Hollow-core microstructured polymer optical fiber. *Optics Letters*, 31(2):172–174, 2006.

[17] M.K. Szczurowski, O. Frazão, J.M. Baptista, K. Nielsen, O. Bang, and W. Urbańczyk. Sensing characteristics of birefringent microstructured polymer optical fiber. In *Proceedings of SPIE*, volume 7753, pages 77533Z–4, 2011.

[18] M.C.J. Large, A. Argyros, F. Cox, M.A. van Eijkelenborg, S. Ponrathnam, N.S. Pujari, I.M. Bassett, R. Lwin, and G.W. Barton. Microstructured polymer optical fibres: new opportunities and challenges. *Molecular Crystals and Liquid Crystals*, 446:219–231, 2006.

[19] G. Emiliyanov, J.B. Jensen, P.E. Bang, O.and Hoiby, L.H. Pedersen, E.M. Kjær, and L. Lindvold. Localized biosensing with Topas microstructured polymer optical fiber. *Optics Letters*, 32:460–462, 2007.

[20] G. Emiliyanov, J.B. Jensen, P.E. Bang, O.and Hoiby, L.H. Pedersen, E.M. Kjær, and L. Lindvold. Localized biosensing with Topas microstructured polymer optical fiber: Erratum. *Optics Letters*, 32 (9):1059, 2007.

[21] G.E. Town, R.M. Chaplin, M.J. Wimford, and D. Baer. Randomly microstructured polymer optical fibre. In *Proceedings of ACOFT*, page 4519226, 2006.

[22] M.C.J. Large, S. Ponrathnam, A. Argyros, N.S. Pujari, and F. Cox. Solution doping of microstructured polymer optical fibres. *Optics Express*, 12(9):1966–1971, 2004.

[23] M.A. van Eijkelenborg, A. Argyros, and S.G. Leon-Saval. Polycarbonate hollow-core microstructured optical fiber. *Optics Letters*, 33(21):2446–2448, 2008.

[24] A. Dupuis, N. Guo, Y. Gao, N. Godbout, S. Lacroix, C. Dubois, and M. Skorobogatiy. Prospective for biodegradable microstructured optical fibers. *Optics Letters*, 32:109, 2007.

[25] K. Nielsen, A.J.L. Rasmussen, H.K. adn Adam, P.C.M. Planken, O. Bang, and P.U. Jepsen. Bendable, low-loss Topas fibers for the terahertz frequency range. *Optics Express*, 17:8592–8601, 2009.

[26] S. Atakaramians, S. Afshar V., H. Ebendorff-Heidepriem, M. Nagel, B.M. Fischer, D. Abbott, and T.M. Monro. THz porous fibers: design, fabrication and experimental characterization. *Optics Express*, 17(16):14053–15062, 2009.

[27] S.H. Law, J.D. Harvey, R.J. Kruhlak, M. Song, E. Wu, G.W. Barton, M.A. van Eijkelenborg, and M.C.J. Large. Cleaving of microstructured polymer optical fibres. *Optics Communications*, 258(2):193–202, 2006.

[28] K.O. Hill, Y. Fujii, D.C. Johnson, and Kawasaki B.S. Photosensitivity in optical waveguides: application to reflection filter fabrication. *Applied Physics Letters*, 32 (10):647, 1978.

[29] R. Kashyap. *Fiber Bragg gratings*. Accademic press, 1999.

[30] J. Canning. Fibre gratings and devices for sensors and lasers. *Laser and Photonics Reviews*, 2(4):275, 2008.

[31] A. Martinez, M. Dubov, I. Khrushchev, and I. Bennion. Direct writing of fiber Bragg gratings by femtosecond laser. *Electronics Letters*, 40 (19):1170–1172, 2004.

[32] A. Othonos. Fiber Bragg gratings. *Review of Scientific Instruments*, 68(12):4309–4341, 1997.

[33] B.J. Eggleton, P.S. Westbrook, R.S. Windeler, S. Spälter, and T.A. Strasser. Grating resonances in air-silica microstructured optical fibers. *Optics Letters*, 24(21):1460–1462, 1999.

[34] G.D. Marshall, D.J. Kan, A.A. Asatryan, L.C. Botten, and M.J. Withford. Transverse coupling to the core of a photonic crystal fiber: the photo-inscription of gratings. *Optics Express*, 15 (12):7876–7887, 2007.

[35] W.J. Tomlinson, I.P. Kaminow, E.A. Chandross, R.L. Fork, and W.T. Silfvast. Photoinduced refractive index increase in poly(methyl-methacrylate) and its applications. *Applied Physics Letters*, 16(12):486–9, 1970.

[36] Z. Xiong, G.D. Peng, B. Wu, and P.L. Chu. Highly tunable Bragg gratings in single-mode polymer optical fibers. *IEEE Photonics Technology Letters*, 11:352–354, 1999.

[37] C. Wochnowski, S. Metev, and G. Sepold. UV-laser-assisted modification of the optical properties of polymethylmethacrylate. *Applied Surface Science*, 154:706–711, 2000.

[38] K. Kalli, H.L. Dobb, D.J. Webb, K. Carroll, C. Themistos, M. Komodromos, G.-D. Peng, Q. Fang, and I.W. Boyd. Development of an electrically tuneable Bragg grating filter in polymer optical fibre operating at 1.55 μm. *Measurement Science and Technology*, 18(10):3155–3164, 2007.

[39] X. Yu, J. andTao and Tam H. Trans-4-stilbenemethanol-doped photosensitive polymer fibers and gratings. *Optics Letters*, 29 (2):156–158, 2004.

[40] G.D. Peng, Z. Xiong, and P.L. Chu. Photosensitivity and gratings in dye-doped polymer optical fibers. *Optical Fiber Technology*, 5(2):242–251, 1999.

[41] C. Zhang, K. Carroll, D.J. Webb, I. Bennion, K. Kalli, G. Emiliyanov, O. Bang, E. Kjær, and G.D. Peng. Recent progress in polymer optical fibre gratings. In *Proceedings of SPIE*, volume 7004, page 70044G, 2008.

[42] A. Argyros. *Bragg reflection and bandgaps in microstructured optical fibres*. PhD thesis, Optical Fibre Technology Centre and School of Physics University of Sydney, March 2006.

[43] Z.F. Zhang, C. Zhang, X.M. Tao, G.F. Wang, and G.D. Peng. Inscription of polymer optical fiber Bragg grating at 962 nm and its potential in strain sensing. *IEEE Photonics Technology Letters*, 22:1562–1564, 2010.

[44] I.P. Johnson, K. Kalli, and D.J. Webb. 827 nm Bragg grating sensor in multimode microstructured polymer optical fiber. *Electronics Letters*, 46(17):1217–1218, 2010.

[45] S. Yin, P.B. Ruffin, and F.T.S. Yu. *Fiber optic sensors*. CRC Press, 2nd edition, 2008.

[46] J. Zubia and J. Arrue. Plastic optical fibers: an introduction to their technological processes and applications. *Optical Fiber Technology*, 7(2):101–140, 2001.

[47] K. Peters. Polymer optical fiber sensors - a review. *Smart Materials and Structures*, 20(1):013002, 2011.

[48] O. Abdi, K. Peters, M. Kowalsky, and T. Hassan. Validation of a single-mode polymer optical fiber sensor and interrogator for large strain measurements. *Measurement Science and Technology*, 22(7):075207, 2011.

[49] S. Kiesel, K. Peters, T. Hassan, and M. Kowalsky. Large deformation in-fiber polymer optical fiber sensor. *IEEE Photonics Technology Letters*, 20(6):416–418, 2008.

[50] M. Silva-López, A. Fender, W.N. MacPherson, J.S. Barton, J.D.C. Jones, D. Zhao, H. Dobb, D.J. Webb, L. Zhang, and I. Bennion. Strain and temperature sensitivity of a single-mode polymer optical fiber. *Optics Letters*, 30:3129–3131, 2005.

[51] D. Gallego and H. Lamela. High sensitivity interferometric polymer optical fiber ultrasound sensors for optoacoustic imaging and biomedical application. In *Proceedings of SPIE*, volume 7753, pages 775370–4, 2011.

[52] D. Gallego and H. Lamela. Optoacoustic fiber optic interferometric sensors for biomedical applications. In *Proceedings of SPIE*, volume 8028, pages 80280O–7, 2011.

[53] L. Peng, X. Yang, L. Yuan, L. Wang, E. Zhao, F. Tian, and Y. Liu. Gaseous ammonia fluorescence probe based on cellulose acetate modified microstructured optical fiber. *Optics Communications*, 284(19):4810–4814, 2011.

[54] J. Wang and L. Wang. Carbon dioxide gas sensor derived from a 547-hole microstructured polymer optical fiber preform. *Optics Letters*, 35(19):3270–3272, 2010.

[55] X. Yu, K.S. Lok, Y.C. Kwok, Y. Zhang, H. Wei, and W. Tong. Chemiluminescence detection in liquid-core microstructured optical fibers. *Sensors & Actuators B: Chemical*, 160(1):800–803, 2011.

[56] F.M. Cox, A. Argyros, and M.C.J. Large. Liquid-filled hollow core microstructured polymer optical fiber. *Optics Express*, 14(9):4135–4140, 2006.

[57] X.H. Yang and L.L. Wang. Fluorescence pH probe based on microstructured polymer optical fiber. *Optics Express*, 15(25):16478–16483, 2007.

[58] M.C.J. Large S. Kalluri F.M. Cox, A. Argyros. Surface enhanced raman scattering in a hollow core microstructured optical fiber. *Optics Express*, 15:13675–13681, 2007.

[59] J.B. Jensen, P.E. Hoiby, G. Emiliyanov, O. Bang, L.H. Pedersen, and A. Bjarklev. Selective detection of antibodies in microstructured polymer optical fibers. *Optics Express*, 13:5883–5889, 2005.

[60] J. Wójcik, P. Mergo, J. Klimek, G. Wójcik, K. Skorupski, J. Pędzisz, and J. Kopeć. Technology of high birefringent microstructured polymer optical fibers. *Photonics Letters of Poland*, 2(1):4–6, 2010.

[61] C.M.B. Cordeiro, G. Chesini, C.H. Brito Cruz, M.A.R. Franco, E.C.S. Barretto, R. Lwin, and M.C.J. Large. Microstructured-core optical fibre for evanescent sensing applications. *Optics Express*, 14(26):13056–13066, 2006.

[62] A. Wang, B.T. Kuhlmey, F.M. Cox, M.C.J. Large, and A. Docherty. Side-hole fiber sensor based on surface plasmon resonance. *Optics Letters*, 34(24):3890–3892, 2009.

[63] M.C.J. Large, D. Blacket, and C.-A. Bunge. Microstructured polymer optical fibers compared to conventional POF: novel properties and applications. *IEEE Sensors Journal*, 10(7):1213–1217, 2010.

[64] R. Lwin, A. Argyros, S.G. Leon-Saval, and M.C.J. Large. Strain sensing using long period gratings in microstructured polymer optical fibres. In *Proceedings of SPIE*, volume 7753, 2011.

[65] J. Witt, M. Steffen, M. Schukar, and K. Krebber. Investigation of sensing properties of microstructured polymer optical fibres. In *Proceedings of SPIE*, volume 7714, pages 77140F–12, 2010.

[66] D. Sáez-Rodríguez, J.L. Cruz Munoz, I. Johnson, D.J. Webb, M.C.J. Large, and A. Argyros. Long period fibre gratings photoinscribed in a microstructured polymer optical fibre by UV radiation. In *SPIE Proceedings*, volume 7357, pages 73570L–8, 2009.

[67] D. Sáez-Rodríguez, J.L. Cruz, I. Johnson, D.J. Webb, M.C.J. Large, and A. Argyros. Water diffusion into UV inscripted long period grating in microstructured polymer fiber. *IEEE Sensors Journal*, 10(7):1169–1173, 2010.

[68] J. Witt, M. Steffen, M. Schukar, and K. Krebber. Investigation of sensing properties of long period gratings based on microstructured polymer optical fibres. In *Proceedings of SPIE*, volume 7653, pages 76530I–4, 2010.

[69] A. Grillet, D. Kinet, J. Witt, M. Schukar, K. Krebber, F. Pirotte, and A. Depre. Optical fiber sensors embedded into medical textiles for healthcare monitoring. *IEEE Sensors Journal*, 8(7):1215–1222, 2008.

[70] A.D. Kersey, M.A. Davis, H.J. Patrick, M. LeBlanc, K.P. Koo, C.G. Askins, M.A. Putnam, and E.J. Friebele. Fiber grating sensors. *Journal of Lightwave Technology*, 15:1442–1463, 1997.

[71] Y.-J. Rao. In-fibre Bragg grating sensors. *Measurement Science and Technology*, 8(4):355–375, 1997.

[72] F.M. Haran, J.K. Rew, and P.D. Foote. A strain-isolated fibre Bragg grating sensor for temperature compensation of fibre Bragg grating strain sensors. *Measurement Science and Technology*, 9(8):1163–1166, 1998.

[73] C. Zhang, W. Zhang, D.J. Webb, and G.-D. Peng. Optical fibre temperature and humidity sensor. *Electronics Letters*, 46:643–644, 2010.

[74] H.B. Liu, H.Y. Liu, G.D. Peng, and P.L. Chu. Strain and temperature sensor using a combination of polymer and silica fibre Bragg gratings. *Optics Communications*, 219:139–142, 2003.

[75] X. Chen, C. Zhang, D.J. Webb, G.-D. Peng, and K. Kalli. Bragg grating in a polymer optical fibre for strain, bend and temperature sensing. *Measurement Science and Technology*, 21:094005, 2010.

[76] D.J. Webb, H. Dobb, K.E. Carroll, K. Kalli, M. Aressy, S. Kukureka, A. Argyros, M.C.J. Large, and M.A. van Eijkelenborg. Fibre Bragg gratings recorded in microstructured polymer optical fibre. In *Optical Fiber Sensors*, page ThE64. Optical Society of America, 2006.

[77] K.E. Carroll, C. Zhang, D.J. Webb, K. Kalli, A. Argyros, and M.C.L. Large. Thermal response of Bragg gratings in PMMA microstructured optical fibers. *Optics Express*, 15(14):8844–8850, 2007.

[78] http://www.physics.usyd.edu.au/cudos/mofsoftware/.

[79] J. Canning, E. Buckley, B. Groothoff, N. andLuther-Davies, and J. Zagari. UV laser cleaving of air–polymer structured fibre. *Optics Communications*, 202:139–143, 2002.

[80] O. Abdi, K.C. Wong, T. Hassan, K.J. Peters, and M.J. Kowalsky. Cleaving of solid single mode polymer optical fiber for strain sensor applications. *Optics Communications*, 282:856–861, 2009.

[81] T. Geernaert, G. Luyckx, E. Voet, T. Nasilowski, K. Chah, M. Becker, H. Bartelt, W. Urbanczyk, J. Wojcik, W. De Waele, J. Degrieck, H. Terryn, F. Berghmans, and H. Thienpont. Transversal load sensing with fiber Bragg gratings in microstructured optical fibers. *IEEE Photonics Technology Letters*, 21(1):6–8, 2009.

[82] I.P. Johnson, D.J. Webb, K. Kalli, M.C.J. Large, and A. Argyros. Multiplexed fbg sensor recorded in multimode microstructured polymer optical fibre. In *Photonic Crystal Fibers IV. Proceeding of SPIE*, volume 7714, pages 77140D–1–10, 2010.

[83] H.Y. Liu, G.D. Peng, P.L. Chu, Y. Koike, and Y. Watanabe. Photosensitivity in low-loss perfluoropolymer (CYTOP) fibre material. *Electronics Letters*, 37(6):347–348, 2001.

[84] D.J. Webb. Polymer photonic crystal fibre for sensor applications. In *Proceedings of SPIE*, volume 7726, pages 77260Q–8, 2010.

[85] Br´uel & Kjær. Test of fiber optic transducer system on vestas v90. Technical report, Br´uel & Kjær, 2011.

[86] S. Andresen, F.K. Nielsen, T.R. Licht, M.N. Rasmussen, and M. Kirkelund. Fibre Bragg grating vibration transducer based on novel mechanical sensing element for monitoring applications. In *Proceedings of SPIE*, volume 7753, pages 77537M–4, 2011.

[87] D.J. Webb, K. Kalli, C. Zhang, M. Komodromos, Argyros. A., M.C.J. Large, G. Emiliyanov, O. Bang, and E. Kjær. Temperature sensitivity of Bragg gratings in PMMA and TOPAS microstructured polymer optical fibres. In *Proceedings of the SPIE - The International Society for Optical Engineering*, volume 6990, pages 69900L–1–10, 2008.

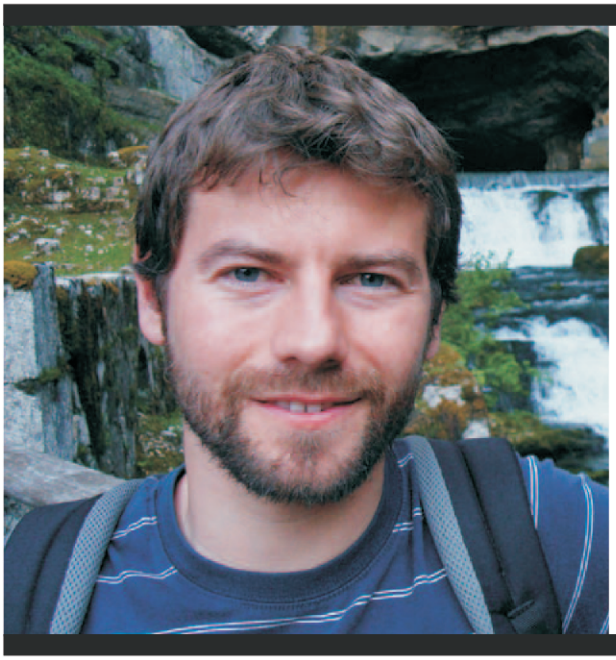

ISBN: 87-92062-80-6

Published by:
DTU Fotonik
Department of Photonics Engineering
Technical University of Denmark
Ørsteds Plads, building 343
DK-2800 Kgs. Lyngby

Alessio Stefani was born in 1984 a Merate, Italy. He graduated in Physical Engineering at the Politecnico di Milano in 2008, specializing in photonics and lasers. He did his master thesis work at the Photonics Engineering department at the technical University of Denmark on "Optical deposition of carbon nanotubes for saturable absorbers". Here, he obtained also his Ph.D. in 2012.

DTU Fotonik
Department of Photonics Engineering

Printed in Denmark by SaloPrint, 2620 Albertslund